I.

NB. blz 39
59
73
85
ontbraken ook al in origineel v. Kesteren.

PETER JUSTESEN

THE TURBULENT WAVE BOUNDARY LAYER

A THEORETICAL STUDY

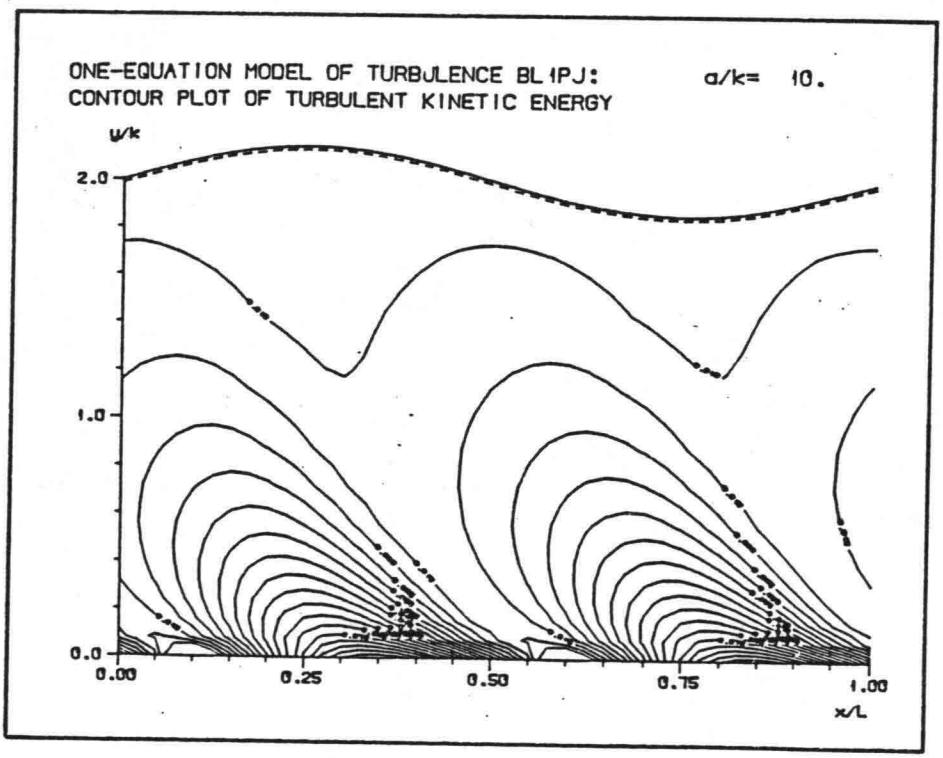

INSTITUTTET FOR
STRØMNINGSMEKANIK OG
VANDBYGNING

Institute of hydrodynamics and hydraulic engineering

TECHNICAL UNIVERSITY OF DENMARK - BUILDING 115 - DK-2800 LYNGBY

ISVA

LYNGBY, JANUARY 1985

LIST OF CONTENTS

0. PREFACE 4

1. INTRODUCTION 5

2. FLOW EQUATIONS AND TURBULENCE MODELS .....
   2.1 Introduction 8
   2.2 The flow equations 8
   2.3 Eddy viscosity models of turbulence 10
   2.4 Mixing-length theory, zero-equation models 12
   2.5 Transport equation for turbulent kinetic energy, one-equation models 14
   2.6 Transport equation for rate of dissipation, two-equation models 18
   2.7 Other turbulence models and their equations ... 20
   2.8 Numerical methods for turbulent boundary layer flows 21
   2.9 Definition of parameters and variables 22

3. REVIEW OF EARLIER WORKS ON OSCILLATORY TURBULENT BOUNDARY LAYER FLOW .....
   3.1 Introduction 26
   3.2 Simple models 26
   3.3 Models with a time-invariant eddy viscosity ... 27
   3.4 Models with a time-varying eddy viscosity 28
   3.5 Works with turbulence modelling 29
   3.6 Measurements in a turbulent wave boundary layer 30

4. BLOBAK, A ZERO-EQUATION MODEL .....
   4.1 Introduction 33
   4.2 Construction of model 33
   4.3 Numerical solution 38
   4.4 Implementation 43
   4.5 Quantities derived from the zero-equation model
   4.6 Presentation of results 43

5. BL1PJ, A ONE-EQUATION MODEL .....
5.1 Introduction 62
5.2 Construction of model 62
5.2.1 The equations 62
5.2.2 Boundary conditions 63
5.2.3 Local equilibrium in TKE 65
5.2.4 The choice of numerical constants 66
5.3 Numerical solution 67
5.3.1 Strategy for the numerical solution ... 67
5.3.2 Solution of the flow equation 69
5.3.3 Solution of the k-equation 72
5.3.4 Implementation 75
5.3.5 Stability and accuracy of numerical scheme 75
5.4 Quantities derived from the one-equation model 75
5.5 Results from the one-equation model 78
5.5.1 Local equilibrium in TKE 78
5.5.2 Velocities and shear stresses 78
5.5.3 Boundary layer extension 80
5.5.4 Budget for turbulent kinetic energy ... 82
5.5.5 Eddy viscosities 92
5.5.6 Numerical aspects 96

6. BL2PJ, A TWO-EQUATION MODEL .....
6.1 Introduction 98
6.2 Construction of model 98
6.2.1 The equations 98
6.2.2 Boundary conditions 99
6.2.3 Constants in the z-equation 99
6.3 Numerical solution 101
6.3.1 General procedure 101
6.3.2 Solution of the z-equation 101
6.3.3 Implementation 103
6.4 Assessment of model capabilities 103

7. APPLICATION OF BLOBAK AND BL1PJ TO SEDIMENT TRANSPORT CALCULATIONS .....
7.1 General 104
7.2 Short theoretical introduction 104

7.3 Model implementation 106
7.4 Theoretical results and comparison with measurements 107

8. CONCLUSIONS 113

9. REFERENCES 116

10. LIST OF SYMBOLS 121

APPENDICES:

A. The computer programme BL0BAK.
B. The computer programme BL1PJ.
C. The computer programmes TKECIR and TKECON.
D. The computer programme JONCAR.
E. The computer programme SEDIPJ.
F. Linearization of k-difference equation.
G. Figures and diagrams.

0. PREFACE

The present report is submitted as one of the requirements for the Master of Science degree (civilingeniør) at the Technical University of Denmark.

The work has been carried out at the Institute of Hydrodynamic and Hydraulic Engineering (ISVA). The author is indebted to the supervisor Dr. techn. Jørgen Fredsøe for good advice and guidance

Lyngby, January 1985

1. INTRODUCTION

Oscillatory turbulent shear flow is encountered in several important physical phenomena. Flows like pulsating blood flow in arteries and the flow past helicopter blades are of this type. So is the bottom boundary layer beneath sea water waves. This report is concerned with the latter phenomenon.

In the largest part of the water body the wave induced motion can be treated as a potential flow. The orbital motion can be determined from first order or higher order wave theories.

Close to the bottom the no-slip condition will retard the flow and cause a boundary layer to develop. In nature this boundary layer will for most practical purposes be turbulent and the bed will be rough. Usually the boundary layer is confined to a thin layer close to the bed having a typical thickness of 0.2 m under surface gravity waves. The turbulence intensity in this rather thin layer can be very high and strongly unsteady.

The understanding of the hydrodynamics of this flow is not only of great academic/scientific interest, but it has also a wide range of applications in practical engineering.

An inherent part of a wind wave generation or wave refraction model is the description of wave attenuation caused by friction and energy dissipation in the bottom layer. The bottom boundary layer may be even more important in sediment transport computations. A popular phrase is that 'the sediment is suspended by the wave and carried away by the currents'. Detailed knowledge about the bed friction and eddy viscosity distribution is essential for the solution of this problem.

Over the years models of varying complexity and level have been proposed. Simple models consider the flow in each half period neglecting the memory in the turbulence. Assuming a logarithmic velocity profile computationally efficient models can be established using the integrated flow equation. One step further is to solve the flow equation effecting turbulent clo-

sure through a prescribed constant or harmonically varying eddy viscosity. Next turbulence modelling is introduced to improve the description of the turbulent processes.

These different approaches may have their individual justification in practical cases. Depending on the particular phenomenon that is under consideration the simplest and most efficient method which gives the required information should be chosen. Simpler models can be useful when they are included as parts of complex models for e.g. sediment transport. For example it would be a very computer intensive task to make a sediment transport model for the surf zone in which the flow description was obtained using a second-order closure model. More advanced models are on the other hand needed to confirm in which cases simpler models can be employed and to understand the basic structures in the flow.

The object of this study is to investigate the use of turbulence modelling in connection with the turbulent wave boundary layer. Two theoretical models are established and their results are checked against available measurements. A third model is constructed but not implemented so no results are thus being presented for this model. Finally, the effects of a refined flow model in connection with sediment transport computations are considered through a few examples.

All efforts in this paper are directed towards the pure wave boundary layer. The important issue of combined wave-current motion has not been treated.

Following this introduction the equations associated with turbulent boundary layers are compiled in chapter 2. A review of the existing methods in turbulence modelling is given and the parameters in the turbulent wave boundary layer are defined.

Chapter 3 is a review of earlier works on oscillatory turbulent boundary layer flow with the purpose of introducing the reader briefly to the development of this specific topic.

In chapter 4 we discuss the zero-equation model BLOBAK which

is the first of the models compiled in this study. Chapter 5 contains a similar discussion of the one-equation model BL1PJ, whereas chapter 6 is a description of the two-equation model BL2PJ which has not yet been implemented.

An example of application of the models developed in this report to sediment transport is presented in chapter 7.

Whenever possible figures from the chapters 4 and 5 have been enclosed in a larger format in Appendix G which also contains some additional diagrams that are not included in the report.

2. FLOW EQUATIONS AND TURBULENCE MODELS

2.1 Introduction

In this chapter we look at the basis for calculation of turbulent flows using turbulence models. First the flow equations are derived, then the existing models are described in an ascending order with respect to the number of equations involved. This review is not intended to be exhaustive, but should provide the reader with a general introduction to the topic. In addition it constitutes the basis for this work on turbulence models. Special attention has been paid to two-dimensional turbulent shear boundary layers over a plane and rough bed.

The last section is devoted to the definition of the standard set of parameters and variables that we will use in this report.

2.2 The flow equations

The general local flow equation, which should be fulfilled in all points in a flow field is

$$\rho \frac{dv_i}{dt} = \rho g_i + \frac{\partial \sigma_{ij}}{\partial x_j} \qquad (2.1)$$

where σ_{ij} is the stress tensor. σ_{ij} are the normal stresses, while the other elements are the shear stresses in the fluid. The stress tensor is reflecting the dynamics in the flow and is related to the deformation tensor e_{ij} through the expression

$$\sigma_{ij} = -p\delta_{ij} + 2\mu e_{ij} \qquad (2.2)$$

In eq. (2.2) p is pressure, δ_{ij} is the Kronecker delta and μ is the dynamic viscosity. The relation expresses the physical requirements in the relation between stresses and deformations and is often called a constitutive equation. The deformation tensor is a kinematic quantity and can be found from the velocity field as

$$e_{i,j} = (v_{i,j} + v_{j,i})/2 \qquad (2.3)$$

When the equations above are combined the so-called Navier-Stokes equations are obtained

$$\frac{dv_i}{dt} = -\frac{1}{\rho}\frac{\partial p}{\partial x_i} + g_i + \nu \frac{\partial^2 v_i}{\partial x_j \partial x_j} \qquad (2.4)$$

ν is the kinematic viscosity.

The most important assumptions made in the derivation of (2.4) are

(i) the fluid is homogeneous and isotropic

(ii) the fluid is incompressible

(iii) elements of the stress tensor and the deformation tensor are related through linear relationships. A fluid with this characteristic is often referred to as a 'Newtonian fluid'.

The equations (2.4) are valid for a laminar flow. If the flow is turbulent, the velocities are separated into a mean part and a fluctuating part

$$v_i = U_i + u_i \qquad (2.5)$$

By definition, the time average of u_i is zero

$$\overline{u_i} = 0 \qquad (2.6)$$

Substitution of (2.5) into the Navier-Stokes equations and subsequently time averaging yields

$$\frac{\partial U_i}{\partial t} + U_j \frac{\partial U_i}{\partial x_j} = -\frac{1}{\rho}\frac{\partial p}{\partial x_i} + g_i + \frac{\partial}{\partial x_j}\left(-\overline{u_i u_j}\right) + \nu \frac{\partial^2 U_i}{\partial x_j \partial x_j} \qquad (2.7)$$

The term including the fluctuating velocity components is called the 'Reynolds stresses'. These stresses describe the exchange of momentum between different parts of the fluid that are due to

the turbulent fluctuations.

In addition to the three flow equations provided by (2.7) there is also the continuity equation, which for an incompressible fluid has the form

$$\frac{\partial U_i}{\partial x_i} = 0 \qquad (2.8)$$

2.3 Eddy viscosity models of turbulence

The problem with the Navier-Stokes equations for the turbulent flow is the modelling of the Reynolds stresses. An exact solution to (2.7) would require a time and space resolution which is inachievable even with todays main frame computers because of the CPU-time and core memory requirements. To overcome this, the Reynolds stresses are modelled to obtain a limited number of equations which can be solved. This procedure involves the introduction of empirical constants that have to be verified experimentally. It is known as the 'closure problem'.

Most commonly used has been the eddy viscosity concept which was introduced by Boussinesq in 1877. The turbulent stresses are assumed to be proportional to the gradients in the mean velocity field. The following relation is introduced

$$\overline{u_i u_j} = \frac{2}{3} k \delta_{ij} - \varepsilon \left(\frac{\partial U_i}{\partial x_j} + \frac{\partial U_j}{\partial x_i} \right) \qquad (2.9)$$

ε is the eddy viscosity and is a function of both t and x_i. k is the turbulent kinetic energy defined by

$$k = \frac{1}{2} \left(\overline{u_1^2} + \overline{u_2^2} + \overline{u_3^2} \right) \qquad (2.10)$$

It is seen that the second term in (2.9) includes quantities from the mean flow. The first term is included for consistency reasons. For the normal stresses (i=j) eq. (2.9) yields

$$\overline{u_1^2} = -2\varepsilon \frac{\partial U_1}{\partial x_1} \quad ; \quad \overline{u_2^2} = -2\varepsilon \frac{\partial U_2}{\partial x_2} \quad ; \quad \overline{u_3^2} = -2\varepsilon \frac{\partial U_3}{\partial x_3} \qquad (2.11)$$

It follows from the continuity equation that the sum of the terms in (2.11) is zero. The inclusion of the first term in (2.9) makes (2.9) and (2.10) consistent.

The additional term in (2.9) can be interpreted as a pressure and can be included in the pressure gradient. When (2.9) is substituted into (2.7), the following form of the Navier-Stokes equations is obtained

$$\frac{\partial U_i}{\partial t} + U_j \frac{\partial U_i}{\partial x_j} = -\frac{1}{\rho}\frac{\partial p^*}{\partial x_i} + g_i + \frac{\partial}{\partial x_j}\left[(\varepsilon+\nu)\frac{\partial U_i}{\partial x_j}\right] \qquad (2.12)$$

where

$$p^* = p + 2k/3 \qquad (2.13)$$

On the upper edge of the boundary layer towards a potential flow k vanishes and $p^* = p$. It means that the pressure gradient in (2.12) can be found from the ambient flow.

In a two-dimensional shear boundary layer (2.12) is reduced to

$$\frac{\partial U}{\partial t} + U\frac{\partial U}{\partial x} + V\frac{\partial U}{\partial y} = -\frac{1}{\rho}\frac{\partial p^*}{\partial x} + \frac{\partial}{\partial y}\left[(\varepsilon+\nu)\frac{\partial U}{\partial y}\right] \qquad (2.14)$$

The term

$$\frac{\partial}{\partial x}\left[(\varepsilon+\nu)\frac{\partial U}{\partial x}\right]$$

is neglected since the velocity gradient in the y-direction is assumed to be much larger than in the x-direction. On the other hand, since the velocity in the x-direction is likely to be much larger than in the y-direction the equation for V is redundant. Hence the continuity equation can be left out of the analysis.

Considering only flow above a hydraulically rough bed, it can be assumed that

$$\varepsilon >> \nu$$

that is to say that the viscous stresses are negligible compared

with the Reynolds stresses. Eq. (2.14) is then reduced to

$$\frac{\partial U}{\partial t} + U\frac{\partial U}{\partial x} + V\frac{\partial U}{\partial y} = -\frac{1}{\rho}\frac{\partial p^*}{\partial x} + \frac{\partial}{\partial y}\left(\varepsilon\frac{\partial U}{\partial y}\right) \qquad (2.15)$$

The pressure gradient is found from the outer velocity

$$\frac{1}{\rho}\frac{\partial p}{\partial x} = -\frac{\partial U_o}{\partial t} - U_o\frac{\partial U_o}{\partial x} \qquad (2.16)$$

If (2.16) is substituted into (2.15) the following equation emerges

$$\frac{\partial U}{\partial t} + U\frac{\partial U}{\partial x} + V\frac{\partial U}{\partial y} = \frac{\partial U_o}{\partial t} + U_o\frac{\partial U_o}{\partial x} + \frac{\partial}{\partial y}\left(\varepsilon\frac{\partial U}{\partial y}\right) \qquad (2.17)$$

Taking the outer flow to be uniform the convective terms in (2.17) can be neglected. This yields the equation for the two-dimensional turbulent shear boundary layer flow over a hydraulically rough bed

$$\frac{\partial U}{\partial t} = \frac{\partial U_o}{\partial t} + \frac{\partial}{\partial y}\left(\varepsilon\frac{\partial U}{\partial y}\right) \qquad (2.18)$$

Now, the problem of determining ε remains. In the following sections various methods for this are discussed.

2.4 Mixing-length theory, zero-equation models

A turbulence model that does not include transport equations for turbulence quantities is called a zero-equation model. Without exception these models employ the eddy viscosity concept. The eddy viscosity distribution can be found from experiments, by sheer guess, or it can be related to the mean flow through algebraic formulae.

When dealing with the oscillatory boundary layer the constant-eddy-viscosity model has been extensively used during the last decades, as it will be seen in the review presented in Chapter 3. Such a model can hardly be called a turbulence model. Since the flow is highly unsteady, it is felt that the simplest time-variation expected must be a periodic behaviour of the eddy

viscosity.

In 1925 Prandtl suggested that the eddy viscosity is proportional to a mean fluctuating velocity V and a 'mixing-length'

$$\varepsilon \sim V l_m \qquad (2.1$$

This expression was conceived by analogy with the kinetic gas theory in which the dynamic viscosity is related to the mean velocity of the molecules $V_{m,1}$ and the 'free paths' of the molecules L

$$\mu \sim L V_{m,1}$$

Prandtl took the velocity scale V as

$$V = l_m \left|\frac{\partial U}{\partial y}\right| \qquad (2.2$$

The mixing-length is defined as the distance that a fluid lump has to be displaced by the turbulent motion in the transverse flow direction from y_1 to y_2 so that its velocity differs from the surrounding mean velocity by V.

Assuming that the constant of proportionality is unity, eqs. (2.19) and (2.20) can be merged to give

$$\varepsilon = l_m^2 \left|\frac{\partial U}{\partial y}\right| \qquad (2.2$$

This is the Prandtl mixing-length hypothesis. It includes only one unknown parameter: l_m. In wall boundary layers the mixing-length

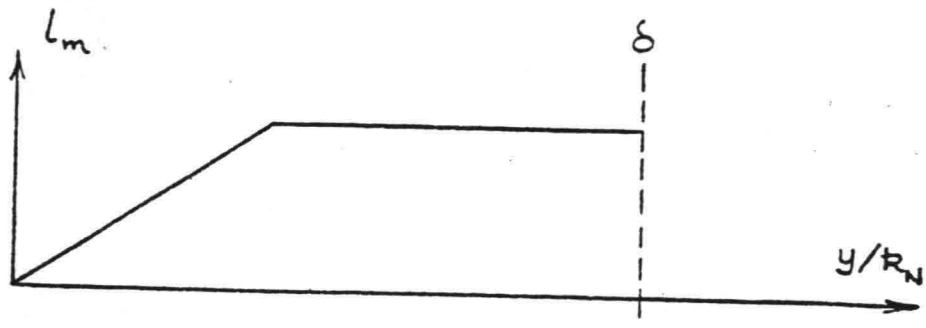

Fig. 2.1 Mixing-length distribution in a wall boundary layer

is often assumed to be proportional to the distance from the wall since this distance determines the maximum eddy size. Far away from the wall l_m can be regarded as being constant. The variation is depicted in Fig. 2.1.

The boundary layer thickness δ is defined e.g. as the distance from the wall to the point where the velocity has reached 99 % of the ambient velocity.

It must be emphasized that the distribution of l_m is purely empirically specified. When a viscous sublayer is present over a smooth wall the mixing-length distribution must be modified. Traditionally the van-Driest damping function is used,

$$l_m = \varkappa y \left[1 - \exp\left(-\frac{y U_f}{A\nu}\right)\right] \qquad (2.22)$$

A is a function of the pressure gradient.

The mixing-length hypothesis has worked well in a number of applications. However, when processes like convective or diffusive transport of turbulence are important it is not appropriate because it assumes that the turbulence intensity is a local phenomena determined only by the local flow parameters. In fact the zero-equation model assumes local equilibrium in turbulent kinetic energy as will be shown in chapter 5. A further weakness is that the eddy viscosity vanishes when the mean velocity gradient is zero. This implies that in the oscillatory boundary layer the eddy viscosity must be zero twice every period.

To remove the weaknesses of the turbulence model we shall introduce the transport equation for turbulent kinetic energy in the next section.

2.5 Transport equation for turbulent kinetic energy, one-equation models

The first important improvement of the mixing-length theory is to determine the velocity scale V in (2.19) from a transport equation rather than from the mean flow field.

It is physically most reasonable to utilize $\sqrt{k}$ as the velocity scale. k is the turbulent kinetic energy of the turbulent motion (per unit mass) defined in eq. (2.10). From this expression it is seen that k is a direct measure of the intensity of the turbulent fluctuations in all three directions. Since this energy is contained in the large-scale eddies, $\sqrt{k}$ becomes a velocity scale for the large-scale motion.

Now, using this velocity scale together with a prescribed length scale l the eddy viscosity can be expressed as

$$\varepsilon = \sqrt{k}\, l \tag{2.23}$$

This expression is known as the Kolmogorov-Prandtl relation because Kolmogorov and Prandtl introduced it independently in 1942 and 1945 respectively. The distribution of k has to be found from the solution to a transport equation for k which we shall derive in the following.

Insert eq. (2.5) into the Navier-Stokes equations (2.4) and multiply by the velocity fluctuation u_i. This leads to

$$u_i \frac{d(U_i+u_i)}{dt} = -u_i \frac{1}{\rho}\frac{\partial p}{\partial x_i} + u_i g_i + u_i \nu \frac{\partial^2 (U_i+u_i)}{\partial x_j \partial x_j} \tag{2.24}$$

The first term is time-averaged

$$\overline{u_i \frac{d(U_i+u_i)}{dt}} = \overline{u_i \frac{\partial (U_i+u_i)}{\partial t}} + \overline{u_i (U_j+u_j) \frac{\partial (U_i+u_i)}{\partial x_j}}$$

$$= \overline{u_i}\frac{\partial U_i}{\partial t} + \overline{u_i \frac{\partial u_i}{\partial t}} + \overline{u_i} U_j \frac{\partial U_i}{\partial x_j} + \overline{u_i u_j}\frac{\partial U_i}{\partial x_j}$$

$$+ U_j \overline{u_i \frac{\partial u_i}{\partial x_j}} + \overline{u_i u_j \frac{\partial u_i}{\partial x_j}} \tag{2.25}$$

Using the continuity equation (2.8) which also holds for the velocity fluctuation u_i we derive

$$\overline{u_i u_j \frac{\partial u_i}{\partial x_j}} = \overline{\frac{\partial}{\partial x_j}\left(\frac{1}{2} u_i u_i u_j\right)} \tag{2.26}$$

Taking advantage of eqs. (2.25) and (2.26) time-averaging of

(2.24) is seen to give

$$0 + \frac{\partial k}{\partial t} + 0 + \overline{u_i u_j}\,\frac{\partial U_i}{\partial x_j} + U_j\,\frac{\partial k}{\partial x_j} + \frac{\partial}{\partial x_j}\left(\tfrac{1}{2}\,\overline{u_i u_i u_j}\right)$$

$$= -\frac{1}{\rho}\,\overline{u_i\,\frac{\partial p}{\partial x_i}} + \nu\,\overline{u_i\,\frac{\partial^2 u_i}{\partial x_j \partial x_j}}$$

which can be rearranged to yield the transport equation for k

$$\frac{\partial k}{\partial t} + U_j\frac{\partial k}{\partial x_j} = -\frac{\partial}{\partial x_j}\left[\overline{u_j\left(\frac{p}{\rho} + \tfrac{1}{2}u_i u_i\right)}\right] - \overline{u_i u_j}\frac{\partial U_i}{\partial x_j} + \nu\,\overline{u_i\,\frac{\partial^2 u_i}{\partial x_j \partial x_j}} \qquad (2.27)$$

① ② ③ ④ ⑤

The terms are identified as follows

① : local time derivative of k
② : convective transport of k
③ : diffusive transport of k due to
  (i) pressure work
  (ii) velocity fluctuations
④ : production of k due to interaction between the Reynolds stresses and the velocity gradients of the mean flow. A corresponding dissipation term appears in the energy equatio for the mean flow, see e.g. Tennekes and Lumley [44]
⑤ : dissipation term which accounts for the energy that is dissipated as heat through the cascade process

Unfortunately the exact k-equation (2.27) is not directly applicable since it contains new unknown correlations in the diffusion and dissipation terms. Again, this is the closure problem. To overcome the difficulty model assumptions will be introduced.

The diffusive transport is assumed proportional to the gradient of k and the eddy viscosity

$$-\overline{u_j\left(\frac{p}{\rho} + \tfrac{1}{2}u_i u_i\right)} = \frac{\varepsilon}{\sigma_k}\,\frac{\partial k}{\partial x_j} \qquad (2.28)$$

where σ_k is an empirical diffusive constant. At high Reynolds numbers the dissipation is recognized to be independent of viscosity and governed by the large-scale motion which is characterized by k and l. Dimensional analysis yields the relation

$$-\nu \overline{u_i \frac{\partial^2 u_i}{\partial x_j \partial x_j}} = c_1 \frac{k^{3/2}}{l} \qquad (2.29)$$

c_1 is an empirical constant to be determined from experiments.

With these modelled terms and using the eddy viscosity expression for the Reynolds stresses the k-equation transforms to

$$\frac{\partial k}{\partial t} + U_j \frac{\partial k}{\partial x_j} = \frac{\partial}{\partial x_j}\left[\frac{\varepsilon}{\sigma_k} \frac{\partial k}{\partial x_j}\right] + \varepsilon\left(\frac{\partial U_i}{\partial x_j} + \frac{\partial U_j}{\partial x_i}\right)\frac{\partial U_i}{\partial x_j} - c_1 \frac{k^{3/2}}{l} \qquad (2.30)$$

It should be recognized that this is in fact a transport equation for the sum of the three normal stresses σ_{ii}.

In a two-dimensional boundary layer this expression reduces to

$$\frac{\partial k}{\partial t} + U\frac{\partial k}{\partial x} + V\frac{\partial k}{\partial y} = \frac{\partial}{\partial y}\left[\frac{\varepsilon}{\sigma_k} \frac{\partial k}{\partial y}\right] + \varepsilon\left(\frac{\partial U}{\partial y}\right)^2 - c_1 \frac{k^{3/2}}{l} \qquad (2.31)$$

The term

$$\frac{\partial}{\partial x}\left[\frac{\varepsilon}{\sigma_k} \frac{\partial k}{\partial x}\right]$$

has been neglected since the variations in k are assumed to be much larger in the y-direction than in the x-direction. The production term on the other hand

$$\varepsilon \frac{\partial V}{\partial x} \frac{\partial U}{\partial y}$$

has been left out as it is thought to be a higher order term.

When the outer flow is uniform we can neglect the convective terms in (2.31) and the simplest form of the k-equation emerges

$$\frac{\partial k}{\partial t} = \frac{\partial}{\partial y}\left[\frac{\varepsilon}{\sigma_k} \frac{\partial k}{\partial y}\right] + \varepsilon\left(\frac{\partial U}{\partial y}\right)^2 - c_1 \frac{k^{3/2}}{l} \qquad (2.32)$$

Turbulence models that consist of the flow equation, the transport equation for k, and a specified length scale are called one-equation models of turbulence and are normally based on the eddy viscosity concept.

The inclusion of the memory effect in the turbulence represents one step forward in comparison with the zero-equation models. However, when the effects of convection and diffusion of

the length scale are important a transport equation for either the length scale or a related quantity must be added to the turbulence model. This may be relevant in recirculating flows or rapidly changing flows. Not very many workers in the field do in fact have fruitful experience with the use of one-equation models, e.g. Hanjalic and Launder [12], Rodi [36], Reynolds [35]. But Reynolds encourages further research into the topic. The next possibility is a two-equation model which will be dealt with in the proceeding section.

2.6 Transport equation for rate of dissipation, two-equation models

The length scale specification inherent in the one-equation model can be replaced by a transport equation for a turbulent quantity

$$z = k^m l^n \tag{2.33}$$

where m and n can be any numbers. Several of these combinations have been proposed and tried so far. Little success has been given using the length scale itself. Instead the isotropic energy dissipation rate

$$z = c_1 k^{3/2} l^{-1} \tag{2.34}$$

has been used extensively. The reason for this peculiarity remains unrevealed.

Appropriate differentiation, multiplication and averaging of the Navier-Stokes equations will yield the transport equation for the dissipation rate. We shall not carry these calculations through here, the reader is referred to for instance Davidov [7] or Harlow and Nakayama [14]. Following Hanjalic and Launder [13] this equation reads for high Reynolds numbers

$$\frac{dz}{dt} = -2\nu \frac{\partial U_i}{\partial x_j}\left(\overline{\frac{\partial u_i}{\partial x_l}\frac{\partial u_j}{\partial x_l}} + \overline{\frac{\partial u_l}{\partial x_i}\frac{\partial u_l}{\partial x_j}}\right) - 2\nu \overline{\frac{\partial u}{\partial x_j}\frac{\partial u_i}{\partial x_l}\frac{\partial u_j}{\partial x_l}}$$

① ② ③

$$-2\overline{\left[\nu\frac{\partial^2 u_i}{\partial x_j \partial x_l}\right]^2} - \frac{\partial}{\partial x_j}\overline{u_j z'} - \frac{\nu}{\rho}\frac{\partial}{\partial x_i}\overline{\left[\frac{\partial p}{\partial x_l}\frac{\partial u_i}{\partial x_l}\right]} \qquad (2.35)$$

④ ⑤ ⑥

The role of the individual terms are

① : total derivative of z
② : generation term
③ & ④ : these terms should be taken together. ③ accounts for the 'generation rate of vorticity fluctuations through the self-streching action of turbulence.' ④ represents the decay of the dissipation rate ultimately through the action of viscosity. Together the terms control the dynamics of the energy cascade process
⑤ : diffusion of z due to velocity fluctuations
⑥ : diffusion of z due to pressure fluctuations

When the terms are modelled in a manner similar to the k-equation we obtain the following equation

$$\frac{\partial z}{\partial t} + U_i\frac{\partial z}{\partial x_i} = \frac{\partial}{\partial x_i}\left[\frac{\varepsilon}{\sigma_z}\frac{\partial z}{\partial x_i}\right] + c_4\frac{z}{k}\varepsilon\left(\frac{\partial U_i}{\partial x_j} + \frac{\partial U_j}{\partial x_i}\right)\frac{\partial U_i}{\partial x_j} - c_5\frac{z\sqrt{k}}{l}c_1 \qquad (2.36)$$

The constants c_4, c_5 and σ_z must be found from experiments. In the two-dimensional case a reduced form can be derived

$$\frac{\partial z}{\partial t} + U\frac{\partial z}{\partial x} + V\frac{\partial z}{\partial y} = \frac{\partial}{\partial y}\left(\frac{\varepsilon}{\sigma_z}\frac{\partial z}{\partial y}\right) + c_4 z\frac{\varepsilon}{k}\left(\frac{\partial U}{\partial y}\right)^2 - c_5\frac{z\sqrt{k}}{l}c_1 \qquad (2.37)$$

which is further simplified to

$$\frac{\partial z}{\partial t} = \frac{\partial}{\partial y}\left(\frac{\varepsilon}{\sigma_z}\frac{\partial z}{\partial y}\right) + c_4 z\frac{\varepsilon}{k}\left(\frac{\partial U}{\partial y}\right)^2 - c_5 c_1 z\frac{\sqrt{k}}{l} \qquad (2.38)$$

when the convective terms are neglected.

A two-equation turbulence model may consist of the flow equation, the transport equation for the turbulent kinetic energy, the transport equation for the dissipation rate, and the Kolmogorov-Prandtl expression to link the quantities together. Such a model is often referred to as a k-ε model in the literature.

Within the framework of the eddy viscosity concept it is the

most advanced turbulence model that can be established. In many flows, however, when the individual Reynolds stresses play very important roles transport equations can be derived that eliminate the need for the eddy viscosity.

2.7 Other turbulence models and their equations

More general than the transport equation for turbulent kinetic energy is the transport equations for the six Reynolds Stresses. Exact equations can be derived from the Navier-Stokes equations, see e.g. Tennekes and Lumley [44] or Hinze [16]. Here we quote Rodi [36]

$$\frac{\partial \overline{u_i u_j}}{\partial t} + U_l \frac{\partial \overline{u_i u_j}}{\partial x_l} = -\frac{\partial}{\partial x_l}\left(\overline{u_l u_i u_j}\right) - \frac{1}{\rho}\left(\frac{\partial \overline{u_j p}}{\partial x_i} + \frac{\partial \overline{u_i p}}{\partial x_j}\right)$$

rate of change — convective transport — diffusive transport

$$- \overline{u_i u_l}\frac{\partial U_j}{\partial x_l} - \overline{u_l u_j}\frac{\partial U_i}{\partial x_l} + \overline{\frac{p}{\rho}\left(\frac{\partial u_i}{\partial x_j} + \frac{\partial u_j}{\partial x_i}\right)}$$

stress production — pressure strain

$$- 2\nu \overline{\frac{\partial u_i}{\partial x_l}\frac{\partial u_j}{\partial x_l}}$$

viscous dissipation (2.39)

The contraction of this equation is seen to yield (2.27). It should be noted that the pressure strain term is not present in (2.27) because of the continuity.

Modelling of the terms in (2.39) that contain new unknown correlations has to be introduced. Then a turbulence model in which one or more of the six equations available in (2.39) replace the k-equation can be made. An increase in computational work is inevitable and flows where the length scale determination is crucial are not better described by this method. However, in cases where transport of the individual stresses is important such a stress-equation model can significantly improve the results.

Recently a new line of thinking has been introduced in the field of turbulence modelling. The approach is called Large-Eddy Simulation (LES). The notion is that only the large-scale motions that are directly affected by the boundary conditions are treated by three-dimensional time-dependent numerical computations. The spatial resolution in this model gives a minimum scale that can be described. The small-scale motion is assumed to have a structure so that its statistics and their effects upon the large scales can be specified by a few parameters. It is referred to as the subgrid-scale modelling.

It is not straightforward to use the large-eddy simulation method. Of course the crucial point is the interaction between the large- and the small-scale motions.

As this method is mentioned for completeness rather than for details the reader is referred to reviews by e.g. Rogallo and Moin [37] and Ferziger [8].

2.8 Numerical methods for boundary layer flows

Given the fact that, to quote Bradshaw [4], 'for every one person who knows enough about turbulence to produce a plausible set of differential equations to describe it, there are tens and hundreds who know (or can learn) enough about numerical analysis to solve those equations', we shall not give a discussion of the methods that are available for the field of fluid dynamics. Suffice it to give a few of the key references. Keller [25] has provided a review paper which describes the current stage of finite difference methods (FDM) in boundary layer problems. Also Blottner [3] deals with FDM methods for this purpose. Bradshaw, Cebeci and Whitelaw [5] have dedicated a book to the calculation of boundary layer flows. Here a wide range of flows are discussed.

When it comes to the finite element method (FEM) in connection with turbulent flows the literature is less generous. This method was initially developed in conjecture with solid mechanics. Recently Shen [38] has given an introduction to FEM in

fluid mechanics. But one will have to revert to research papers and conference proceedings for detailed information on the topic.

(22)

2.9 Definition of parameters and variables

The definition of a standard set of variables and parameters seems to be very useful. The object of study in this work is the oscillatory turbulent boundary layer over a hydraulically rough bed. When the 'amplitude Reynolds number' defined by

$$RE = \frac{U_{1m}\, a}{\nu} \qquad (2.40)$$

is sufficiently large the rough boundary layer can be regarded fully turbulent. Jonsson [22] suggests the following 'practical limits'

$RE=10^4$ for $1 \leq a/k_N \leq 10$ (2.41a)

$RE=(a/k_N)10^3$ for $10 \leq a/k_N \leq 10^3$ (2.41b)

Then the flow may be characterized by three parameters

k_N Nikuradse roughness of bed roughness elements (m) (2.41a)

ω cyclic frequency of ambient velocity (rad/s) (2.41b)

$U_{1\bullet}$ velocity amplitude of ambient flow (m/s) (2.41c)

The amplitude of the particle motion in the ambient flow is

$$a=U_{1\bullet}/\omega \qquad (2.42)$$

The parameters above may be joined in one single dimensionless number characterizing the boundary layer

$$a/k_N = U_{1\bullet}/(\omega k_N) \qquad (2.43)$$

which is the amplitude/roughness ratio.

In this work we shall make use of the following basic ways of non-dimensioning quantities of interest utilizing the parameters in eq. (2.42)

time	$t^* = \omega t$	(2.44a)
space	$y^* = y/k_N$	(2.44b)
velocity	$U^* = U/U_{1,\infty}$	(2.44c)

Further, we will use

shear stress	$\tau^* = \tau/(\rho U_{1,\infty}^2)$	(2.45a)
friction velocity	$U_\tau^* = U_\tau/U_{1,\infty}$	(2.45b)
eddy viscosity	$\varepsilon^* = \varepsilon/(U_{1,\infty} k_N)$	(2.45c)
turbulent kinetic energy	$k^* = k/U_{1,\infty}^2$	(2.45d)
length scale	$l^* = l/k_N$	(2.45e)
displacement thickness	$\delta^* = \delta/k_N$	(2.45f)
boundary layer thickness	$\delta_1^* = \delta_1/k_N$	(2.45g)
momentum thickness	$\theta^* = \theta/k_N$	(2.45h)
production, dissipation and diffusion of t.k.e.	$\phi^* = \phi/(U_{1,\infty}^3/k_N)$	(2.45i)

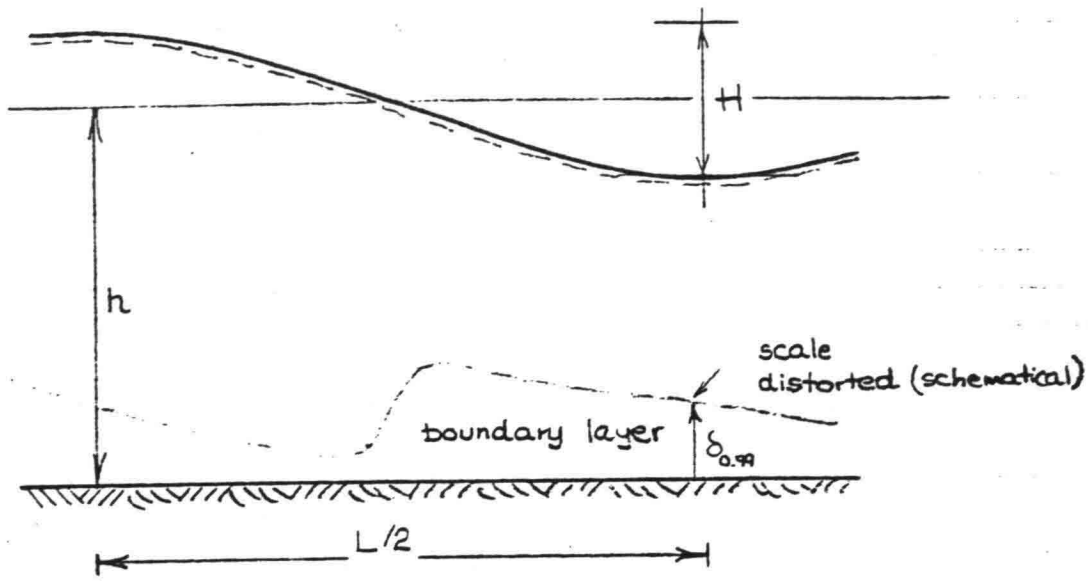

Fig. 2.2 Definition sketch

Usually the starting point in a practical case will be that a wave is described by its parameters H, T and h. Given this the bottom particle amplitude can be worked out. From Stokes' theory is obtained

$$a = \frac{H}{2} \frac{1}{\sinh kh} \tag{2.46}$$

Similarly the velocity amplitude is

$$U_{1m} = \frac{\pi H}{T} \frac{1}{\sinh kh} \tag{2.47}$$

where H is the wave height, k is the wave number and h is the water depth.

If the convective terms are dropped in the boundary layer equations first order wave theory can be adopted. This implies that only the first term in (2.46) and (2.47) should be retained. The particle velocity at the bottom is then described by

$$U_b = U_1 \cdot \cos(kx-\omega t) \tag{2.48}$$

For simplicity, when the convective terms are neglected in the governing equations, x will be taken as $x=\pi/(2k)$. Eq. (2.48) is then reduced to

$$U_b = U_1 \cdot \sin(\omega t) \tag{2.49}$$

The bottom roughness must also be available. It is traditionally taken as

$$k_N = 2.5 d_{50} \qquad (2.50)$$

where d_{50} is the median grain size of the bottom particles.

To end this section we shall discuss the determination of a boundary layer thickness. In simple models where the momentum equation is used with a prescribed velocity profile the boundary layer thickness enters the problem in a natural way as the upper limit of integration. The situation is depicted in Fig. 2.3 with a solid curve. If we have, instead, a velocity profile like the dashed curve in Fig. 2.3 it is less obvious how a boundary layer thickness is defined. One way is illustrated in the figure. Here δ_1 is defined as the minimum distance from the bed to a level where the velocity is equal to the ambient velocity. Such a definition implies that δ_1 can be infinite or very large when all velocities are less than the free stream velocity. And it is not a measure for the region where shear stresses and turbulence are important, as it would be expected from the boundary layer thickness. Instead $\delta_{0.99}$ can be defined as the minimum distance to the level where the velocity is 99 % of the free stream velocity. It may be argued that this is not a precise quantity if the curvature of the velocity profile is small. As it will be seen in chapters 4, 5 and 6 we shall use the displacement thickness and momentum thickness in this report as they are integral quantities that can be determined independently of the difficulties mentioned above.

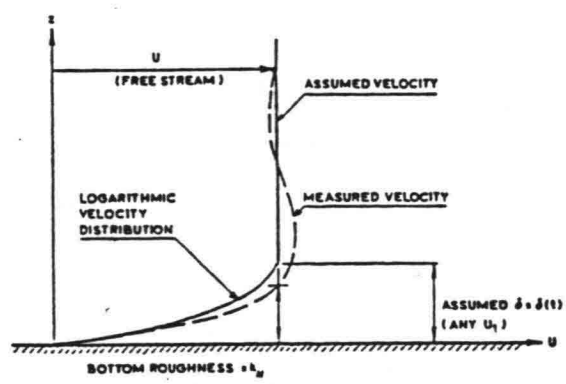

Fig. 2.3 Definition of a boundary layer thickness

3. REVIEW OF EARLIER WORKS

3.1 Introduction

A natural and necessary part of the present project has been a study of the available earlier works within the field of turbulent oscillatory boundary layers including both theoretical and experimental material. The literature is, as one would expect, very extensive due to the great importance of this area in practical engineering. Despite this fact, the review is, like chapter 2 not intended to be thorough but to provide a survey of the different approaches that have been pursued over the last two decades.

The theoretical developments are naturally divided into four sections. Then follows a review of experimental works and existing data from the laboratory.

Review papers have been published by Jonsson [21] and Knight [27]. Unfortunately these comprehensive works do not give the latest developments within the field when it comes to inclusion of turbulence modelling.

Recently Sleath [41] has written a book devoted to the different processes at the sea bed. Sections on the turbulent boundary layer are also included and constitute the newest review.

3.2 Simple models

Perhaps the most simple models that can be found are those in which the form of the velocity profile is prescribed. Fredsøe [9] used a logarithmic velocity profile and by substituting this into the depth-integrated momentum equation he obtained an ordinary differential equation in the parameter $z=U_* \kappa / U_f$ which was easily solved numerically. The eddy viscosity is not included directly but can be taken as a function of the instantaneous friction velocity and boundary layer thickness, both of which are determined in the model.

A basic assumption is that the time scale for production and decay of turbulent kinetic energy is small compared with the wave period. It follows that the flow can be studied in each half period starting with a water body at total rest thus disregarding the eddies from previous motion.

The advantage of Fredsøe's model is its simplicity. Since its development it has been employed to describe the flow field in connection with problems like sediment transport in waves, second-order mass transport in waves, and separation behind large cylinders at ISVA.

3.3 Models with a time-invariant eddy viscosity

Lately, many workers have solved the flow equation using a time-invariant eddy viscosity distribution incorporating different layers in their models. Grant and Madsen [11], Christoffersen [6] and Myrhaug [32] have solved this problem with the only difference being the prescription of ε within the boundary layer.

We shall briefly describe the model by Myrhaug [32] here. It is, of course, an eddy viscosity model of turbulence which implies that the linearized flow equation (2.18) is employed. It is reformulated by introduction of the defect velocity

$$U_d = U - U_0 \tag{3.1}$$

to

$$\frac{d}{dy}\left[\varepsilon \frac{du_d}{dy}\right] - i\omega u_d = 0 \tag{3.2}$$

with the assumption that the defect velocity is a harmonic function

$$U_d(y,t) = u_d(y)e^{i\omega t} \tag{3.3}$$

The ordinary differential equation for the defect velocity amplitude (3.2) is subject to the usual boundary conditions

$$u_d\,(y=k_N/30)=0 \quad \text{and} \quad u_d \to 0 \text{ for } y\to\infty \tag{3.4}$$

Now, a two-layer variation for ε is given

$$\frac{\varepsilon_i}{\varkappa U_{f,max}\delta} = \frac{1}{2} - \frac{1}{2}\left(\frac{y}{\delta}-1\right)^2 \quad \text{for } z \le \delta$$

$$\frac{\varepsilon_o}{\varkappa U_{f,max}\delta} = \frac{1}{2} \quad \text{for } z > \delta \tag{3.5}$$

where the distance δ is not a boundary layer thickness but apparently a 'tuning parameter' that can be used to fit theoretical findings to experimental data.

The inspiration for the quadratic variation of ε in the inner layer and a constant value in the outer layer stems from the experiments by Jonsson and Carlsen, cf. Fig. 4.17. A rather laborious analytical solution to (3.2) can now be obtained. Fairly good agreement with the experiments is found for velocities and shear stresses but the model fails to describe the eddy viscosity in detail.

The other models that were mentioned use different profiles for ε in eq. (3.5), many of them employing a linear variation in the inner layer. Together these models can be used to determine the bed shear stress and energy dissipation associated with travelling waves.

3.4 Models with a time-varying eddy viscosity

Recently Throwbridge and Madsen [45] published a paper describing a model containing a time-variant eddy viscosity distribution instead of the constant ε in the models in section 3.3. Now ε is assumed to be a sum of a constant part and a harmonic component. This model is like Myrhaug's also a two-layer model and analytical solutions are developed through tedious manipulations. The advantage over the ε-invariant models seems to be that a third harmonic in all quantities is also included. Comparison with the measurements by Jonsson and Carlsen indicates that this third harmonic is indeed found reasonably well in connection with velocities. Unfortunately no results for τ and ε are presented!

3.5 Works with turbulence modelling

Turbulence modelling of the turbulent oscillatory flow was initiated by Bakker [1]. Assuming a local equilibrium in turbulent kinetic energy he used a mixing-length hypothesis relating the eddy viscosity to the local mean velocity gradient

$$\varepsilon = l_m^2 \left|\frac{\partial U}{\partial y}\right| \qquad (3.6)$$

l_m is the mixing-length, cf. section 2.4. Utilizing (3.6) in the linearized flow equation Bakker formulated a partial differential equation in an 'internal shear velocity'. Boundary conditions for this problem were implicit since the bed shear stress was not known a priory. In later publications, Bakker and van Doorn [2] and van Kesteren and Bakker [47], this formulation has been retained. In a report by van Doorn [46] the partial differential equation was formulated in the local mean velocity thus simplifying the boundary conditions.

The method has been revised and implemented using a different numerical approach in this report. The reader is therefore refered to chapter 4 for a detailed discussion of this zero-equation model of turbulence.

Johns [19] effectively made the same model as Bakker although a different formulation and numerical method was employed. Two years later Johns [20] had made a one-equation model of turbulence for the oscillatory flow. This model effects closure at the level of the turbulent kinetic energy equation and is identical to the one developed in chapter 5 of this report apart from the fact that Johns retained the advective terms in the equations. A hybrid numerical method consisting of both finite difference and pseudo-spectral tecniques was used. Johns puts emphasis on the mass transport in the bottom boundary layer. For a discussion of the calculated variations for the turbulent energy and the eddy viscosity see chapter 5.

To the knowledge author there exists one example only of higher closure in connection with turbulent oscillatory boundary layers. Sheng [39] has used a model which included the k-

equation, a length-scale transport equation and a transport equation for the Reynolds stress $\overline{-uv}$.

A detailed evaluation of his results is not really possibly because only velocities and shear stresses for $a/k_N = 124$ (Jonsson and Carlsens experiments) are depicted in the paper. These quantities are reproduced acceptably well even by the constant eddy viscosity models.

In order to judge the model performance properly computations for a range of a/k_N-values are needed.

3.6 Measurements in a turbulent wave boundary layer

Perhaps the most referenced set of measurements in a turbulent wave boundary layer over a rough bottom is due to Jonsson [21] and Jonsson and Carlsen [23]. These measurements include only ensemble-mean values and were obtained by a micro-propeller in an oscillating water tunnel. Unfortunately the two tests were made for low values of a/k_N equal to 28.4 and 124 respectively. In nature this ratio is often of the order of 10^3. The flow in a water tunnel is uniform. Therefore the advective terms in the model equations can be neglected.

A problem inherent in these experiments is the artificial bottom roughness as depicted in Fig. 3.1. All theoretical models make exclusive use of the equivalent sand roughness parameter k_N

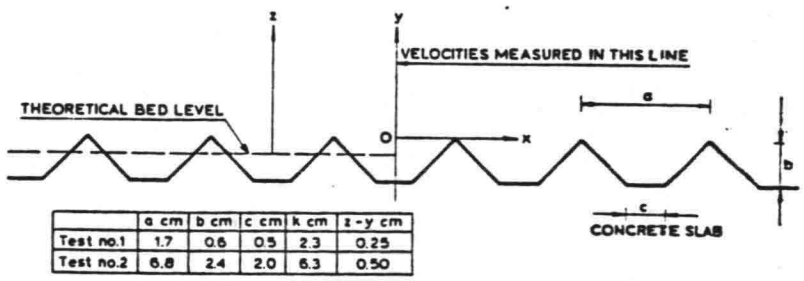

	a cm	b cm	c cm	k cm	z-y cm
Test no.1	1.7	0.6	0.5	2.3	0.25
Test no.2	6.8	2.4	2.0	6.3	0.50

Fig. 3.1 Bottom roughness, Jonsson and Carlsen [23].

as it was originally defined by Nikuradse. k_N appears in the usual logarithmic velocity profile which is strongly associated with a bed that is covered with a layer of roughness elements like sand grains. Such a layer is characterized by the absence of any directionality whereas the roughness elements used by Jonsson and Carlsen were triangular rods placed normal to the flow direction at constant intervals.

Based on these speculations it must be emphasized that the nature of the bottom roughness elements can have an impact on the results. Especially at lower a/k_N-values, a phenomenon like vortex shedding may change the flow pattern considerably depending on the roughness elements. This is said to underline that a comparison between measurements over an artificial roughened bed and theoretical models using the traditional roughness concept cannot be expected to yield perfect results since they may represent different flow situations. Nonetheless, measurements are so few at present so that it may be the only possibility.

Apart from velocity profiles and shear stress profiles obtained by integrating the equation of motion, Jonsson and Carlsen also presented eddy viscosities derived from the other quantities. ε is, however, a difficult quantity to evaluate when it is done using the definition

$$\varepsilon = \frac{\tau/\rho}{\frac{\partial U}{\partial y}} \qquad (3.7)$$

especially when both the numerator and the denominator are small quantities. Following this ε will be poorly determined far from the bed where the turbulence intensity is negligible. (31)

Introduction of Laser-Doppler Anemometry made direct measurements of the turbulent velocity fluctuations possible. Consequently the Reynolds stresses and the turbulent kinetic energy can be determined directly. The expression for ε, eq. (3.7) may then be more useful.

In the rough wall case Bakker and van Doorn [2] made mean velocity measurements whereas Kemp and Simons [26] also included the fluctuations to obtain the turbulent kinetic energy. But

only experiments for very low a/k_N-values in the order of 1-10 were performed.

For smooth walls two separate works exist. Tanaka et al. [43] made wind tunnel experiments obtaining an amplitude Reynolds number (cf. 2.40) of $6.10 \cdot 10^5$. Eddy viscosity and TKE distributions were presented only in cases with combined wave-current motion. A very comprehensive investigation for pure oscillatory flow in a wind tunnel has been reported by Hino et al. [15]. An amplitude Reynolds number of $3.8 \cdot 10^5$ was attained.

From the available experimental data it seems that theoretical models over smooth beds are much easier to check against measurements at present.

Finally we mention the work by Kamphuis [24] who determined the friction factor f_w in the rough wall case by direct measurement of the bottom shear stress.

No field measurements have been encountered during this study.

4. BLOBAK, A ZERO-EQUATION MODEL

4.1 Introduction

In this chapter we shall look at a zero-equation model for the turbulent wave boundary layer. The method is based on earlier works by Bakker [1], Bakker and van Doorn [2] and van Doorn [46]. But the choice of dimensionless variables is different. In the present work they are selected as outlined in chapter 2. Furthermore, deviations are present in the numerical method.

4.2 Construction of model

The flow equation governing the mean velocity field in a uniform two-dimensional boundary layer flow was established in chapter 2,

$$\frac{\partial U}{\partial t} = \frac{\partial U_o}{\partial t} + \frac{\partial}{\partial y}\left(\epsilon \frac{\partial U}{\partial y}\right) \qquad (4.1)$$

where

$U = U(y,t)$,
$\epsilon = \epsilon(y,t)$,
$U_o = U_o(t)$.

Now, define a defect velocity as the difference between the local mean velocity U and the ambient flow velocity U_o

$$U_d = U - U_o \qquad (4.2)$$

Eq. (4.1) then simplifies to

$$\frac{\partial U_d}{\partial t} = \frac{\partial}{\partial y}\left(\epsilon \frac{\partial U_d}{\partial y}\right) \qquad (4.3)$$

In the zero-equation model the eddy viscosity is related to the mean velocity through an algebraic equation. In this case we use Prandtl's mixing-length theory,

$$\varepsilon = l_m^2 \left| \frac{\partial U}{\partial y} \right| \tag{4.4}$$

where l_m is the mixing-length.

The mixing-length is, usually, assumed to be proportional to the distance from the wall because the size of the eddies may be governed by this. In steady boundary layers the constant of proportionality is the von Karman constant, κ, which most frequently is taken as 0.40. Mathematically the mixing-length is written

$$l_m = \kappa y \tag{4.5}$$

Although there is no certain evidence supporting this simple variation of the mixing-length in an unsteady boundary layer, we shall apply (4.5) in this model as a qualified guess. It is noticed that for large a/k_w where the oscillatory wave motion can be recognized to attain a quasi-steady behaviour during each half-period, it is in agreement with a 'steady flow' solution to prescribe eq. (4.5).

If eqs. (4.4) and (4.5) are substituted into eq. (4.3), we obtain

$$\frac{\partial U_d}{\partial t} = \frac{\partial}{\partial y} \left(\varkappa^2 y^2 \frac{\partial U_d}{\partial y} \left| \frac{\partial U_d}{\partial y} \right| \right) \tag{4.6}$$

This is the governing differential equation for the flow in a turbulent wave boundary layer under the given assumptions. Bakker derived a different version of (4.6) in his earliest work [1], where he defined an 'interior friction velocity'

$$p = \text{sign}(\tau) \sqrt{|\tau| / \rho} \tag{4.7}$$

Equation (4.6) appeared as

$$\frac{\partial p}{\partial t} = \varkappa y \frac{\partial^2 (p|p|)}{\partial y^2} \tag{4.8}$$

The disadvantage in this formulation is that the boundary conditions should be given in terms of the shear stress (through

eq. (4.7)) and not in the mean velocity, as is the case with (4.6). In consequence of this Bakker later [46] reformulated the problem together with van Doorn to conform to (4.6).

Before we can formulate the boundary conditions for (4.6), the choice of the bed coordinate has to be considered.

The y-coordinate for the lowermost mesh-point is determined by analogy with the usual logarithmic velocity profile in a steady turbulent flow above a rough bed,

$$\frac{U}{U_f} = \frac{1}{\varkappa} \ln \frac{y}{k_N/30} \qquad (4.9)$$

where U=0 at a distance above the theoretical bed level, cf.

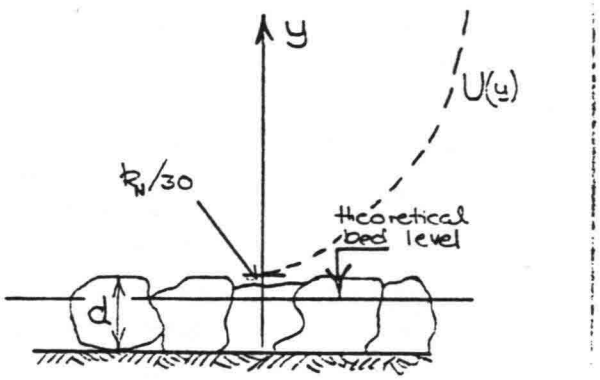

Fig. 4.1 Definition of bed coordinate

Fig. 4.1. Normally the boundary condition is

$$U(y=k_N/30)=0 \qquad (4.10)$$

From (4.9) we get

$$\frac{\partial U}{\partial y} = \frac{U_f}{\varkappa y} \qquad (4.11)$$

and

$$\varepsilon = \frac{\tau/\rho}{\frac{\partial U}{\partial y}} = \varkappa U_f y \qquad (4.12)$$

It is seen that concordance between (4.9),(4.12) and (4.4),(4.5) is achieved when the boundary condition is prescribed according to (4.10). The bed coordinate must be

$$y_b = k_N / 30 \qquad (4.13)$$

The boundary conditions associated with eq. (4.6) are the following

1. The velocity vanishes at the bed due to the no-slip condition. From (4.2) is obtained

$$U_d(y=y_o) = -U_o \qquad (4.14)$$

2. At the edge of the computational region towards the ambie flow the velocity must match with the outer velocity, tha is

$$U_d(y=y_b) = 0 \qquad (4.15)$$

3. Further, an initial vertical velocity distribution has to be given. This can either be a stagnant fluid where

$$U_d(y) = 0$$

since the ambient flow velocity is zero at the start, or can be a profile found in an earlier run.

4. An arbitrary variation af the ambient flow velocity can b prescribed. In the present model the situation is restricted to a pure oscillatory motion characterized by

$$U_o(t) = U_1 \sin(\omega t) \qquad (4.16)$$

It follows from eq. (4.16) that we must require periodici in the solution

$$U(y,t+T)=U(y,t)$$

When the usual dimensionless quantities defined in Chapter 2 are inserted into eq. (4.6)

Time: $t^* = 2\pi t/T = \omega t$ (4.17a)

y-coordiante: $y^* = y/k_N$ (4.17b)

Velocities: $U^* = U/U_1$. (4.17c)

the following dimensionless differential equation is found

$$\frac{\partial U_d^*}{\partial t^*} = \varkappa^2 \frac{a}{k_N} \frac{\partial}{\partial y^*} \left([y^*]^2 \frac{\partial U_d^*}{\partial y^*} \left| \frac{\partial U_d^*}{\partial y^*} \right| \right) \tag{4.18}$$

The initial value problem consisting of eq. (4.18) with the dimensionless boundary and initial conditions is depicted in Fig. 4.2.

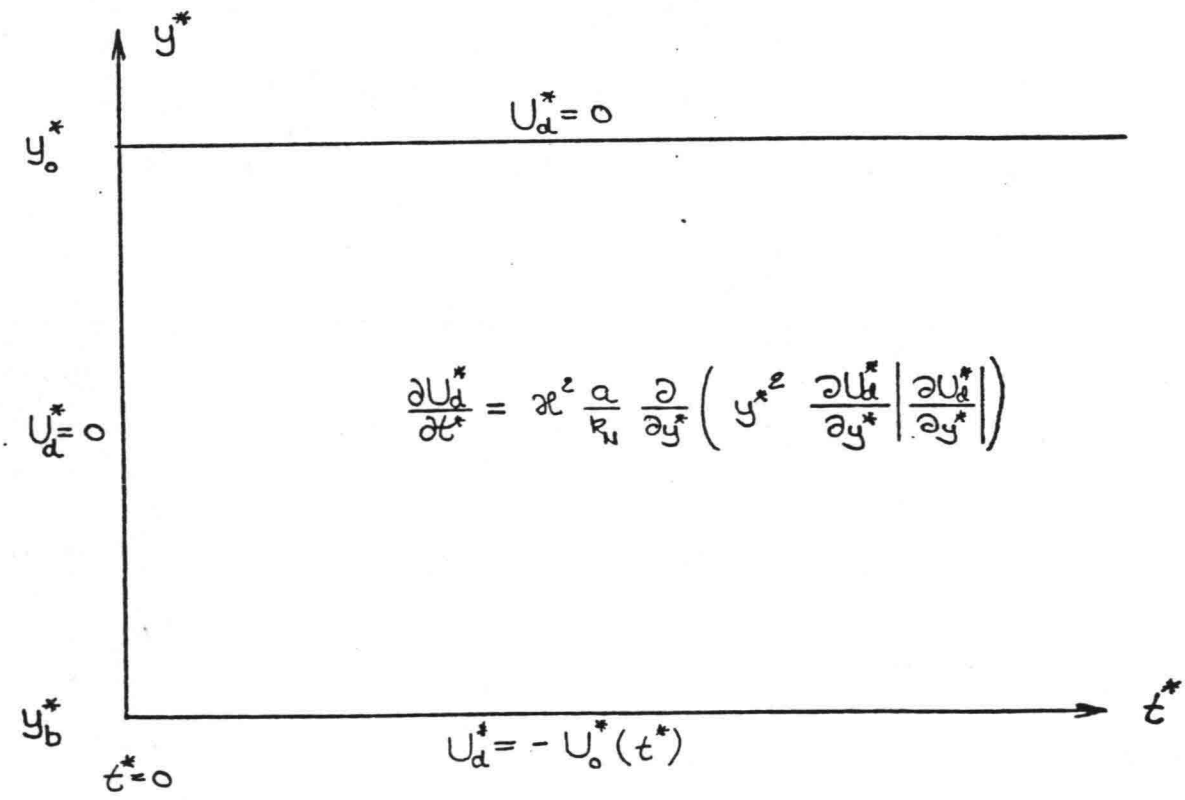

Fig. 4.2 Initial value problem for the defect velocity

The upper limit for the region of computation, y_∞, is determined so that the gradient in the mean velocity vanishes at this boundary. It follows that also the shear stress and the eddy viscosity disappear. The adequate value of y_∞ is found by trial and error.

4.3 Numerical solution

The only way to solve the initial value problem is to apply a numerical method of solution. Bakker and van Doorn used a finite difference method (FDM), and we will do the same. The choice is based on the fact, that FDM must be considered faster to implement than a similar finite element method (FEM) would be. The expense may be a longer computer time to obtain the same accuracy in the computations.

In FDM a mesh of points is placed over the region of solution. To increase the efficiency of the method the mesh is refined in areas where the solution has the largest variations. In the present case large gradients in the velocity are anticipated close to the bed. Consequently the mesh is refined close to the bed. There exists a number of ways to achieve this. Bakker and van Doorn employed the so-called 'Staggered Grid'. The notion is that an arbitrary number of grids with increasing fineness are superimposed. As the meshwidth becomes smaller, the mesh extends less and less from the bed. In this way a refined description of the solution is obtained near the bed without the expense of an intolerable requirement in CPU-time and memory.

It seems to be more straightforward to vary the distance between the mesh points in a single mesh. This can be achieved either by incorporating a coordinate straining in the differential equation using an equidistant mesh, or by varying the mesh size in the original coordinate system and take this variance into account. In this case the coordinate straining is chosen, whereas the latter method is applied in the next chapter.

The transformation of the derivative has been used,

$$\frac{\partial}{\partial y^*} = \frac{c}{\exp(\xi^*)} \frac{\partial}{\partial \xi^*} \tag{4.22}$$

Now, the numerical scheme for the solution of (4.21) is set-up in the mesh shown in Fig. 4.3.

An implicit Crank-Nicolson scheme is applied, see e.g. [25]. Equal weight is given to the previous and the present timestep. The second order derivative in eq. (4.21) is found by centering the first order derivatives in points between the mesh points as shown in Fig. 4.3 and then using central estimates for the second order derivatives.

Using first order difference approximations the following difference equation is obtained (*, which indicates dimensionless quantaties are omitted from this point to the end of the section),

$$f_j = (U_d^{i,j} - U_d^{i-1,j}) - \frac{a}{k_v} \frac{x^2 c\, \Delta t}{2 \Delta \xi \exp(\xi)} \left[\left\{ 1 - \frac{1}{\exp\{\frac{1}{2}(\xi_{j+1} + \xi_j)\}} \right\}^2 \cdot \frac{1}{\Delta \xi^2} \cdot \right.$$

$$\left\{ (U_d^{i,j+1} - U_d^{i,j}) \left| U_d^{i,j+1} - U_d^{i,j} \right| + (U_d^{i-1,j+1} - U_d^{i-1,j}) \left| U_d^{i-1,j+1} - U_d^{i-1,j} \right| \right\}$$

$$- \left\{ 1 - \frac{1}{\exp\{\frac{1}{2}(\xi_j + \xi_{j-1})\}} \right\}^2 \cdot \frac{1}{\Delta \xi^2} \left\{ (U_d^{i,j} - U_d^{i,j-1}) \left| U_d^{i,j} - U_d^{i,j-1} \right| \right.$$

$$\left. \left. + (U_d^{i-1,j} - U_d^{i-1,j-1}) \left| U_d^{i-1,j} - U_d^{i-1,j-1} \right| \right\} \right], \quad j = 2, \ldots, N+1 \tag{4.23}$$

Since eq. (4.21) is nonlinear, eq. (4.23) is the same. The N equations contained in (4.23) can generally be formulated as N nonlinear equations with N unknowns

$$f_j(\underline{z}) = 0 \qquad , \quad j = 2, \ldots, N+1 \tag{4.24}$$

where

$$\underline{z} = \{z_2, \ldots, z_{N+1}\} = \{U_d^{i,2}, \ldots, U_d^{i,N+1}\}$$

are the N unknowns. The system is solved using Newton's iterative method, see e.g [30] and [48].

At a given stage in the iteration procedure a residual vector can be written

$$\underline{f}^n = \{f_j(\underline{z}^n)\}$$

The residual vector for the next iteration step can be expanded as a Taylor series

$$f_j^{n+1} = f_j^n + \sum_{l=2}^{N+2} \left(\frac{\partial f_j}{\partial z_l}\right)^n (z_l^{n+1} - z_l^n) + \ldots \quad ; \; j = 2, \ldots, N+2 \tag{4.25}$$

where

$$\left(\frac{\partial f_j}{\partial z_l}\right)^n = \frac{\partial f_j(\underline{z}^n)}{\partial z_l}$$

The aim is to have $\underline{f}^{n+1} = 0$. An approximation to this is found from (4.25) by truncating the series after the shown term, and solving the resultant system of linear equations

$$\underline{\underline{A}}(\underline{z}^{n+1} - \underline{z}^n) = -\underline{f}^n \tag{4.26}$$

where

$$A_{kl} = \frac{\partial f_k}{\partial z_l}(\underline{z}^n)$$

The partial derivatives in $\underline{\underline{A}}$ are found from (4.23). Defining

$$C_j = \frac{a}{k_N} \frac{\chi^2}{2} \frac{c\,\Delta t}{\Delta\xi \exp(\xi_j)} \tag{4.27}$$

and

$$S_j = \left[1 - \frac{1}{\exp\{\frac{1}{2}(f_j + \xi_{j-1})\}}\right]^2 \frac{1}{\Delta\xi^2} \tag{4.28}$$

we find that

$$\frac{\partial f_j}{\partial U_\alpha^{j-1}} = -2 S_j C_j \operatorname{sign}\left(U_\alpha^j - U_\alpha^{j-1}\right)\left(U_\alpha^j - U_\alpha^{j-1}\right) \tag{4.29}$$

$$\frac{\partial f_j}{\partial U_\alpha^j} = 1 + 2 S_j C_j \operatorname{sign}\left(U_\alpha^j - U_\alpha^{j-1}\right)\left(U_\alpha^j - U_\alpha^{j-1}\right) + 2 S_{j+1} C_j \operatorname{sign}\left(U_\alpha^{j+1} - U_\alpha^j\right)\left(U_\alpha^{j+1} - U_\alpha^j\right) \tag{4.30}$$

$$\frac{\partial f_j}{\partial U_d^{j,n+1}} = -2S_{j+1}C_j \operatorname{sign}\left(U_d^{j,j+1}-U_d^{j,j}\right)\left(U_d^{j,j+1}-U_d^{j,j}\right) \qquad (4.31)$$

All other elements in $\underline{\underline{A}}$ are zero. The system (4.26) is of the tridiagonal type

$$D_j^n\left(U_d^{j-1,n+1}-U_d^{j-1,n}\right)+E_j^n\left(U_d^{j,n+1}-U_d^{j,n}\right)+F_j^n\left(U_d^{j+1,n+1}-U_d^{j+1,n}\right)=G_j^n \qquad (4.32)$$

where the coefficients D_j^n, E_j^n and F_j^n are given by (4.29) - (4.31) and the right-hand side is

$$G_j^n = -f_j^n \qquad (4.33)$$

Eqs. (4.32) are solved by the so-called Double-Sweep-Method, as it is described in e.g. [33] and [48]. It is noticed that if the mesh points had been equidistant in the original coordinate system, then the system of equations (4.32) would have had a symmetric coefficient matrix. Generally we have for the coefficients

$$E_j^n = 1-D_j^n-F_j^n \qquad (4.34)$$

No special attention has been paid to the issue of stability. The timestep has been decreased until a stable solution was reached. In practice this has always been the case when 800 timesteps were used during one period. Because of coordinate straining the Crank-Nicolson scheme can not be expected to be unconditionally stable, as would have been the case with a uniform mesh. (42)

The mesh has been refined by an increased straining and additional mesh points until the numerical solution remained invariant to further refinements. Henceforth the solution has been accepted. All iteration cycles are controlled by an accuracy parameter related to the relative change in the solution from one iteration step to the next. When a certain accuracy has been reached in all points, the iteration is stopped. Typically a relative change of 10^{-5} to 10^{-6} has been demanded.

The periodicity condition for U is not directly included in this solution procedure. When the specified initial velocity distribution is not from a periodic solution it contains a transient part which has to be damped out through a number of periods of calculations. This issue is discussed in section 4.6.

4.4 Implementation

The zero-equation model is implemented through the programme BLOBAK (Boundary Layer 0-Equation Bakker). The structure and operation procedure for BLOBAK are discussed in Appendix A.

4.5 Quantities derived from the zero-equation model

From the solution to eq. (4.1) a number of quantities can be derived. In connection with an eddy viscosity model the shear stress is defined by

$$\tau/\rho = \epsilon \frac{\partial U}{\partial y} \tag{4.35}$$

If (4.4) and (4.5) are inserted for ϵ, τ becomes

$$\tau/\rho = (\varkappa y)^2 \left(\frac{\partial U}{\partial y}\right)^2 \tag{4.36}$$

In the transformed coordinate system and in dimensionless version eq. (4.36) has the form

$$\tau^* = \varkappa^2 \left[1 - \frac{1}{exp(\xi^*)}\right]^2 \frac{\partial U^*}{\partial \xi^*} \left|\frac{\partial U^*}{\partial \xi^*}\right| \tag{4.37}$$

where (4.20) and (4.22) have been used. The derivatives are approximated by central differences in the numerical method.

The bed shear stress can not be determined from (4.37) since the derivative can not be found numerically. The bed shear stress is therefore taken as the extrapolated value of the shear stress in the two adjacent mesh points. The friction velocity is defined as

$$U_f^* = \sqrt{|\tau_b^*|}\ \mathrm{sign}(\tau_b^*) \tag{4.38}$$

The friction factor f_w is found as

$$f_w = 2\,(U_{f,max}^*)^2 \tag{4.39}$$

The eddy viscosity is determined from (4.35)

$$\varepsilon^* = \frac{\exp(\zeta^*)}{c}\,\frac{\tau^*}{\frac{\partial U^*}{\partial \zeta^*}} \tag{4.40}$$

When the velocity gradient vanishes, $\varepsilon^*=0$. The displacement thickness δ^* is found as

$$\delta^* = -\frac{1}{U_o^*}\int_{\zeta_b^*}^{\infty}\frac{\exp(\zeta^*)}{c}\,(U^*-U_o^*)\,d\zeta^* \tag{4.41}$$

while the momentum thickness θ^* is

$$\theta^* = -\left(\frac{1}{U_o^*}\right)^2\int_{\zeta_b^*}^{\infty}\frac{\exp(\zeta^*)}{c}\,U^*\,(U^*-U_o^*)\,d\zeta^* \tag{4.42}$$

Lundgrens wave viscosity is found from the definition [29]

$$\eta_w^* = \frac{\exp(\zeta^*)}{c}\,\frac{\int_{T^*}|\tau^*|\,dt^*}{\int_{T^*}\left|\frac{\partial U^*}{\partial y^*}\right|\,dt^*} \tag{4.43}$$

where the integrals are determined over one period giving a vertical profile for η_w^*.

The mean specific energy loss E over one period is given by

$$\overline{E} = \overline{\tau_b U_o} \tag{4.44}$$

In order to relate the energy loss to a general parameter the energy loss factor f_e is defined by

$$\overline{E} = \frac{2}{3\pi}\,\rho\, f_e\, U_{im}^3 \tag{4.45}$$

see Jonsson [21]. f_e is important in connection with wave attenuation since a paramount fraction of the energy is lost due to dissipation processes in the nearbed turbulent boundary layer.

4.6 Presentation of results

This section is a discussion of the results that have been compiled using the zero-equation model.

As mentioned in the introduction to this chapter this model has been implemented earlier. It is natural to compare the results obtained from the two different implementations of the same theoretical model. Calculated velocity profiles for the two cases where the ambient velocity is zero and a maximum are shown in Fig. 4.4. Close agreement is observed. To remove the effects

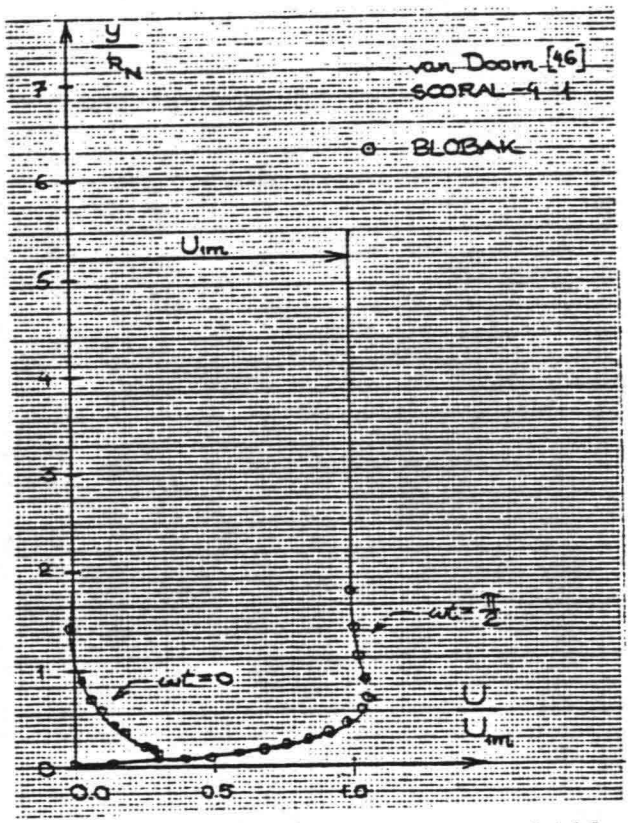

Fig. 4.4 Comparison with van Doorn [46], $a/k_N = 4.47$ SOORAL-4 1.

of a transient component in the solution due to the initial conditions five periods have been used to reach an almost periodic solution. It follows from the nature of the mathematical problem that each half period must yield the same results except for possible opposite signs. In Fig. 4.5 we have plotted the maximum velocity coinciding with zero ambient velocity over 10 half periods of calculation. It is seen how the values for the last two half periods diverge approx. 1 % from each other. Further it can be seen that the transient part is damped out even if the

process becomes more and more slow. All further results in this chapter are based on the fifth period of calculation. Often the mean of the values from the ninth and tenth half period has been used. It has been customary to run four periods without detailed output storing the solution in an external file and then run the fifth period with a detailed output from BLOBAK. A list of the completed runs with BLOBAK is enclosed in Appendix A. Typical running times for BLOBAK on the IBM computers at NEUCC were 20-30 seconds per period using 3 iterations at each timestep.

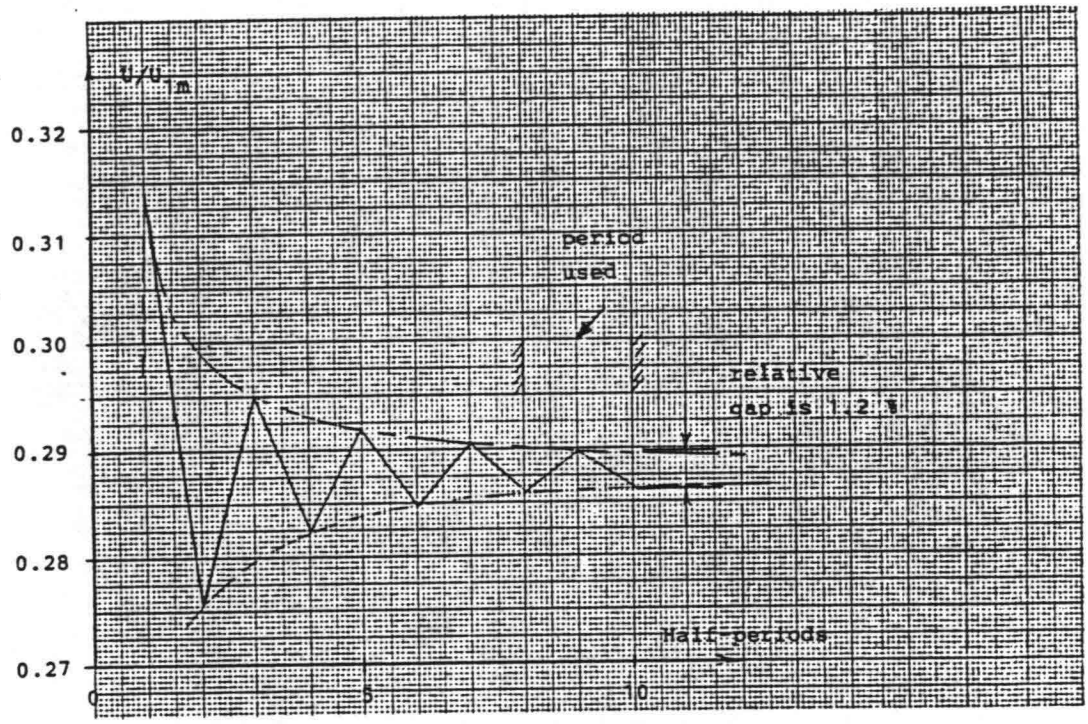

Fig. 4.5 Development of solution, $a/k_N = 10$

A standard mesh containing 43 interior points has been used in all runs except for a/k_N-values larger than 10^3 where points were added to facilitate a non-vanishing solution further away from the bed. The strain factor c in eq. (4.19) has been taken as c=2000. The edge of the computational region was at $y/k_N = 1000$ for N=43 and $y/k_N = 8200$ for N=52.

These requirements were determined by trial and error. The process has been aiming at a good numerical solution. For convenience it was decided that the same mesh was to be used for as wide a range of a/k_N-values as possible even if this would not

be economically sound.

The basic idea in the following will be that we go through the different results that can be found from the model for the a/k_N-value 124 which is also the value in TEST 1 of Jonsson and Carlsen [23] so that results can be compared. Additional diagrams for a/k_N=1000 can be found in Appendix G. The test data from Jonsson and Carlsen have been processed using the programme JONCAR enclosed in Appendix D.

Velocity field.

Velocity profiles are shown in different ways In Fig. 4.6. From Fig. 4.6 (a) and (b) it is seen that close to the bed there is good agreement between theory and measurements. When the experimental results from opposite phases are averaged it is seen that further away from the bed there is a depression in the profiles which is not described by the theory.

The well-known overshoot, which occurs when the fluid particles close to the bed areas accelerated by the pressure gradient at an earlier stage than further away from the bed because of the lower velocities, is described well when the ambient velocity is zero. The overshoot is less accurate when the free stream velocity is a maximum.

It is very important to notice that a logarithmic velocity profile is always found very close to the bed. The presence of this phenomenon is generally recognized and confirmed by the measurements. Often theoretical models include a logarithmic velocity profile close to the bottom. It is referred to as the law of the wall. Here it is inherent in the numerical solution.

Another way of looking at the velocity field is to determine the velocity amplitude as a function of the distance from the bed. As seen from Fig. 4.7 (a) the general shape compares well with experiments but the curve is shifted upwards. The phase lag between the maximum local velocity and the maximum free stream velocity is depicted in Fig. 4.7 (b). Discrepancies are present

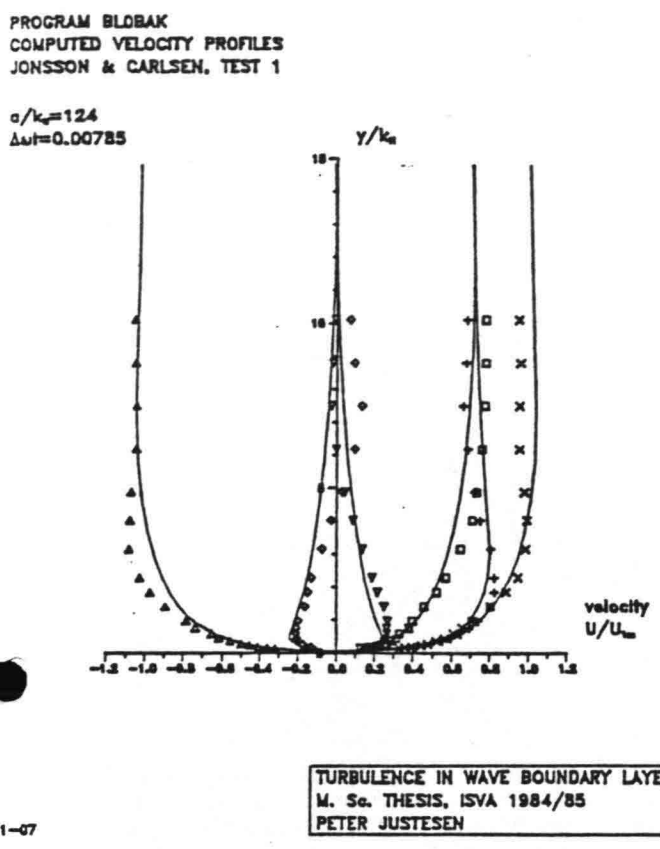

(a)

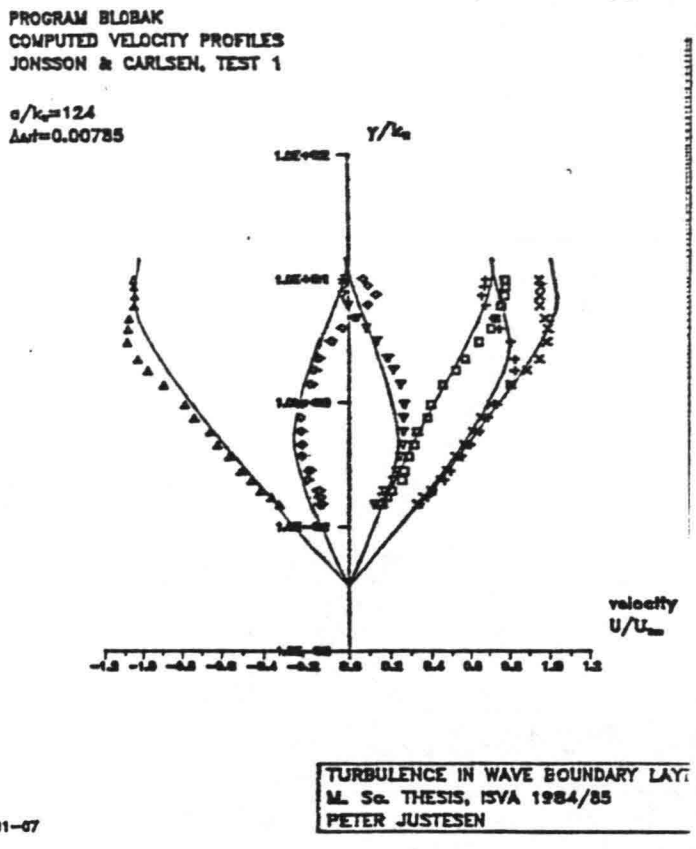

(b)

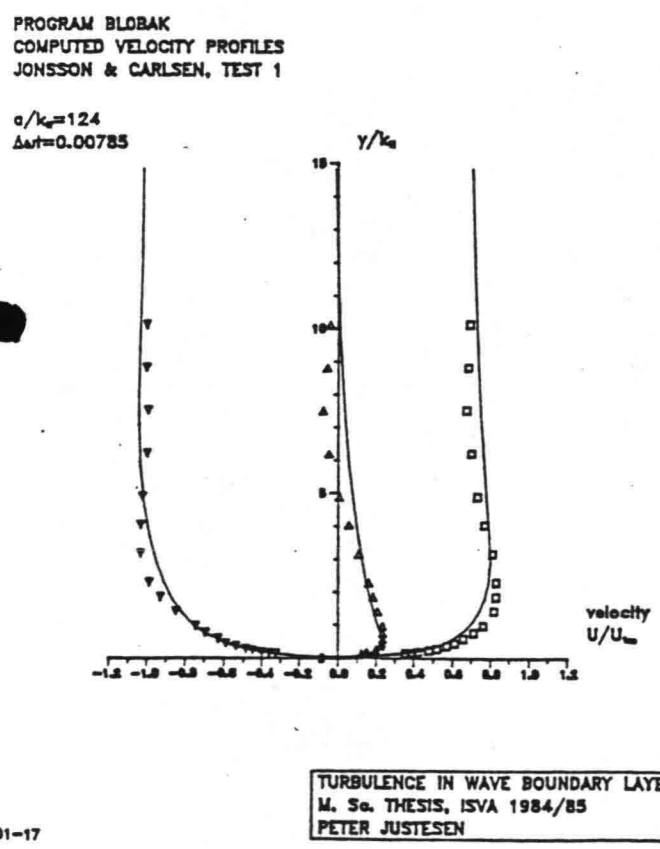

(c)

a. linear plot

b. log. plot

c. linear plot, measured values averaged over two half periods

Fig. 4.6 Velocity profiles for $a/k_N = 124$

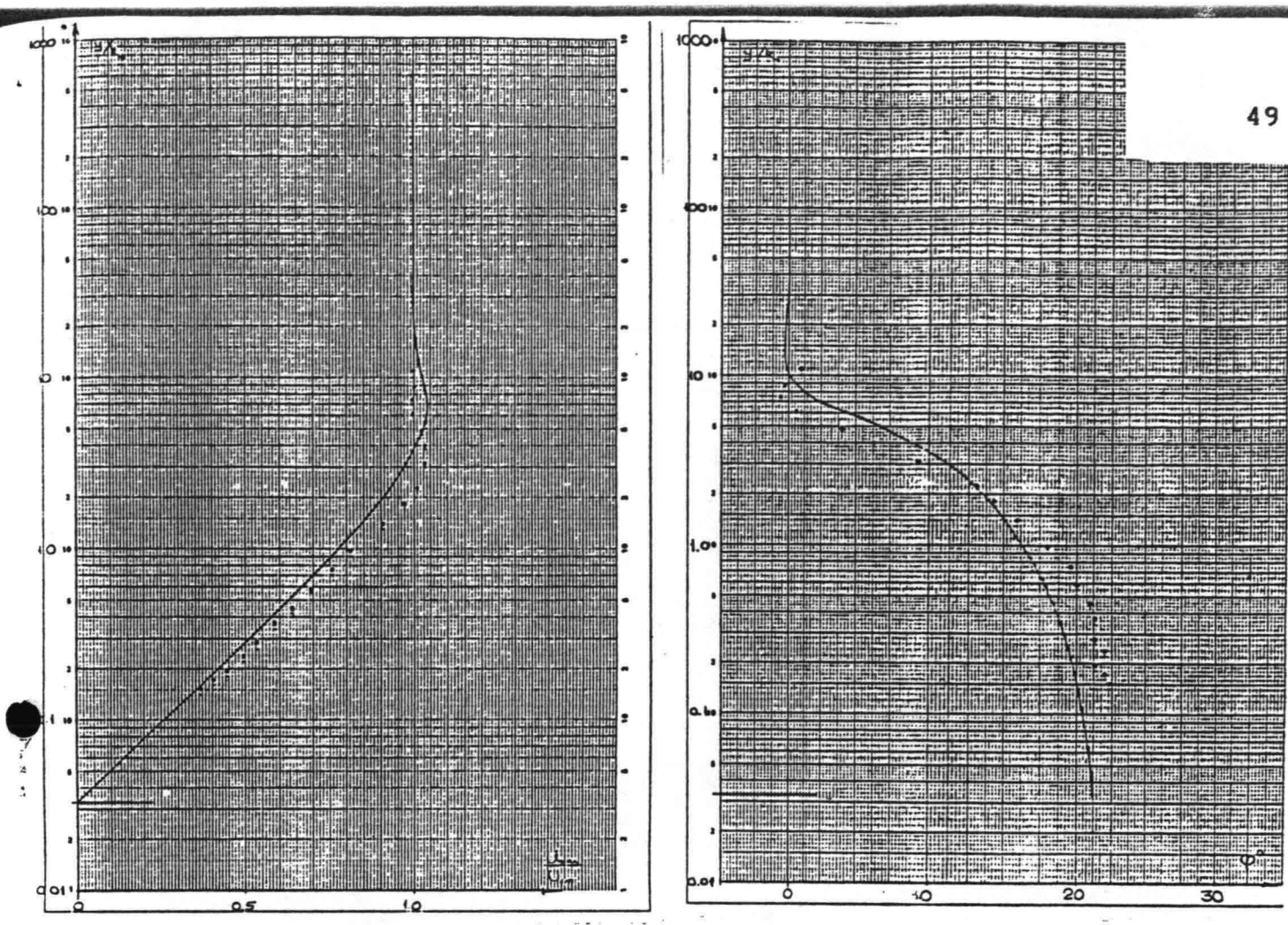

Fig. 4.7 Velocity amplitudes and phases. $a/k_N = 124$

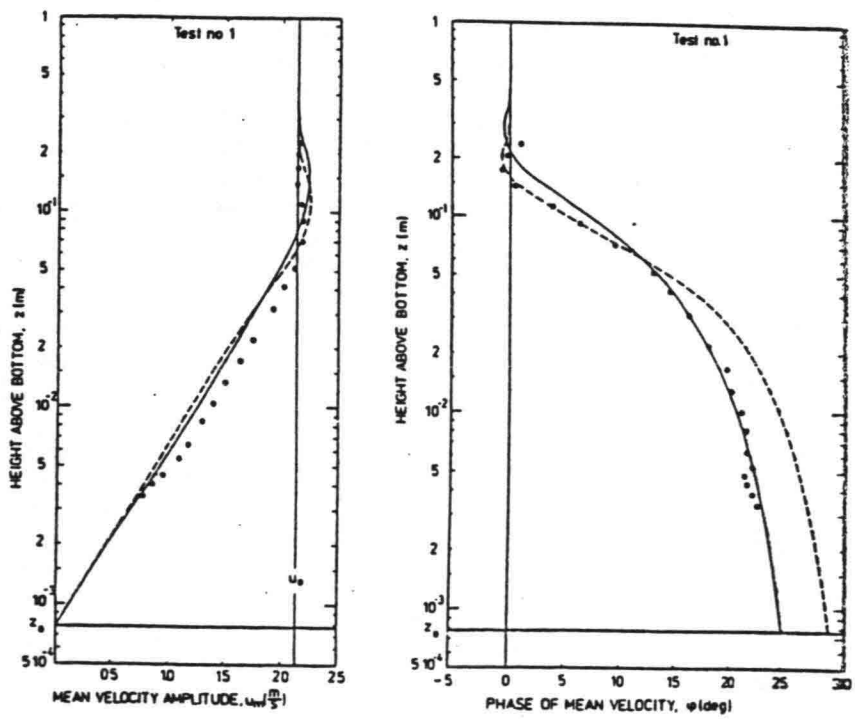

Fig. 4.8 As Fig. 4.7, $a/k_N = 124$. Myrhaug [32].

once more. It may be useful to compare these results with those of Myrhaug [32] who used a two-layer time-invariant eddy viscosity model, cf. chapter 3, to attack the same problem. His curves are shown in Fig. 4.8. The two-layer model yields the same results with respect to the velocity amplitudes whereas the phase shift description is better than that of BLOBAK. This feature may not be an important measure since the phase shift in the experiments was determined from velocity measurements that were 15 degrees apart over the period. An accuracy of less than perhaps 5 degrees can therefore not be expected and this is more than the differences between calculations and measurements.

Calculations have been made for a number of a/k_N-values. In Table 4.1 the maximum overshoot in the velocity profile is shown as a function of a/k_N. Also the phase shift between the maximum defect velocity at the bed and $U_{1\bullet}$ is included.

a/k_N	$U_{\bullet max}/U_{1\bullet}$	ϕ
10^0	1.072	35.2
10^1	1.052	28.8
10^2	1.041	21.6
10^3	1.032	16.2
10^4	1.027	12.6

Table 4.1 Maximum velocity overshoot and phase shift between max. defect velocity at bed and max. outer velocity.

Both the velocity overshoot and the phase angle are seen to decrease with increasing amplitude/roughness ratio.

Shear stresses.

Computed and measured shear stress profiles are shown in Fig. 4.9. Obviously the discrepancies between theory and measurements that were found with respect to the velocity field are also present here. The general shape, however, is reproduced fairly

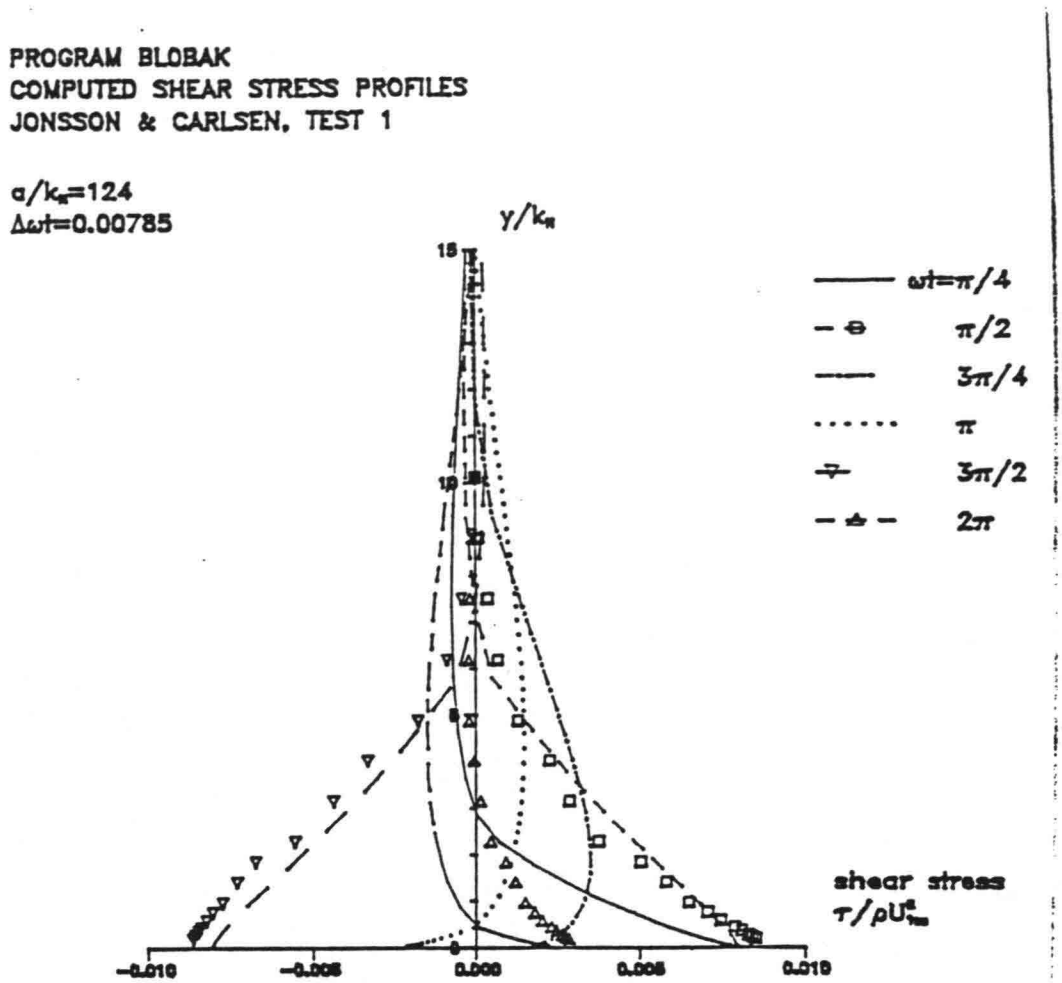

Fig. 4.9 Computed and measured shear stresses.

well. Special attention has been paid to the bed shear stress as this quantity is important when evaluating the energy loss and the friction factor. As previously described the bed shear stress is determined by linear extrapolation from the two mesh points adjacent to the bed. To check this procedure it was investigated whether the result was consistent with the law of the wall. Knowing the velocity in the points near the bed a number of values for U_* can be calculated using eq. (4.9). If the velocity profile is logarithmic the same U_* will be found in all the points. A few examples showed that the same bed shear stress value was found from the two different methods. This also confirmed that the numerical mesh was adequately detailed near the bed. In Fig. 4.10 we have plotted the bed shear stress as a function of time. Jonsson and Carlsen determined τ_b in two ways. One was to assume a logarithmic velocity profile (l.p.) close to the bed as described above. The other was to integrate the flow equation (f.e.) so that

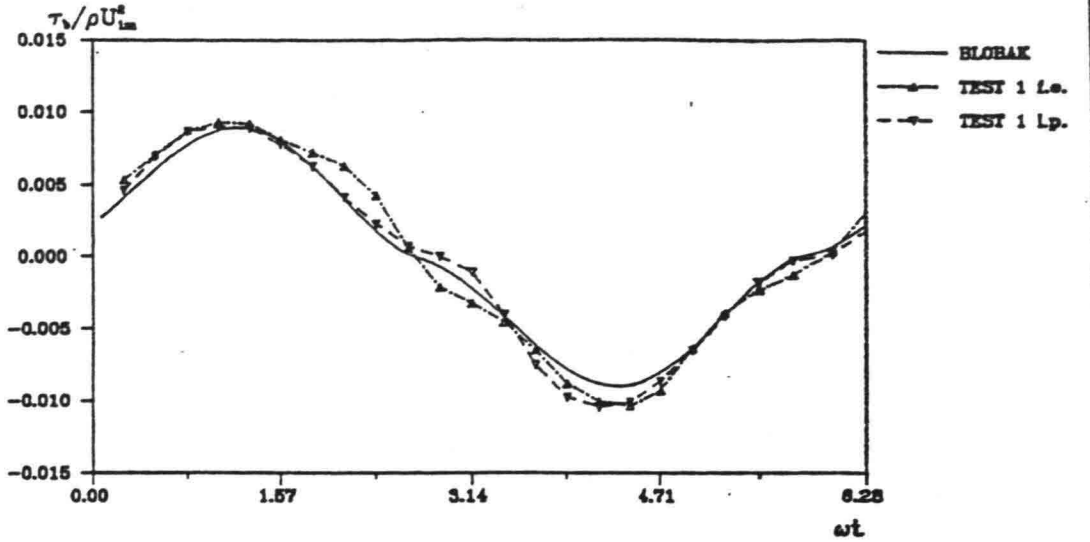

Fig. 4.10 Computed and measured bed shear stress

$$\frac{\tau_b}{\rho} = \int_{k_N/30}^{\infty} \frac{\partial}{\partial t}(U_o - U)\, dy \qquad (4.46)$$

The upper limit of integration is in practice finite since the defect velocity vanishes at a given level. Both curves are shown in Fig. 4.10. The best agreement is found using the law of the wall. This is not surprising because the numerical differentiation contained in the integrand of eq. (4.46) can be a delicate affair.

The friction factor f_w can easily be determined from the bed shear stress variation. Fig. 4.11 shows a number of different results for f_w. Results are included from both BLOBAK and Bakker. Fredsøe's simple model and Myrhaug's two-layer model are shown. Experimental results by Jonsson and Carlsen and Kamphuis [24] are also depicted. The discrepancies between Bakker's results and the present results are significant especially for decreasing a/k_N-values. It should be noted that comparison was only possible in a limited interval for a/k_N due to the amount of data given by Bakker. Referring to the discussion above concerning the bed shear stress it is believed that the present results are the most reliable. Generally all theoretical models fail to describe the variation of f_w when a/k_N is less than, say, 10. In this regime vortex shedding behind the individual roughness elements becomes important. These effects are not included in the present type of models. It should also be expected that the type of roughness elements used in the

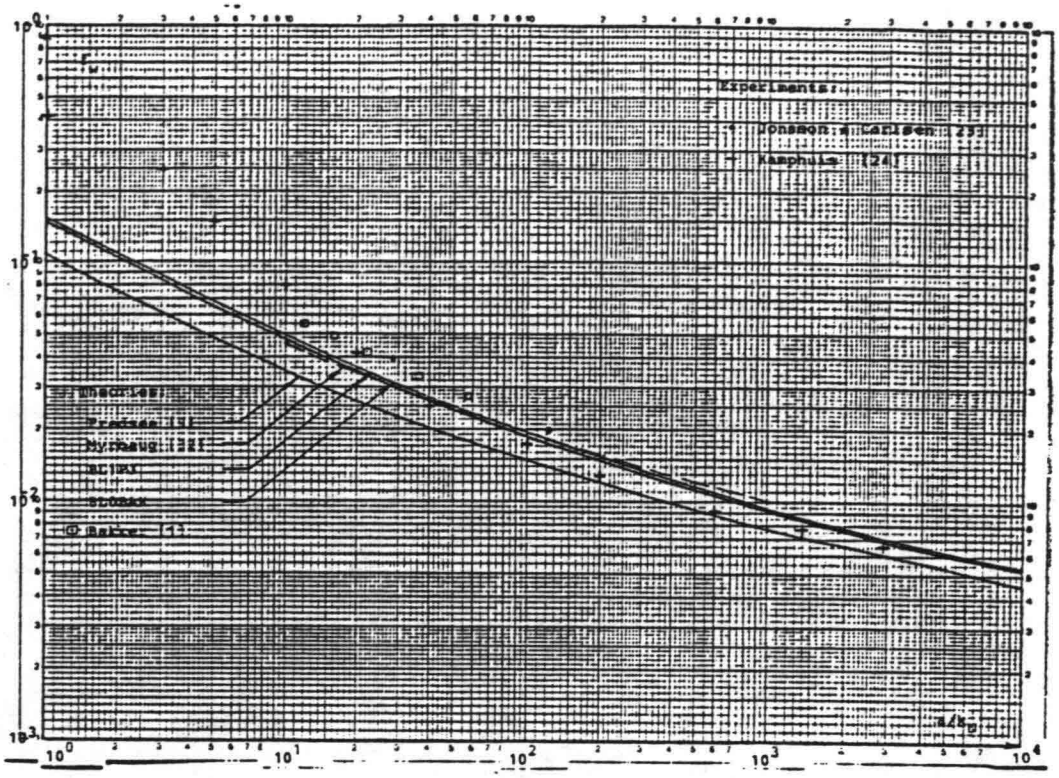

Fig. 4.11 Friction factor f_w as a function of a/k_N

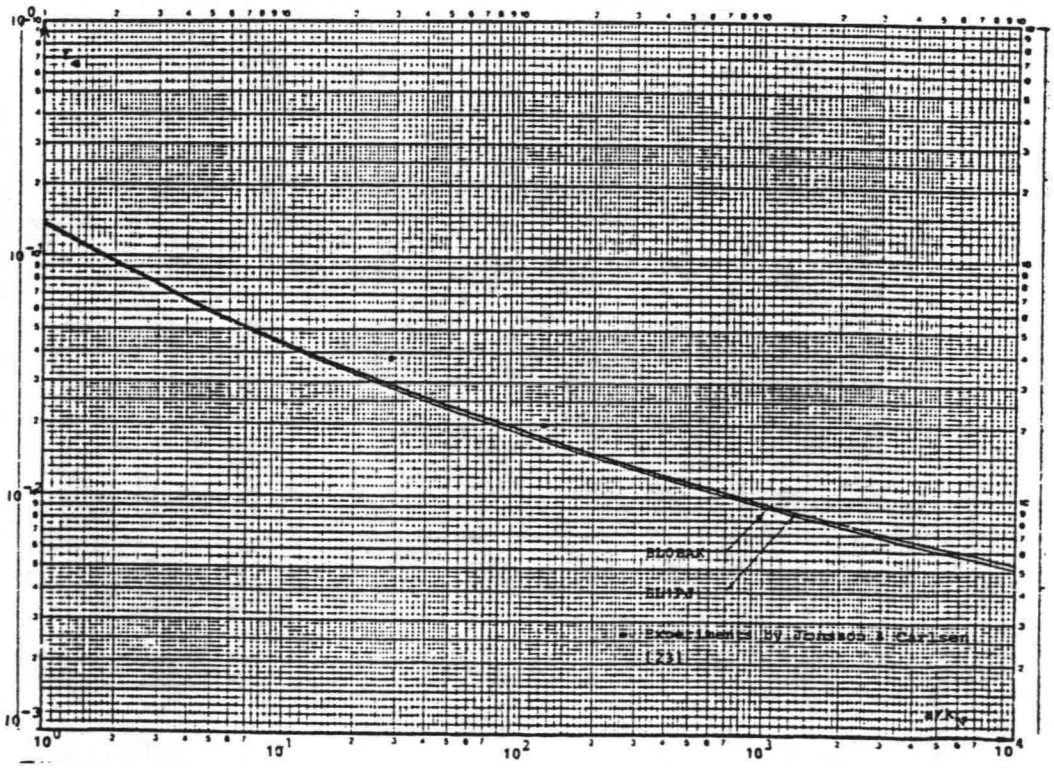

Fig. 4.12 Energy loss factor f_e as a function of a/k_N

experiments has a substantial influence on the results obtained. We shall revert to this aspect later. For larger a/k_N-values the variation of f_v found from the present model fits quite well with the experimental results.

The friction factor is often used instead of the energy loss factor f_e. This factor has been evaluated numerically and the variation is depicted in Fig. 4.12. Comparison with Fig. 4.11 shows that the two quantities f_v and f_e vary in the same way qualitatively. Table 4.2 shows the ratio f_v/f_e for different a/k_N-values as found from BLOBAK. Good agreement with the experimental results is observed.

a/k_N	f_v	f_e	f_v/f_e	
10^0	0.154	0.136	1.13	
10^1	0.0489	0.0453	1.08	
10^2	0.0193	0.0188	1.027	
10^3	0.00935	0.00933	1.002	
10^4	0.00528	0.00533	0.992	
28.4	0.0310	0.0290	1.07	theory
	0.0395	0.0379	1.04	exp.
124	0.0179	0.0175	1.022	theory
	0.0200	0.0197	1.02	exp.

Table 4.2 Computed values of f_v, f_e and f_v/f_e. Experiments by Jonsson and Carlsen.

Apparently this discussion is the first attempt to calculate f_v/f_e theoretically without any assumptions on the variation of τ. A discussion of the topic is given by Skovgaard et al. [40].

Boundary layer extension.

The time-variation of the displacement thickness is depicted in Fig. 4.13 (a) while the momentum thickness appears in Fig.

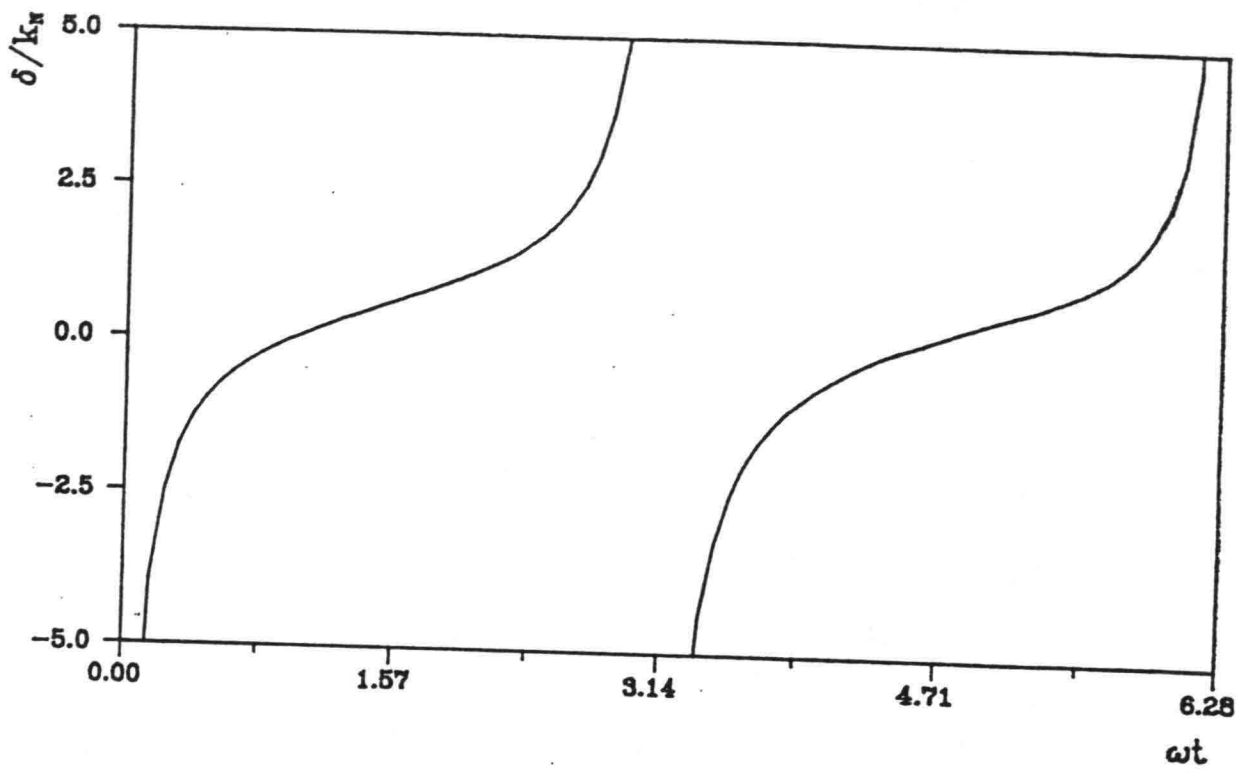

Fig. 4.13 (a) Variation of displacement thickness for $a/k_N = 124$

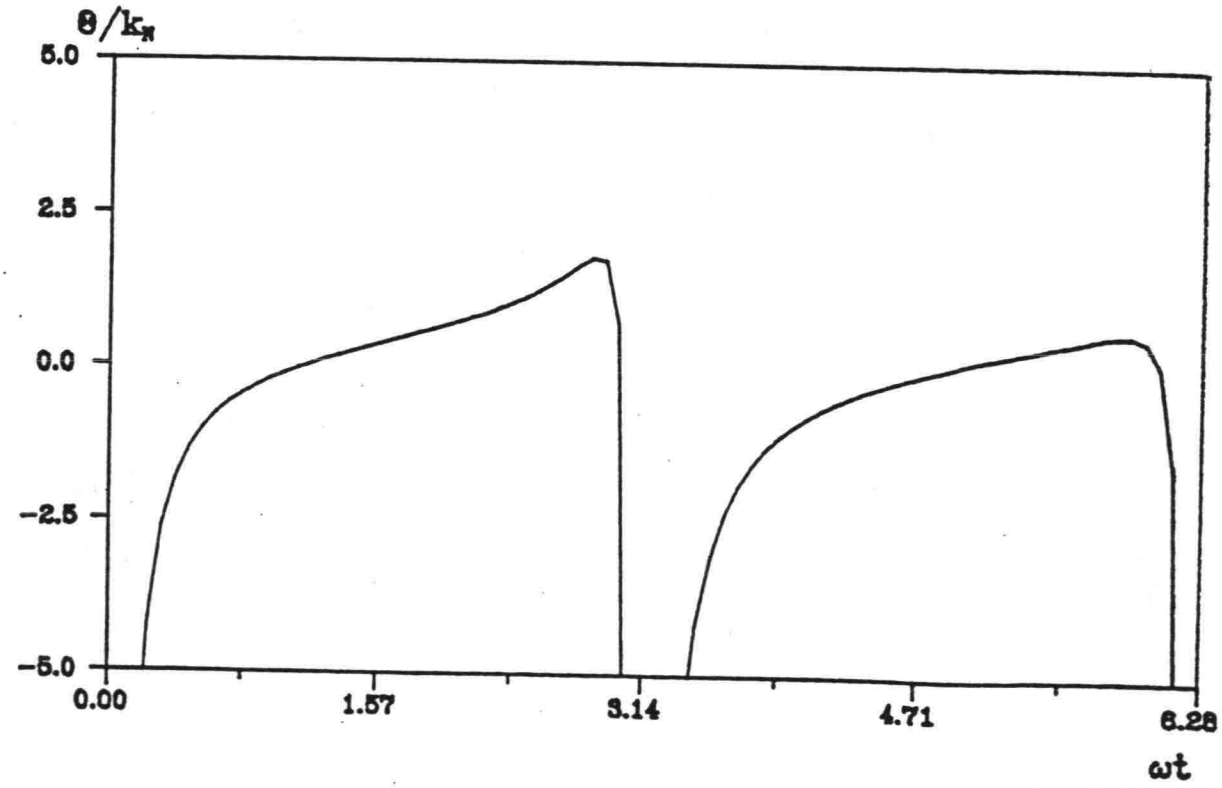

Fig. 4.13 (b) Variation of momentum thickness for $a/k_N = 124$

4.13 (b). The variation of both quantities is slightly different during the two half periods shown. The difference is explained by the remaining transient part of the solution. Worst affected is the momentum thickness. To facilitate comparison with other theories and experiments we have listed the results at $\omega t=\pi/2$ as a function of a/k_N in Table 4.3. Values are also included for the boundary layer thickness δ_1 defined as the minimum distance between the wall and the level where the velocity equals the ambient flow velocity when this is a maximum. For comparison the results by Fredsøe [9] are included as well.

a/k_N	δ/k_N	δ/a	δ_1/k_N	θ/k_N	δ_1/a	
10^0	0.0507	0.0507	0.229	0.015	0.182	
10^1	0.130	0.0130	0.078	0.044	0.074	
10^2	0.395	0.00395	0.036	0.155	0.039	
10^3	1.456	0.00146	0.021	0.641	0.025	
10^4	6.412	0.000641	0.014	0.197	0.017	
124			0.0341	0.197		theory
			0.0210			exp.

Table 4.3 Displacement, boundary layer and momentum thicknesses. Rightmost column shows Fredsøe's theory.

Eddy viscosities

For applications like sediment transport computations the eddy viscosity distribution in the turbulent wave boundary layer is very important. An example of such an analysis is given in chapter 7. Here we shall discuss the results obtained from BLOBAK.

As a start consider the eddy viscosity profiles computed at different timesteps during one period. In Fig. 4.14 it can be seen how the eddy viscosity reaches a peak close to the bed. It then drops to a very small value before there is an increase again. For sufficiently large values of y/k_N the eddy viscosity

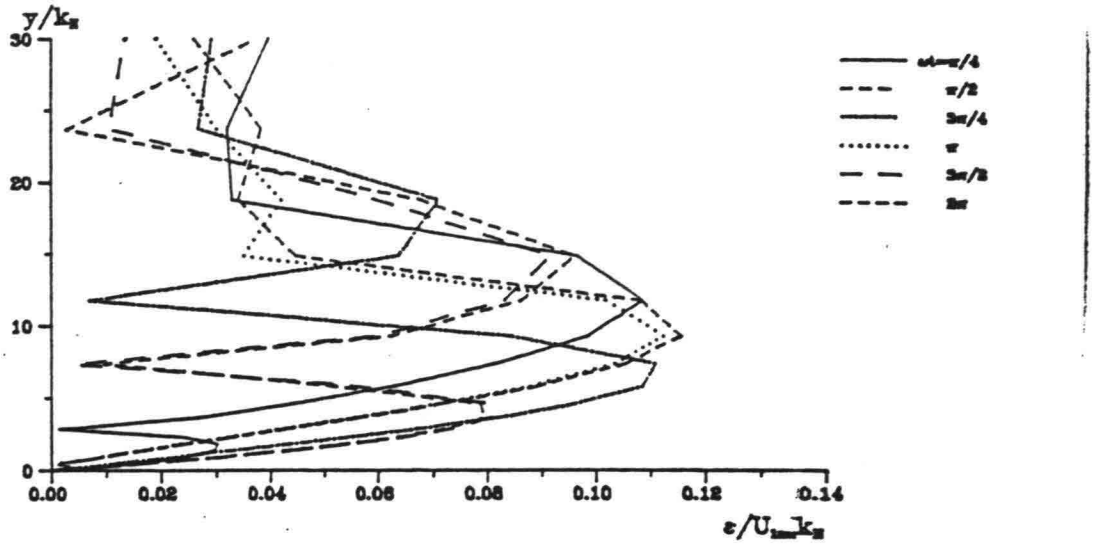

Fig 4.14 Profiles for the eddy viscocity, $a/k_N = 124$

vanishes as there is no turbulence present. The definition equation for ε, eq. (4.4), states that when there is a vertical tangent to the velocity profile the eddy viscosity is zero. If the profiles in Fig. 4.14 are compared with the velocity profiles in Fig. 4.6 it becomes clear that the eddy viscosity does not become exactly zero when it should according to the velocity profiles. The reason for this inaccuracy is the numerical discretization which is causing the peaked profiles shown in Fig. 4.24 as well.

The timeseries for eddy viscosities in specified levels above the bed are probably more useful. They are presented in Fig. 4.15 and four different a/k_N-values are included. The vertical levels have been chosen in terms of y/k_N so that they are physically the same independently of a/k_N. Another possibility would have been to use y/a as the coordinate since the boundary layer extends further away from the bed with increasing a/k_N-ratios. The figure shows that the overall time variation is the same in all levels. Twice every period the eddy viscosity attains a minimum value of zero. It then increases rapidly to reach a maximum value whereafter there is a decrease to the next minimum value. This variation can also be found from simple models like Fredsøe's. But since they take ε as being proportional with U_* the eddy viscosity will vanish in all levels simultaneously when U_* is zero. We see from Fig. 4.15 that the results from BLOBAK contain a phase shift between zero-values of ε in different levels.

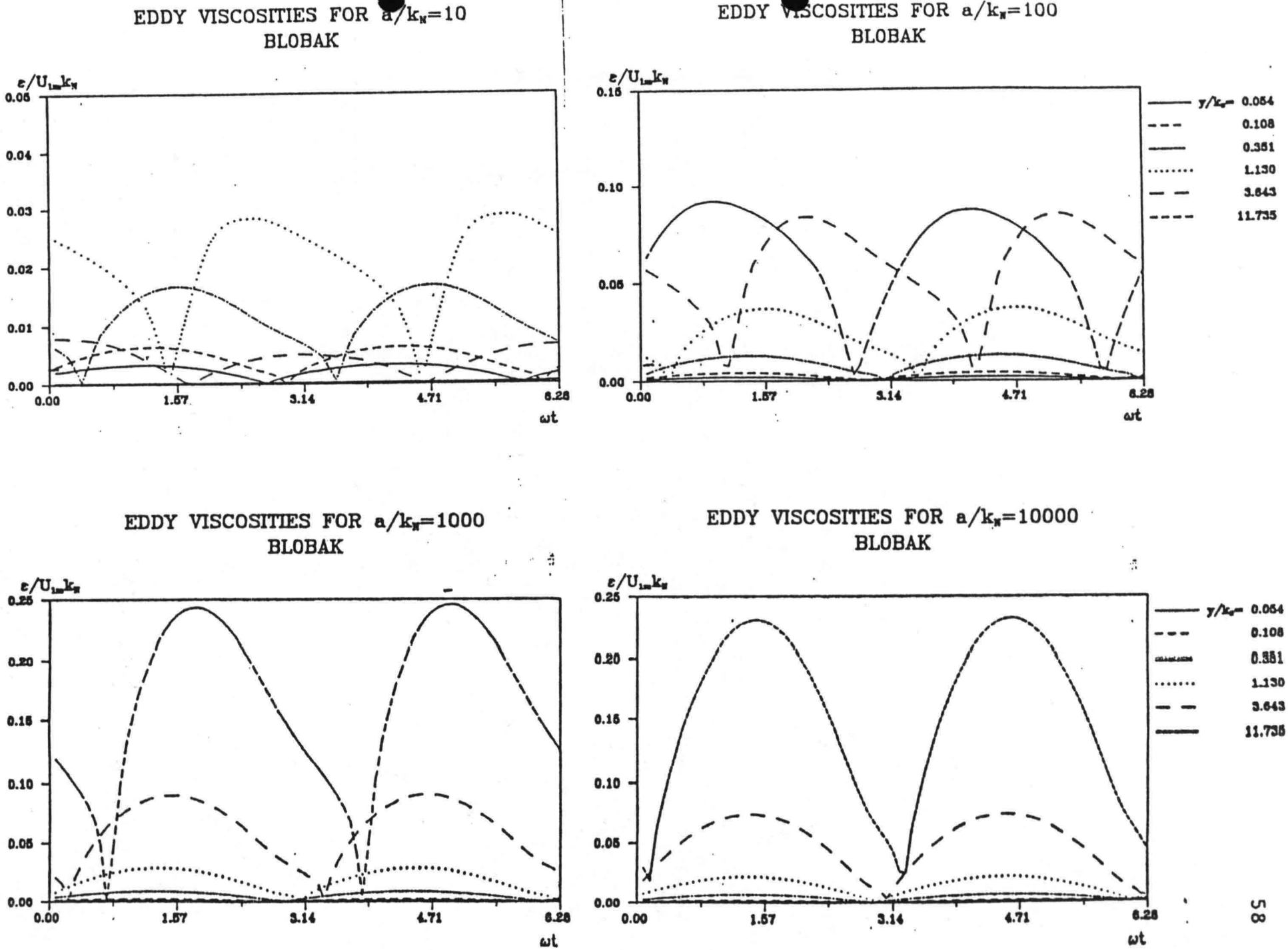

Fig. 4.15 Timeseries for the eddy viscosity.

BLOBAK compares with the experimental results and with the time-invariant eddy viscosity distribution that Myrhaug [32] used in his two-layer model. These variations are depicted in Fig. 4.17. In all cases there is good agreement close to the bed. Further away it appears that BLOBAK overestimates the mean eddy viscosity in comparison with measurements whereas it is close to Myrhaug's (solid line). The results from BL1PJ are discussed in section 5.5.

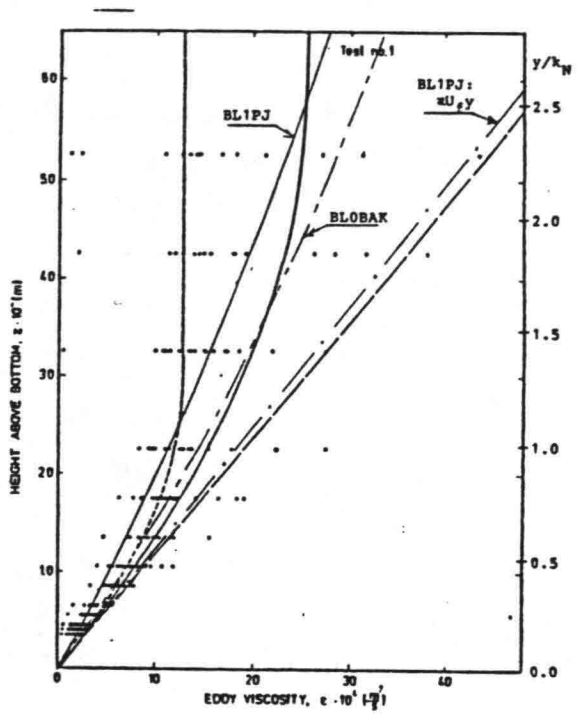

Fig. 4.17 Comparison of mean eddy viscosity with Myrhaug

Consequently it is justified that the two models yield approximately the same velocity field as was noticed previously.

To end the discussion of the eddy viscosity the wave viscosity distribution for $a/k_N = 124$ is shown in Fig. 4.18 together with the results found by Lundgren [29]. It is seen how good agreement is found for very small values of y/k_N. Thereafter BLOBAK overestimates η_w substantially. Again it may be questionable whether the experimental data are reliable. ε is determined as the ratio between two very small quantities when the shear stress becomes small.

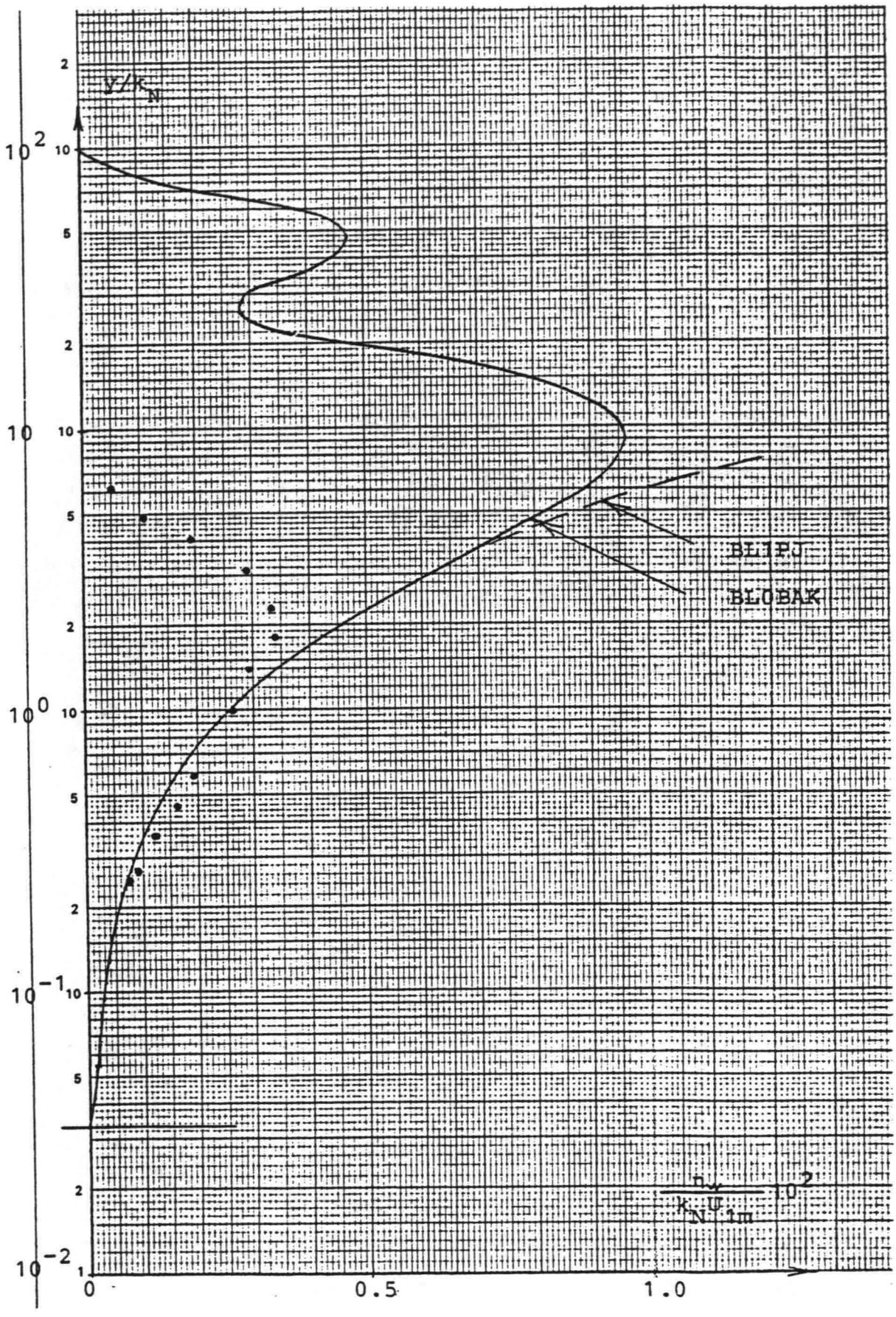

Fig. 4.18 Wave viscosity profile for $a/k_N = 124$

5. BL1PJ, A ONE-EQUATION MODEL

5.1 Introduction

In order to compensate for the shortcomings of the mixing-length theory a one-equation model is developed in this chapter. Such a model includes the calculation of the energy of the turbulent velocity fluctuations from the transport equation for turbulent kinetic energy. The eddy viscosity is no longer taken as a function of the mean velocity field. Consequently the eddy viscosity does not necessarily vanish, when the mean velocity gradient is zero. Further, the transport equation for TKE will model the memory in the turbulence together with diffusion processes. These effects are not comprised in the mixing-length theory, where local equilibrium in TKE is assumed.

5.2 Construction of model

5.2.1 The equations

As was the case with the zero-equation model, the flow equation for the mean velocity field is

$$\frac{\partial U}{\partial t} = \frac{\partial U_e}{\partial t} + \frac{\partial}{\partial y}\left(\varepsilon \frac{\partial U}{\partial y}\right) \qquad (5.1)$$

The flow is assumed to be uniform. The ambient flow is described by first order theory. Hence the convective terms can be neglected. The eddy viscosity ε is expressed as a product of a velocity scale and a length scale

$$\varepsilon = \sqrt{k}\, l \qquad (5.2)$$

in which k is the turbulent kinetic energy defined as

$$k = \frac{1}{2}\overline{u_i u_i} \qquad (5.3)$$

and l is the length scale. Close to the wall in a rough boundary layer l behaves as

$$l = c_3 y \qquad (5.4)$$

while l further away often is taken to be constant. c_3 is a constant which is evaluated later. In this model (5.4) is used to describe l throughout the boundary layer.

To solve eq. (5.1) the k-distribution must be known. It is determined from the solution to the transport equation for the turbulent kinetic energy. From chapter 2 it is known that this equation in a two-dimensional shear boundary layer has the form

$$\frac{\partial k}{\partial t} = \frac{\partial}{\partial y}\left[\frac{\varepsilon}{\sigma_k}\frac{\partial k}{\partial y}\right] + \varepsilon\left(\frac{\partial U}{\partial y}\right)^2 - c_1\frac{k^{3/2}}{l} \qquad (5.5)$$

Rate of change = DIFF + PROD - DISS

The convective terms have been neglected in accordance with eq. (5.1). In eq. (5.5) σ_k and c_1 are empirical constants, the values of which will be enumerated later.

It should be mentioned that if the diffusion term in eq. (5.5) is neglected, then the partial differential equation is reduced to an ordinary differential equation.

5.2.2 Boundary conditions

The equations (5.1) and (5.5) are two coupled second order partial differential equations in U and k. To form a solvable problem proper boundary and initial conditions must be specified. The same conditions are associated with the flow equation as in the preceeding chapter.

(i) At the bed the no-slip condition applies, i. e.

$$U(y=y_b)=0 \qquad (5.6)$$

The bed coordinate is chosen according to the ideas outlined in chapter 4. y_b is taken as $y_b = k_N/30$.

(ii) At the upper boundary of the region of computation is the velocity equal to that of the ambient flow

$$U(y=y_\infty)=U_\infty \tag{5.7}$$

y_∞ must be large enough to ensure that all turbulent quantities vanish at the boundary towards the ambient potential flow.

(iii) The initial velocity distribution can be either a stagnant flow or a distribution obtained in a previous run. Since we only consider a periodic ambient velocity. Hence it is required that the solution has this periodicity, i.e.

$$U(y,t+T)=U(y,t)$$

The velocity of the ambient flow is according to the first order theory given by

$$U_\infty(t)=U_1 \cdot \sin(\omega t) \tag{4.11}$$

Associated with the k-equation are the following initial and boundary conditions.

(i) The turbulent velocity fluctuations are not vanishing at a hydraulically rough bed as would be the case with a smooth wall, where the viscous stresses transfer the Reynolds stresses through the viscous sublayer. Close to the wall the Reynolds stresses are nearly constant. In this region diffusion can be neglected. When k is assumed to attain a quasi-static value at the wall, local equilibrium prevails. It follows that $\tau \sim k$, cf. section 5.2.3. Hence in this model we apply the following boundary condition for k at the wall

$$k_b = \frac{1}{\sqrt{c_1}} \left| \tau_b / \rho \right| \tag{5.8}$$

See e.g. Rodi [36] for a discussion of this boundary condition.

(ii) At the top of the computational region the turbulent quantities disappear. For k this means

$$k(y=y_{\delta})=0 \tag{5.9}$$

(iii) The initial k-distribution must match with the given initial distribution for the velocity.

5.2.3 Local equilibrium in TKE

If production is equal to dissipation eq. (5.5) reduces to

$$\varepsilon\left(\frac{\partial U}{\partial y}\right)^2 = C_1 \frac{k^{3/2}}{l} \tag{5.10}$$

Taking advantage of eq. (5.2) we obtain

$$\varepsilon^2\left(\frac{\partial U}{\partial y}\right)^2 = C_1 k^2 \tag{5.11}$$

When ε is substituted for k the following equatiom emerges analogous to the mixing-length theory

$$\varepsilon = \frac{1}{\sqrt{C_1}} l^2 \left|\frac{\partial U}{\partial y}\right| \tag{5.12}$$

Agreement between eq. (5.12) and the mixing-length theory, eq. (4.4), is achieved when

$$C_3 = \varkappa \sqrt[4]{C_1} \tag{5.13}$$

Rearranging eq. (5.11) gives

$$k = \frac{1}{\sqrt{C_1}} \varepsilon \left|\frac{\partial U}{\partial y}\right| \sim |\tau_b/\rho| \tag{5.14}$$

To summarize, it has been shown that the assumption of local equilibrium of TKE in the boundary layer is equivalent with the mixing-length theory. Furthermore, according to eq. (5.14) k and τ are proportional in a local equilibrium layer. By neglecting the time derivative of k and the diffusion term in eq. (5.5) the

BL1PJ model is similar to the BL0BAK model discussed in chapter 4.

5.2.4 The choise of empirical constants

The present turbulence model contains three empirical constants c_1, c_3 and σ_k. c_1 appears in the dissipation term. According to Launder and Spalding [28] we use

$$c_1 = 0.08 \tag{5.15}$$

The value of c_3 is determined given the requirement that the one-equation model should be reduced to the mixing-length model in the simple case. It follows from eq. (5.13) that

$$C_3 = 0.40 \cdot \sqrt{0.08} = 0.213 \tag{5.16}$$

σ_k is contained in the diffusive term and is effectively proportional to the inverse of a diffusion constant. Hanjalic and Launder [13] have optimized σ_k so that the best possible agreement between calculations and experimental results was achieved for a number of different flows. Their results give σ_k the value

$$\sigma_k = 1.25 \tag{5.17}$$

Later Launder and Spalding [28] make reference to the paper by Hanjalic and Launder and give the similar value of

$$\sigma_k = 1.0 \tag{5.18}$$

Reynolds [35] gives a description of the well known STAN5 boundary layer flow model. In this σ_k is taken as

$$\sigma_k = 2.37 \tag{5.19}$$

The value is obtained by matching results of a zero-equation and a one-equation model.

In BL1PJ the value stated by Launder and Spalding (5.18) is used since it is the commonly accepted value.

Sensibility studies have not been performed in order to see consequences of small changes in the values of the empirical constants.

5.3 Numerical solution

5.3.1 Strategy for the numerical solution

An analytical solution to eqs. (5.1) and (5.5) and the associated conditions cannot be found. Consequently a numerical solution is sought. In analogy with the zero-equation model a finite difference method is applied.

The flow equation and the transport equation for TKE are coupled and should be solved simultaneously. However, results from the zero-equation model indicate that variations in the eddy viscosity are less important for the velocity distribution than the opposite. The k-equation is nonlinear and requires an iterative solution procedure at each timestep. These two effects are combined to form the solution procedure at the timestep t_i as depicted in Fig. 5.1.

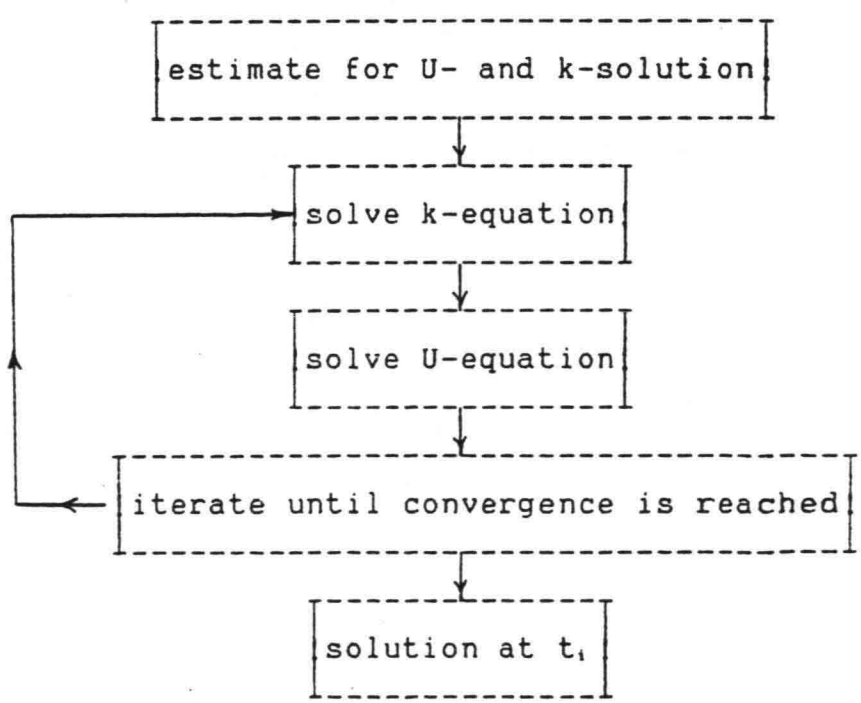

Fig. 5.1 Solution procedure

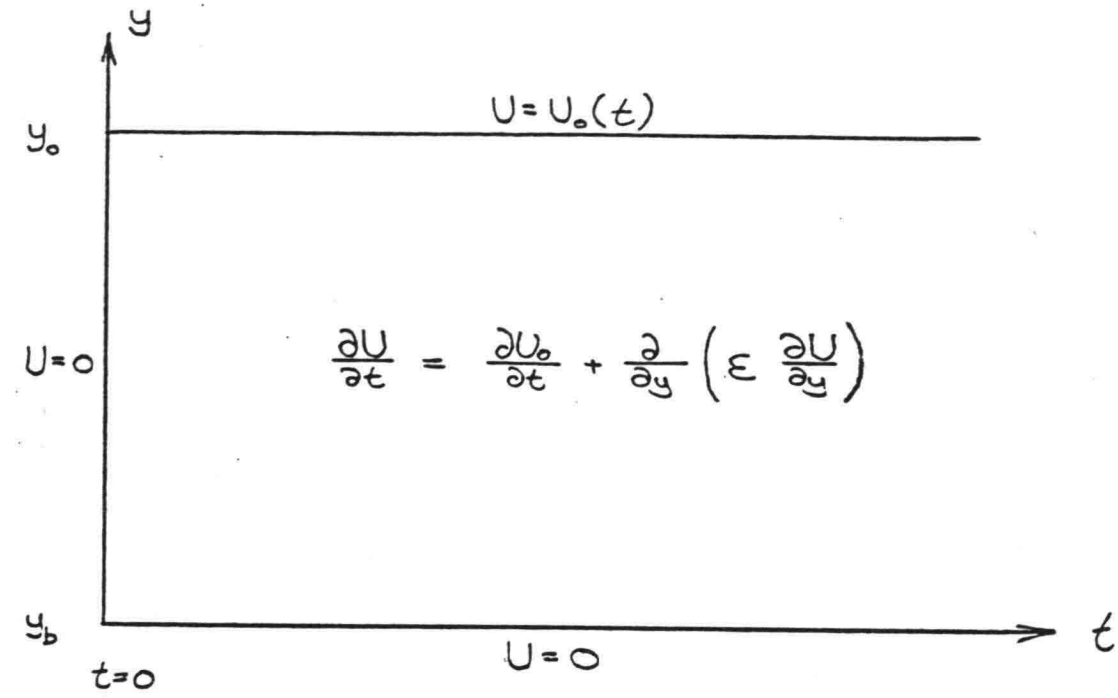

Fig. 5.2 (a) Initial value problem for U

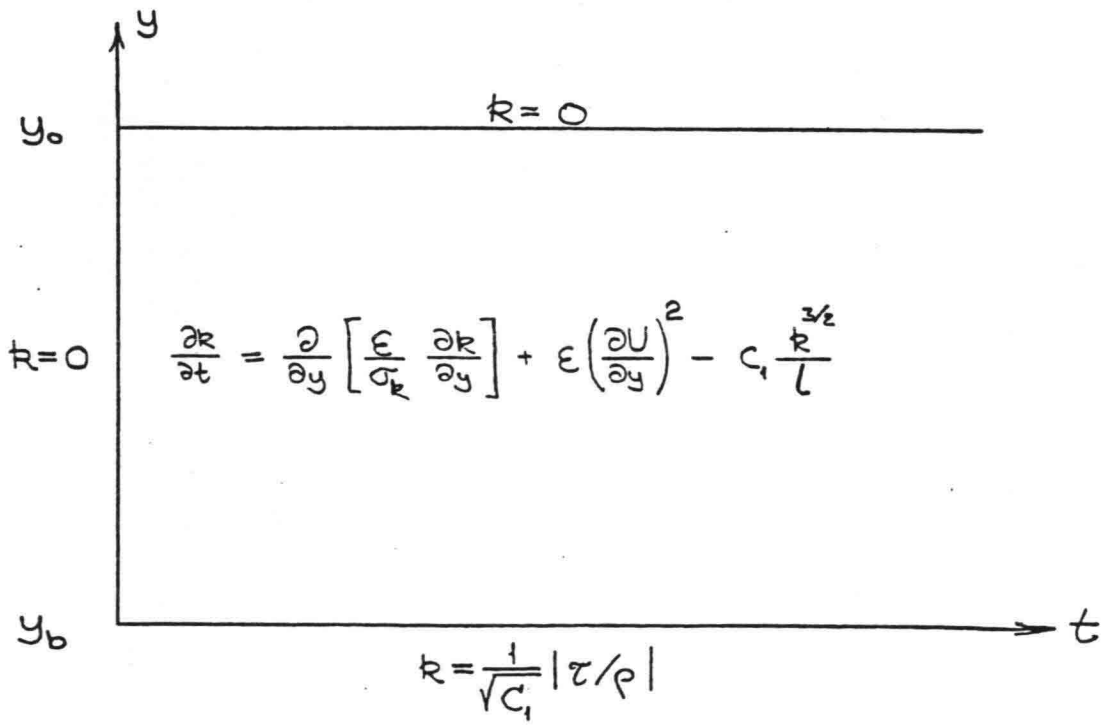

Fig. 5.2 (b) Initial value problem for k

In the proceeding sections it is outlined how the equations are solved independently given the distribution of the 'opposite' quantity. For instance the solution of the flow equation with a known distribution of TKE.

Both initial value problems are illustrated in Fig. 5.2.

5.3.2 Solution of the flow equation

The flow equation

$$\frac{\partial U}{\partial t} = \frac{\partial U_o}{\partial t} + \frac{\partial}{\partial y}\left(\varepsilon \frac{\partial U}{\partial y}\right) \tag{5.1}$$

is a second order partial differential equation of the parabolic type like for instance the well known diffusion equation.

The solution to (5.1) together with the boundary conditions derived in section 5.2.2 is found using the finite difference method. The principles are discussed elsewhere in this report. As eq. (5.1) is linear with a given ε-distribution also the resultant difference equation will be linear. Hence the solution is found directly from the system of linear difference equations.

The mesh points in the computational region are distributed using the transformation (4.19) to give the smallest mesh size close to the solid boundary. In BLOBAK the equations are solved in the transformed coordinate system. In this case we shall operate in the original system taking into account the varying mesh size. The mesh is shown in Fig. 5.3. Notice the small differences in e.g. the numbering between Figs. 4.3 and 5.3.

The individual terms in the differential equation are approximated by

$$\frac{\partial U}{\partial t} \simeq \frac{1}{\Delta t}\left(U_i^j - U_{i-1}^j\right) \tag{5.20}$$

$$\frac{\partial U_o}{\partial t} \simeq \frac{1}{\Delta t}\left(U_{oj} - U_{oj-1}\right) \tag{5.21}$$

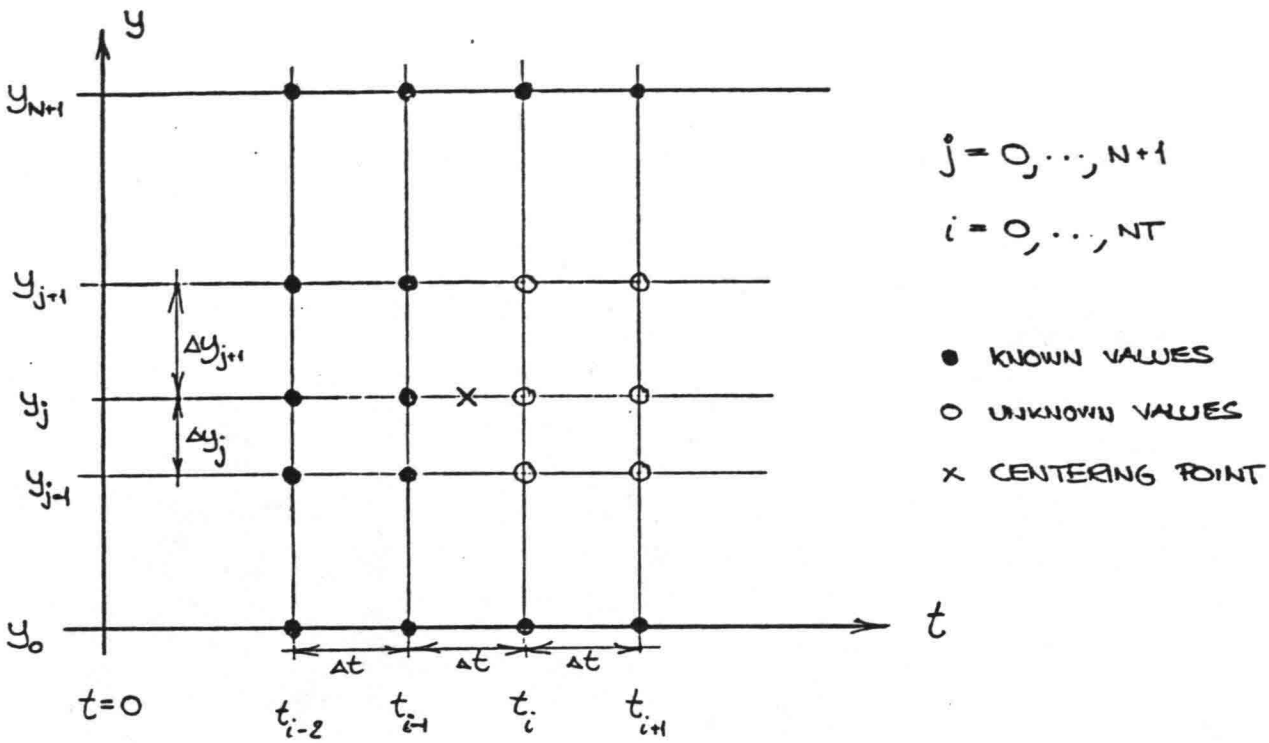

Fig. 5.3 FDM-mesh

$$\frac{\partial}{\partial y}\left(\varepsilon\frac{\partial U}{\partial y}\right) \simeq \frac{1}{\frac{1}{2}(\Delta y_{j+1}+\Delta y_j)}\left[\varepsilon_i^{j+\frac{1}{2}}\frac{1}{\Delta y_{j+1}}(U_i^{j+1}-U_i^j) - \varepsilon_i^{j-\frac{1}{2}}\frac{1}{\Delta y_j}(U_i^j-U_i^{j-1})\right] \quad (5.22)$$

where

$$\varepsilon_i^{j+\frac{1}{2}} = \frac{1}{2}(\varepsilon_i^{j+1}+\varepsilon_i^j) \quad \& \quad \varepsilon_i^{j-\frac{1}{2}} = \frac{1}{2}(\varepsilon_i^j+\varepsilon_i^{j-1}) \quad (5.23)$$

It is possible to determine (5.21) exact as

$$\frac{\partial U_0}{\partial t} = \omega\cos(\omega t) \quad (5.24)$$

since the ambient flow velocity is given by eq. (4.11). However, the use of (5.21) ensures consistency between the differential equation and the difference equation. The right-hand side of (5.1) is weighed between the timesteps t_{i-1} and t_i according to

$$HS=(1-\alpha)HS_{i-1}+\alpha HS_i \quad (5.25)$$

α=0 corresponds to an explicit method of solution, whereas α=1 yields a fully implicit method. When α=0.5 eq. (5.25) is similar to the Crank-Nicolson method, see e.g. [33].

The difference approximation to (5.1) in the point (y_j, t_i) is in the usual dimensionless variables found as

$$f_{u_j} = -\frac{1}{\Delta t}\left(U_i^j - U_{i-1}^j\right) + \frac{1}{\Delta t}\left(U_{0,i} - U_{0,i-1}\right) + \frac{1}{\frac{1}{2}(\Delta y_{j+1} + \Delta y_j)} \frac{a}{R_M} \Bigg\{$$

$$(1-\alpha)\left[\varepsilon_{i-1}^{j+\frac{1}{2}} \frac{U_{i-1}^{j+1} - U_{i-1}^j}{\Delta y_{j+1}} - \varepsilon_{i-1}^{j-\frac{1}{2}} \frac{U_{i-1}^j - U_{i-1}^{j-1}}{\Delta y_j}\right]$$

$$+ \alpha\left[\varepsilon_i^{j+\frac{1}{2}} \frac{U_i^{j+1} - U_i^j}{\Delta y_{j+1}} - \varepsilon_i^{j-\frac{1}{2}} \frac{U_i^j - U_i^{j-1}}{\Delta y_j}\right]\Bigg\}_j \quad j=1,\ldots,N \tag{5.26}$$

Together the equations for all the interior mesh points form a system of linear equations of the tridiagonal type

$$A^j U_i^{j-1} + B^j U_i^j + C^j U_i^{j+1} = D^j{}_j \quad j=1,\ldots,N \tag{5.27}$$

The coefficients A^j, B^j, C^j and D^j are given by

$$A^j = -\frac{1}{\frac{1}{2}(\Delta y_{j+1} + \Delta y_j)} \alpha \varepsilon_i^{j-\frac{1}{2}} \frac{1}{\Delta y_j} \tag{5.28}$$

$$B^j = \frac{R_M}{a}\frac{1}{\Delta t} + \frac{1}{\frac{1}{2}(\Delta y_{j+1} + \Delta y_j)} \alpha \left(\varepsilon_i^{j+\frac{1}{2}} \frac{1}{\Delta y_{j+1}} + \varepsilon_i^{j-\frac{1}{2}} \frac{1}{\Delta y_j}\right) \tag{5.29}$$

$$C^j = -\frac{1}{\frac{1}{2}(\Delta y_{j+1} + \Delta y_j)} \alpha \varepsilon_i^{j+\frac{1}{2}} \frac{1}{\Delta y_{j+1}} \tag{5.30}$$

$$D^j = \frac{R_M}{a}\frac{1}{\Delta t} U_{i-1}^j + \frac{R_M}{a}\frac{1}{\Delta t}\left(U_{0,i} - U_{0,i-1}\right)$$

$$+ \frac{(1-\alpha)}{\frac{1}{2}(\Delta y_{j+1} + \Delta y_j)}\left[\varepsilon_{i-1}^{j+\frac{1}{2}} \frac{U_{i-1}^{j+1} - U_{i-1}^j}{\Delta y_{j+1}} - \varepsilon_{i-1}^{j-\frac{1}{2}} \frac{U_{i-1}^j - U_{i-1}^{j-1}}{\Delta y_j}\right] \tag{5.31}$$

Due to straining of the wall coordinate the coefficient matrix in (5.27) will not be symmetric. The equations are, nonetheless, solved efficiently using the tridiagonal-algorithm also used in BLOBAK.

The explicit solution for U is used as a first guess for the solution to a timestep and is given by

$$U_i^j = U_{i-1}^j + (U_{0,i} - U_{0,i-1}) + \frac{\Delta t}{\frac{1}{2}(\Delta y_{j+1} + \Delta y_j)} \frac{a}{R_N} \left[\varepsilon_{i-1}^{j+\frac{1}{2}} \frac{U_{i-1}^{j+1} - U_{i-1}^j}{\Delta y_{j+1}} - \varepsilon_{i-1}^{j-\frac{1}{2}} \frac{U_{i-1}^j - U_{i-1}^{j-1}}{\Delta y_j} \right] \quad (5.32)$$

5.3.3 Solution of the k-equation

Like the flow equation the transport equation for turbulent kinetic energy

$$\frac{\partial k}{\partial t} = \frac{\partial}{\partial y} \left[\frac{\varepsilon}{\sigma_k} \frac{\partial k}{\partial y} \right] + \varepsilon \left(\frac{\partial U}{\partial y} \right)^2 - c_1 \frac{k^{3/2}}{l}$$

is also of the parabolic type. FDM is used to find the solution in the same region as for the flow equation. Now, since the differential equation is nonlinear the corresponding difference equation contains nonlinearities as well.

The diffusive term can be elaborated to yield

$$\frac{\partial k}{\partial t} = \frac{1}{\sigma_k} \left[\sqrt{k} \frac{\partial k}{\partial y} \frac{\partial l}{\partial y} + l \frac{\partial \sqrt{k}}{\partial y} \frac{\partial k}{\partial y} + \sqrt{k}\, l \frac{\partial^2 k}{\partial y^2} \right] + \varepsilon \left(\frac{\partial U}{\partial y} \right)^2 - c_1 \frac{k^{3/2}}{l} \quad (5.33)$$

The time derivative is approximated as usually

$$\frac{\partial k}{\partial t} \simeq \frac{1}{\Delta t} \left(k_i^j - k_{i-1}^j \right) \quad (5.34)$$

while the remaining derivatives are substituted by

$$\frac{\partial k}{\partial y} \simeq \frac{1}{2} \left\{ \frac{k_i^{j+1} - k_i^j}{\Delta y_{j+1}} + \frac{k_i^j - k_i^{j-1}}{\Delta y_j} \right\} = F_i^j \quad (5.35)$$

$$\frac{\partial^2 k}{\partial y^2} \simeq \frac{1}{\frac{1}{2}(\Delta y_{j+1} + \Delta y_j)} \left\{ \frac{k_i^{j+1} - k_i^j}{\Delta y_{j+1}} - \frac{k_i^j - k_i^{j-1}}{\Delta y_j} \right\} = A_i^j \quad (5.36)$$

$$fk_j = 0 \qquad j \quad j=1,\ldots,N \tag{5.39}$$

The system of linear equations contained in Newton's method is

$$A_j^n \left(k_i^{j-1,n+1} - k_i^{j-1,n}\right) + B_j^n \left(k_i^{j,n+1} - k_i^{j,n}\right) + C_j^n \left(k_i^{j+1,n+1} - k_i^{j+1,n}\right) = D_j^n \tag{5.40}$$

where the coefficients can be derived from (5.39) by partial differentiation. They are given by

$$A_j^n = \frac{\partial fk_j}{\partial k_i^{j-1}} = -\frac{a}{k_N}\frac{\alpha}{\sigma_k}\sqrt{k_i^j}\,\frac{1}{2\Delta y_j}\left\{\left(\frac{\partial l}{\partial y}\right)_j + l_j\frac{F_i^j}{k_i^j} - 2l_j\frac{1}{\frac{1}{2}\left(\Delta y_{j+1}+\Delta y_j\right)}\right\} \tag{5.41}$$

$$\begin{aligned} B_j^n = \frac{\partial fk_j}{\partial k_i^j} = &-\frac{1}{t} + \frac{a}{k_N}\frac{\alpha}{\sigma_k}\left\{\frac{1}{2\sqrt{k_i^j}}\left(\frac{\partial l}{\partial y}\right)_j F_i^j + \sqrt{k_i^j}\left(\frac{\partial l}{\partial y}\right)_j \frac{1}{2}\left(\frac{1}{\Delta y_j} - \frac{1}{\Delta y_{j+1}}\right)\right. \\ &+ l_j F_i^j\,\frac{1}{2}\left(\frac{1}{\Delta y_j} - \frac{1}{\Delta y_{j+1}}\right)\frac{1}{\sqrt{k_i^j}} - \frac{1}{4}l_j\left(F_i^j\right)^2\frac{1}{\left(k_i^j\right)^{3/2}} \\ &\left. + \frac{1}{2\sqrt{k_i^j}}l_j A_i^j - \sqrt{k_i^j}\,\frac{1}{\frac{1}{2}\left(\Delta y_{j+1}+\Delta y_j\right)}\left\{\frac{1}{\Delta y_{j+1}} + \frac{1}{\Delta y_j}\right\}l_j\right\} \\ &+ \frac{a}{k_N}\alpha\left\{\frac{1}{2\sqrt{k_i^j}}\,l_j\left[\left(\frac{\partial U}{\partial y}\right)_i^j\right]^2 - \frac{3}{2}c_1\frac{\sqrt{k_i^j}}{l_j}\right\} \end{aligned} \tag{5.42}$$

$$C_j^n = \frac{\partial fk_j}{\partial k_i^{j+1}} = \frac{a}{k_N}\frac{\alpha}{\sigma_k}\sqrt{k_i^j}\,\frac{1}{2\Delta y_{j+1}}\left\{\left(\frac{\partial l}{\partial y}\right)_j + l_j\frac{F_i^j}{k_i^j} + 2l_j\frac{1}{\frac{1}{2}\left(\Delta y_{j+1}+\Delta y_j\right)}\right\} \tag{5.43}$$

and

$$D_j^n = -fk_j^n \tag{5.44}$$

As a first guess at the solution to the k-equation in the point (y_j, t_i) is used the explicit solution which follows from (5.38) when $\alpha=0$.

$$\begin{aligned} k_i^j = k_{i-1}^j + \frac{a}{k_N}\Delta t\sqrt{k_{i-1}^j}\left\{\frac{1}{\sigma_k}\left[c_3 F_{i-1}^j + \frac{1}{2}l_j F_{i-1}^j\frac{1}{k_{i-1}^j} + l_j A_{i-1}^j\right]\right. \\ \left. + l_j\left[\left(\frac{\partial U}{\partial y}\right)^j\right]^2 - c_1\frac{k_{i-1}^j}{l_j}\right\} \end{aligned} \tag{5.45}$$

5.3.4 Implementation

The one-equation model is implemented through the programme BL1PJ (Boundary Layer 1-Equation Peter Justesen). The structure of and operation procedure for BL1PJ are discussed in Appendix B.

5.3.5 Stability and accuracy of numerical scheme

The discussion in Chapter 4 concerning the zero-equation model applies also here. Practical details are described in section 5.5.6.

5.4 Quantities derived from the one-equation model

From the velocity and TKE distribution a number of characteristic properties of the boundary layer flow can be derived. The eddy viscosity is found directly using the Prandt-Kolmogorov relation

$$\varepsilon^* = \sqrt{k^*}\, l^* \tag{5.41}$$

Given ε^* the shear stresses are determined as

$$\tau^* = \varepsilon^* \frac{\partial U^*}{\partial y^*} \tag{5.42}$$

The bed shear stress τ_b^* is taken as the value found from linear extrapolation of the shear stress in the two mesh points adjacent to the bed point in the FDM-mesh. The friction velocity then becomes

$$U_f^* = \mathrm{sign}(\tau^*)\sqrt{|\tau^*|} \tag{5.43}$$

The friction coefficient f_c and the energy loss factor f_e are determined as described in chapter 4.

By definition the displacement thickness is given by

$$\delta^* = \int_{1/30}^{\infty} \left(1 - \frac{U^*}{U_0^*}\right) dy^* \tag{5.44}$$

while the momentum thickness is expressed by

$$\theta^* = \int_{1/30}^{\infty} \left(1 - \frac{U^*}{U_0^*}\right) \frac{U^*}{U_0^*} \, dy^* \qquad (5.45)$$

In the programme BL1PJ these two integrals are evaluated by numerical integration employing the trapezoidal rule.

$$\delta^* = \sum_{j=1}^{N+1} \left\{ \left(1 - \frac{U_i^{j-1}}{U_{0,i}}\right) + \left(1 - \frac{U_i^{j}}{U_{0,i}}\right) \right\} \cdot \Delta y_j^* / 2 \qquad (5.46)$$

$$\theta^* = \sum_{j=1}^{N+1} \left\{ \left(1 - \frac{U_i^{j-1}}{U_{0,i}}\right) \frac{U_i^{j-1}}{U_{0,i}} + \left(1 - \frac{U_i^{j}}{U_{0,i}}\right) \frac{U_i^{j}}{U_{0,i}} \right\} \cdot \Delta y_j^* / 2 \qquad (5.47)$$

The wave viscosity was defined by Lundgren [29]

$$\eta^* = \frac{\int_T |\tau^*| \, dt^*}{\int_T \left|\frac{\partial U^*}{\partial y^*}\right| dt^*} \qquad (5.48)$$

Until now all quantities could be found also in the zero-equation model. The inclusion of a transport equation for the turbulent kinetic energy allows us to study the budget for TKE within the boundary layer. For this purpose the terms in (5.5) are evaluated. The production term is given by

$$\text{PROD} = \varepsilon^* \left(\frac{\partial U^*}{\partial y^*}\right)^2 \qquad (5.46)$$

and the dissipation is

$$\text{DISS} = c_1 \frac{[k^*]^{3/2}}{l^*} \qquad (5.47)$$

while diffusion is found as

$$\text{DIFF} = \frac{\partial}{\partial y^*} \left[\frac{\varepsilon^*}{\sigma_k} \frac{\partial k^*}{\partial y^*} \right] \qquad (5.48)$$

To determine the diffusive fluxes of TKE we must reach back to the k-profiles. The model assumption is that the flux of k is proportional to the negative gradient of k and the eddy viscosity. This is expressed as

$$Q_x = - \frac{\varepsilon}{\sigma_k} \frac{\partial k}{\partial x} \qquad (5.49)$$

$$Q_y = -\frac{\varepsilon}{\sigma_k}\frac{\partial k}{\partial y} \qquad (5.50)$$

where Q_x and Q_y are fluxes of k in the x- and y-directions respectively. Reference is made to eq. (2.28). It is straightforward to find the vertical diffusive flux Q_z from the k-profile. In the derivation of the k-equation the horizontal diffusion was neglected as it was considered negligible. Even so we shall estimate it from the k-field. Consider a wave of constant form travelling at the velocity c. A new space variable ξ can be defined as

$$\xi = x - ct \qquad (5.51)$$

In the system (ξ, y), which is in fact a frame of reference that is moving along with the wave form, the flow is steady. From eq. (5.51) we deduce that

$$\frac{\partial}{\partial x} = -\frac{1}{c}\frac{\partial}{\partial t} \qquad (5.52)$$

The horizontal diffusive flux can then be estimated as

$$Q_x \cong \frac{1}{c}\,\frac{\varepsilon}{\sigma_k}\,\frac{\partial k}{\partial t} \qquad (5.53)$$

which can be rearranged

$$Q_x / U_{1m}^3 = \frac{k_N}{a}\,\frac{U_{1m}}{c}\,\frac{\varepsilon}{U_{1m} k_N \sigma_k}\,\frac{1}{\omega U_{1m}^2}\,\frac{\partial k}{\partial t} \qquad (5.54)$$

The wave celerity is made nondimensional with the ambient velocity amplitude. This parameter U_{1m}/c is a function of the wave height. In this work the wave motion is described by first order theory which is only valid for small amplitude waves. As a consequence U_{1m}/c is much smaller than unity. Further, if the advective terms had been retained in the equations the parameter U_{1m}/c would have been necessary.

The calculation of Q_x and Q_y takes place in a computer programme TKECIR which at the same time produces automatic plots of the circulation of TKE by means of arrows. The source programme is enclosed in Appendix C.

5.5 Results from the one-equation model

5.5.1 Local equilibrium in TKE

In section 5.2.3 it was shown how the one-equation model could be reduced to the zero-equation model compiled in chapter 4. The first step in the testing procedure for BL1PJ was therefore to verify that these two models yielded the same results within the range of discrepancy that should be anticipated due to the differences in the numerical methods. Indeed, relative deviations of less than 1 % were found on the velocity field and shear stresses. It was concluded on this basis that the local equilibrium option in the programme BL1PJ was working.

5.5.2 Velocities and shear stresses

Velocity amplitudes and phase shifts for $a/k_N = 124$ are shown in Fig. 5.4. The numerical details for this and other computations are discussed in a later section. A comparison of the graphs in Fig. 5.4 with the similar results from BLOBAK shown in Fig. 4.7 reveals that the velocity amplitude is exactly the same whereas the phase shift is slightly smaller. The maximum overshoot and the phase shift between the maximum defect velocity at the bottom and the maximum ambient velocity for different a/k_N-values are listed in Table 5.1. Generally the

a/k_N	U_{max}/U_{1a}	ϕ
10^0	1.054	35.1
10^1	1.047	27.9
10^2	1.038	21.2
10^3	1.031	15.8

Table 5.1 Maximum velocity overshoot and phase shift between max. defect velocity at bed and max. amb. velocity.

overshoot is less than found from BLOBAK. Similarly, the phase shift is smaller although only slightly. The same decrease in both overshoot and phase shift for increasing a/k_N is observed.

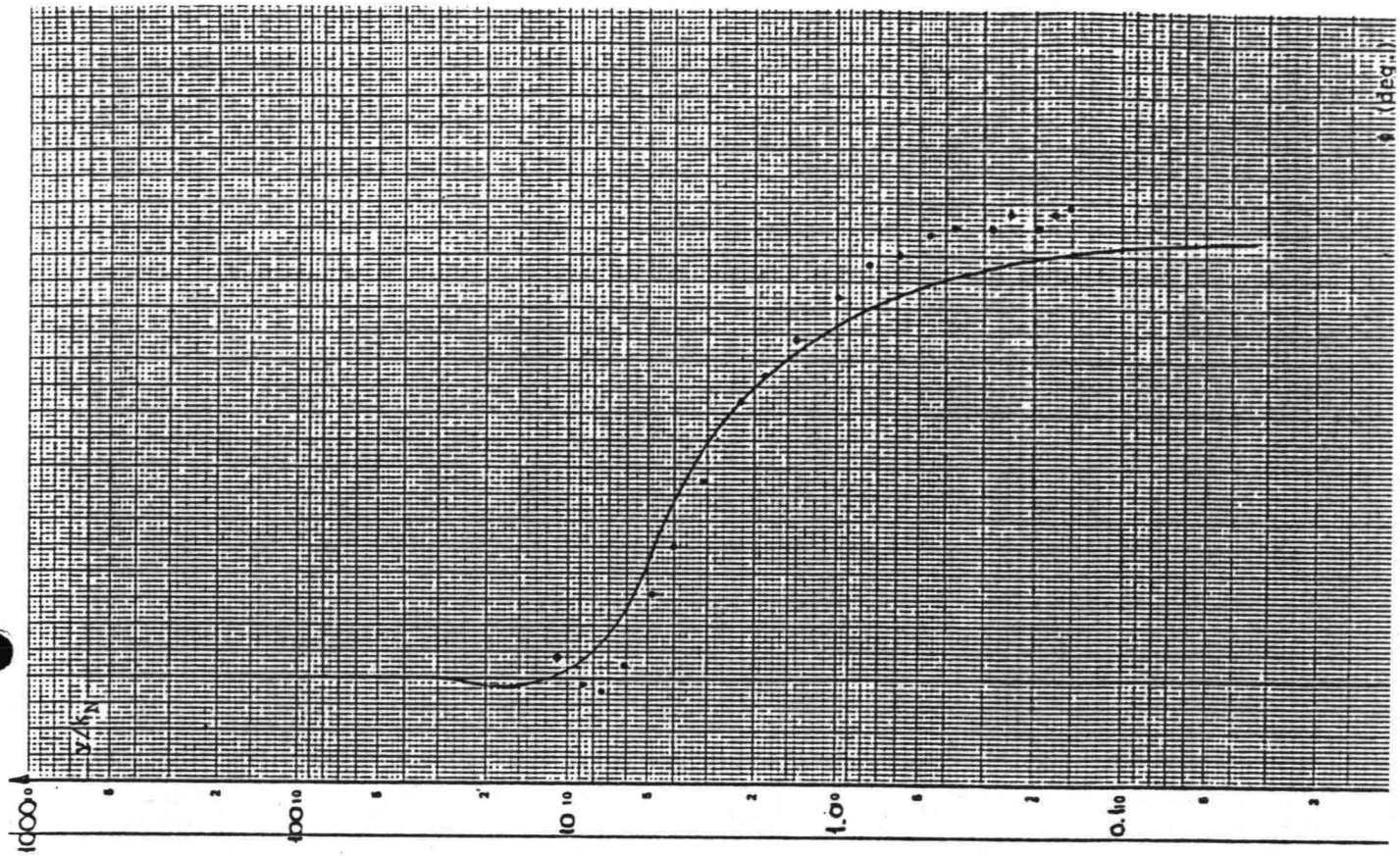

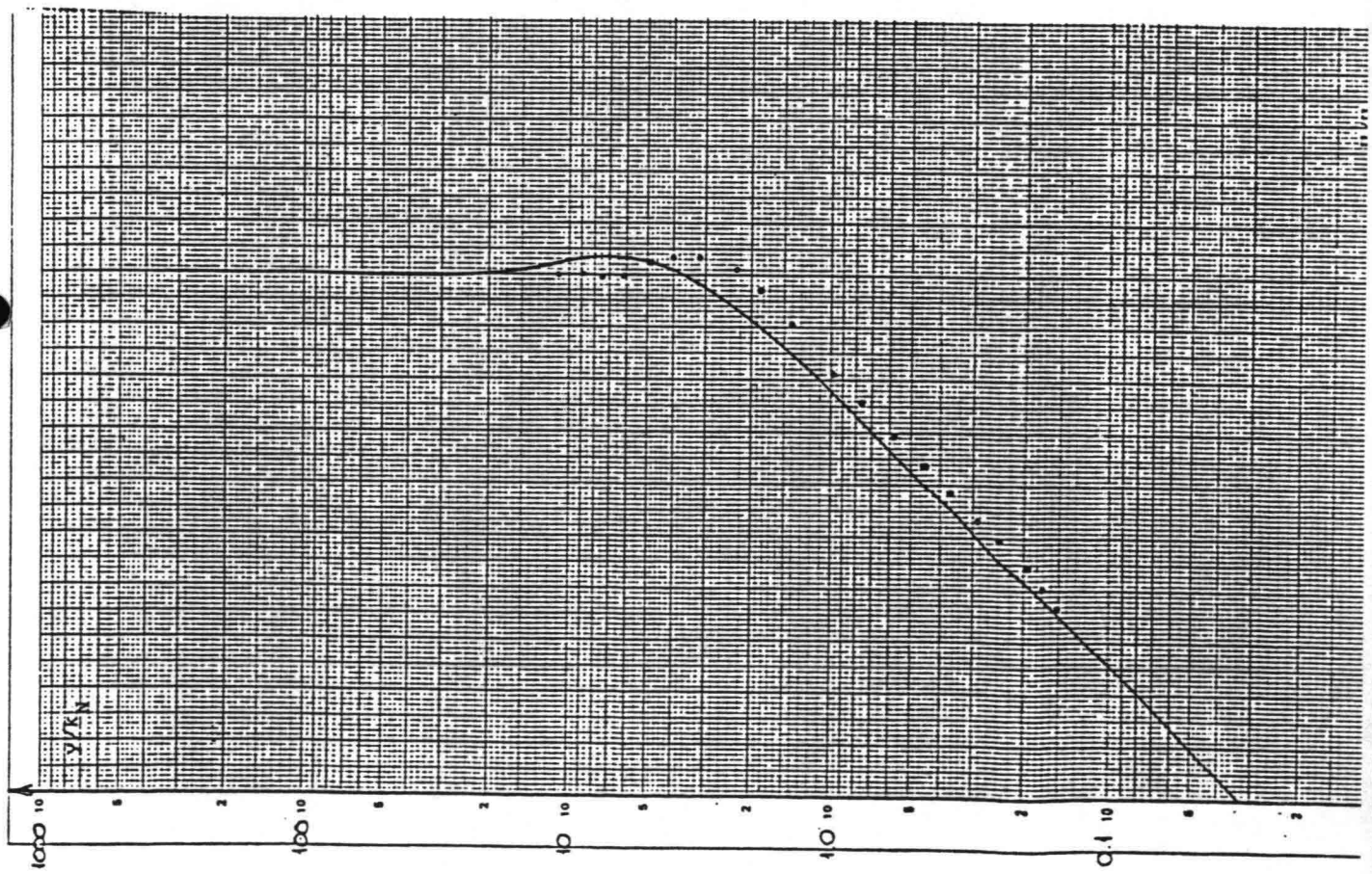

Fig. 5.4 Velocity amplitudes and phase shifts, $a/k_N = 124$

For all practical purposes it can be concluded that the two models yield the same velocity fields.

Next we will consider the shear stresses. The shear stress amplitudes in the case where $a/k_N = 124$ are depicted in Fig. 5.5. The values are consistently smaller than those by BLOBAK. The bed shear stress is some 3-4 % less. The general variation of τ is the same. From the bed shear stress variation the friction factor can be determined. In Table 5.2 the results from BL1PJ are shown. The energy loss factor and the ratio f_w/f_c are included as well. The smaller shear stress values affect both

a/k_N	f_w	f_c	f_w/f_c
10^0	0.149	0.132	1.12
10^1	0.0468	0.0441	1.06
10^2	0.0186	0.0182	1.02
10^3	0.00903	0.00906	1.00
28.4	0.030	0.029	1.04
124	0.0172	0.0170	1.02

Table 5.2 Computed values for f_w, f_c and f_w/f_c.

f_w and f_c whereas the ratio f_w/f_c fits well with experiments, cf. Table 4.2.

5.5.3 Boundary layer extension

The variation of the displacement thickness and the momentum thickness correspond to those obtained from BLOBAK. The explanation is, of course, the similarity in the velocity fileds from which both δ and θ are determined. In Table 5.3 we give the values for both these quantities at $\omega t = \pi/2$.

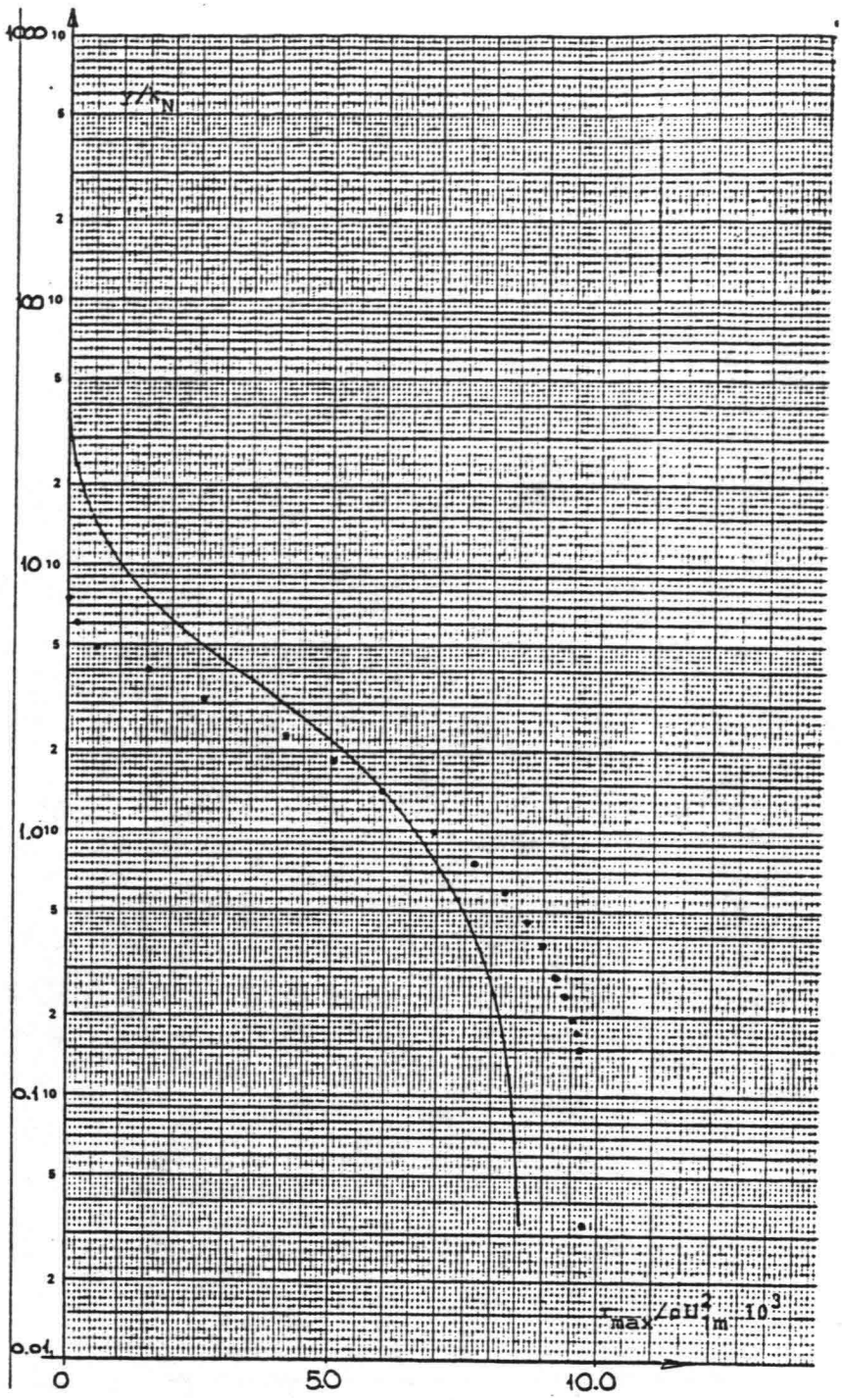

Fig. 5.5 Shear stress amplitudes for $a/k_N = 124$

a/k_N	δ/k_N	θ/k_N
10^0	0.045	0.012
10^1	0.119	0.036
10^2	0.366	0.127
10^3	1.366	0.540

Table 5.4 Displacement and momentum thicknesses.

5.5.4 Budget for turbulent kinetic energy

The major improvement in a one-equation model of turbulence is the ability to describe the generation, circulation and dissipation of the turbulent kinetic energy contained in the turbulent velocity fluctuations. In the mixing-length theory the TKE was ssumed to be in local equilibrium while a redistribution both in the time and space domain can now take place.

An example of calculated profiles for the turbulent kinetic energy for $a/k_N = 1000$ is depicted in Fig. 5.6. Close to the bed the k-distribution resembles the shear stress distribution since the TKE is in a quasi-equilibrium state in that region. This can be seen from Fig. 5.7 (a) where we have plotted the variation of the four terms in the k-equation, eq. (5.5), for four different phases during one half period. In all cases the production and dissipation terms are dominant very close to the wall. At $\omega t = 0(\pi)$, when the ambient flow velocity is zero, all terms small, and of equal magnitude. In the accelerating flow at $\omega t = \pi/4$ the turbulence is spreading from the bed area via the diffusion process. This continues well into the deccelerating part of the period where the boundary layer expands under influence of the adverse pressure gradient. From $\omega t = \pi/2$ where the pressure gradient is zero to $\omega t = 3\pi/4$ the diagrams show that the production and dissipation profiles are getting more flat which indicates the expansion of the boundary layer. Note that in all cases except when the flow is retarding at $\omega t = 3\pi/4$ there is a level in which the production is zero due to a vanishing velocity gradient. Similar diagrams for $a/k_N = 100$ are shown in Fig. 5.7 (b). Here almost the same picture is recognized, the difference being that the activity is closer to the bed.

Although the strength of the individual terms in the k-equation reflects the energy exchange in the boundary layer it is instructive to consider the diffusive fluxes of TKE. Plots of the circulation of TKE have been produced using the computer code TKECIR. First, in Fig. 5.8 (a) the case $a/k_N = 10^3$ and $U_{1.}/c = 0.353$ is shown. This choice of parameters corresponds to a situation where H=5.2 m, T= 8 sec., h= 20m and k_N = 0.005 m - a typical situation in Danish waters. Only the area up to 25 k_N or

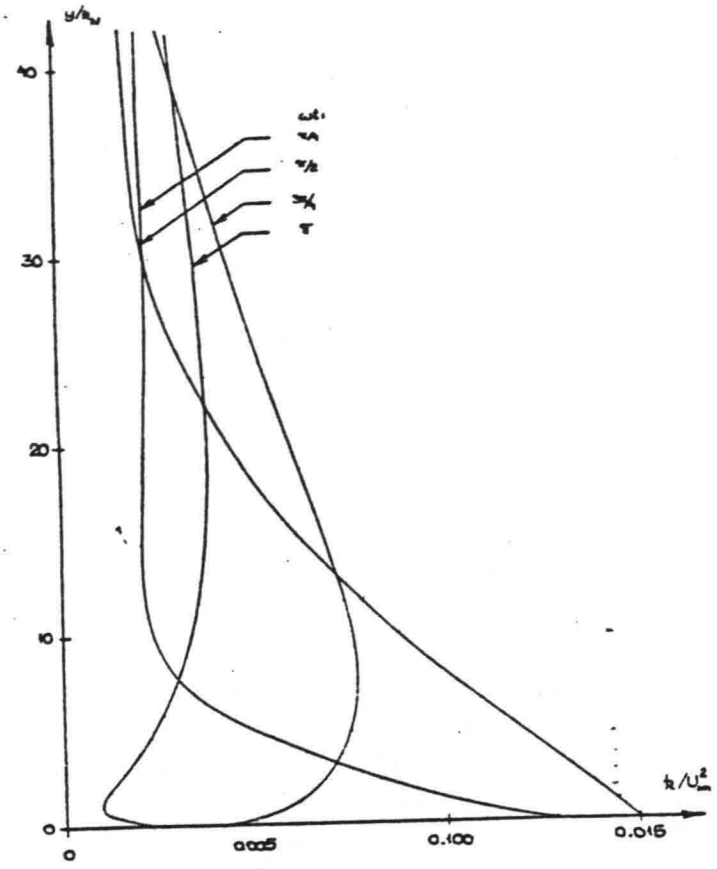

Fig. 5.6 Calculated profiles for turbulent kinetic energy, $a/k_N = 10^3$

0.125 m above the bottom is included in the figure. The wave on top of the diagram shows the variation of the surface elevaton and the ambient velocity at the bottom over one wave length. The flux is shown as vectors indicating direction and magnitude. Virtually all transport is in a vertical direction which means that the neglect of the advective terms and horizontal diffusion is apparently justified.

Just before the ambient velocity is a maximum the production is highest (cf. Fig. 5.6) and there is a significant outward flux of TKE. It is seen how this energy is gradually moving away towards areas with less production and available energy. The memory effect plays an important role in this exchange since energy is not only moved away from highly productive areas near the bed in a vertical direction but is also retained from times with higher production to the period of flow reversal where it is then dissipated. Around $\omega t = O(\pi)$ there is a small flux of TKE towards the bed. The explanation can be found in Fig. 5.6 which shows that the production has a minimum equal to zero close to the bed at this instant.

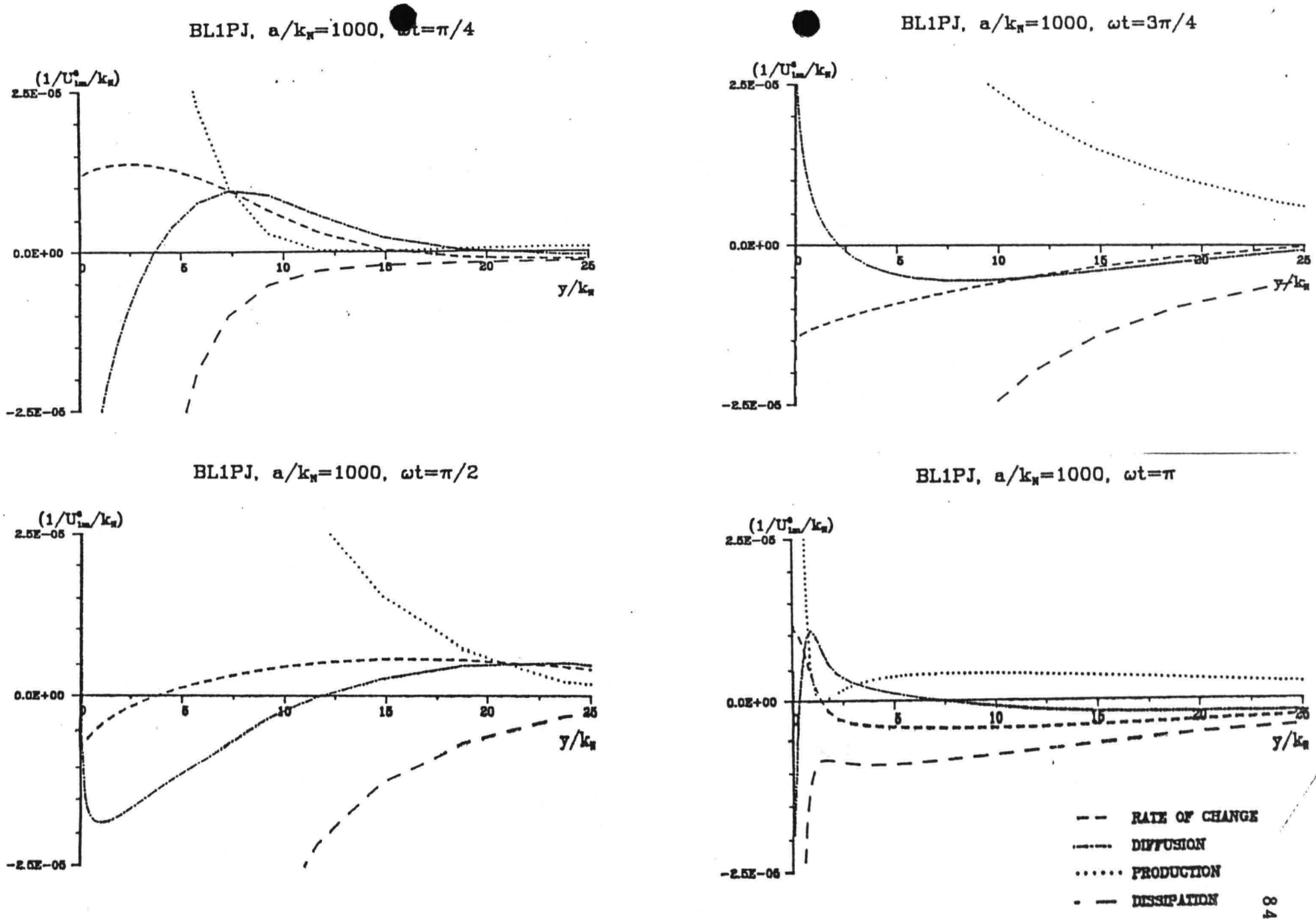

Fig. 5.7 (a) The terms in the k-equation for $a/k_N = 10^3$

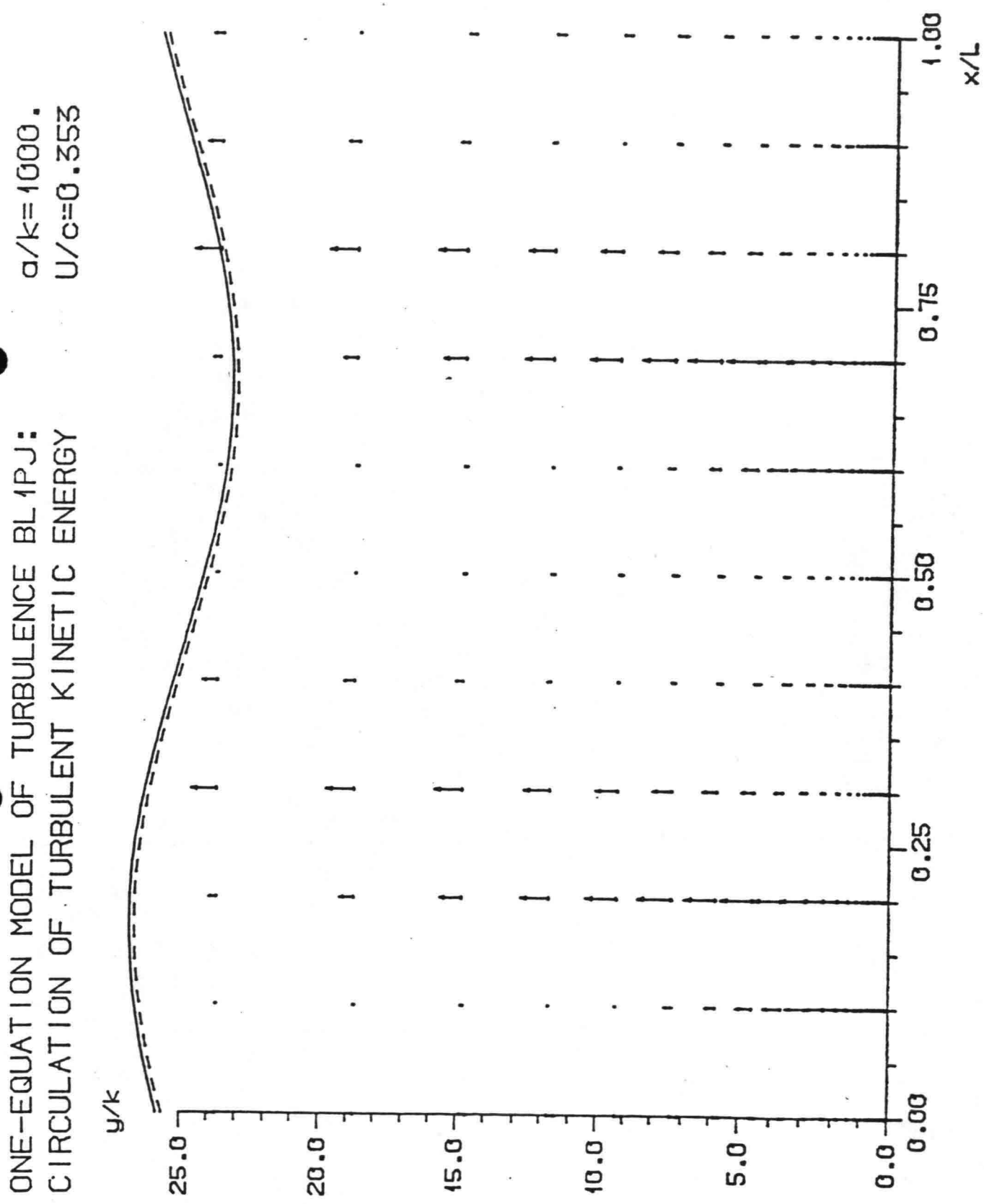

Fig. 5.8 (a) Circulation of TKE for $a/k_w = 10^3$

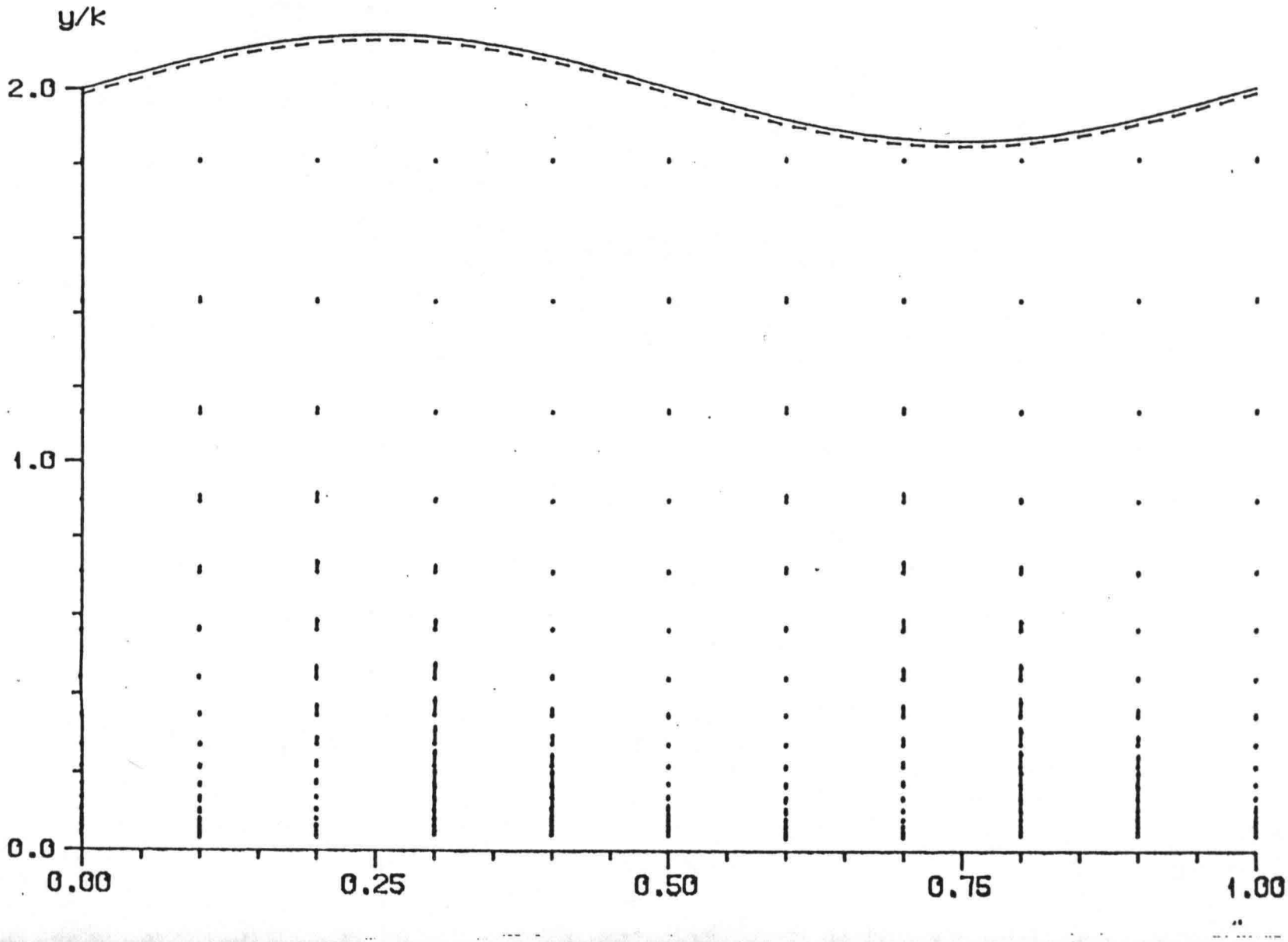

Fig. 5.8 (b) Circulation of TKE for $a/k_w = 10$

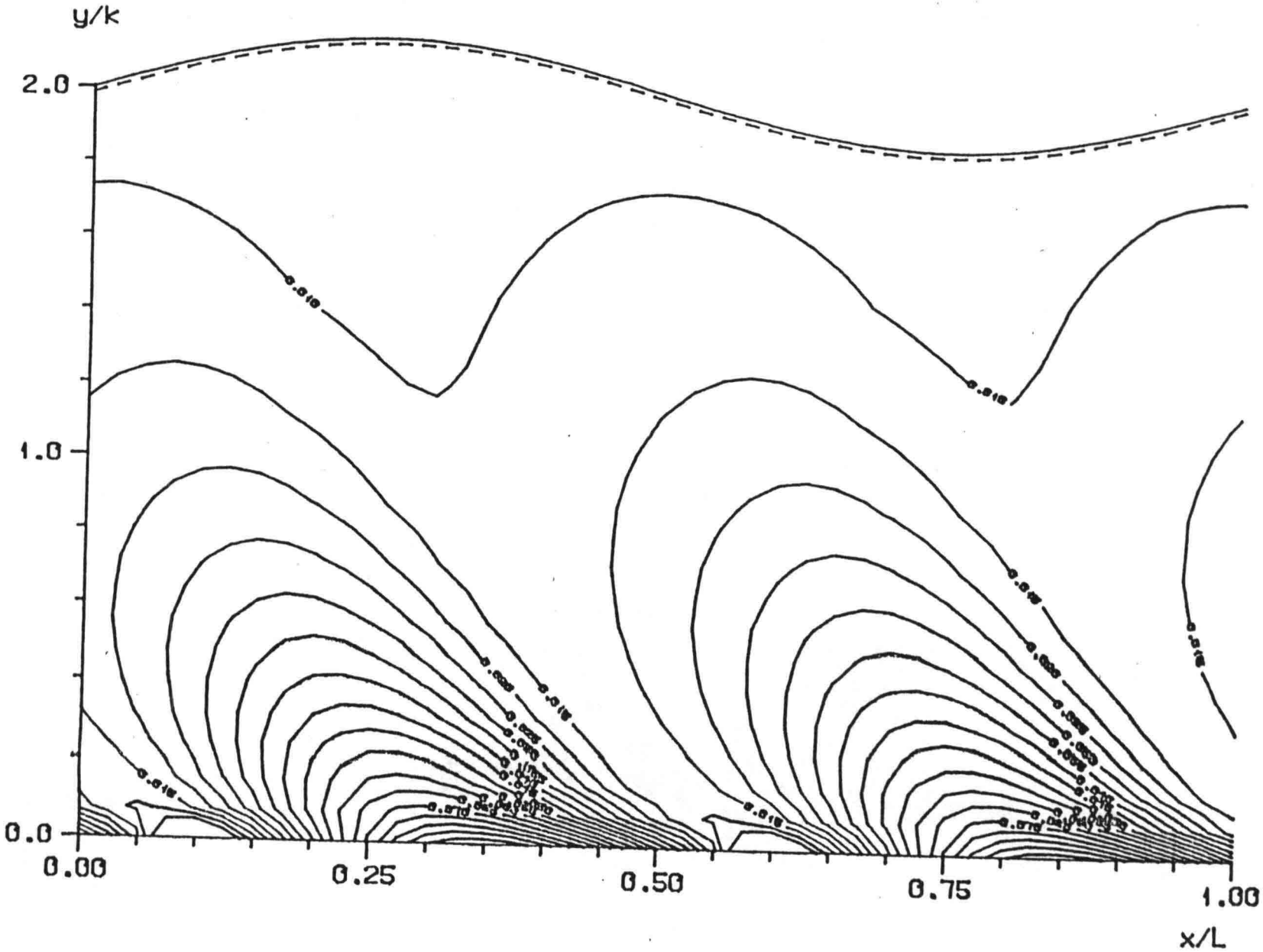

Fig. 5.9 (a) Contour plot of TKE for $a/k_w = 10$

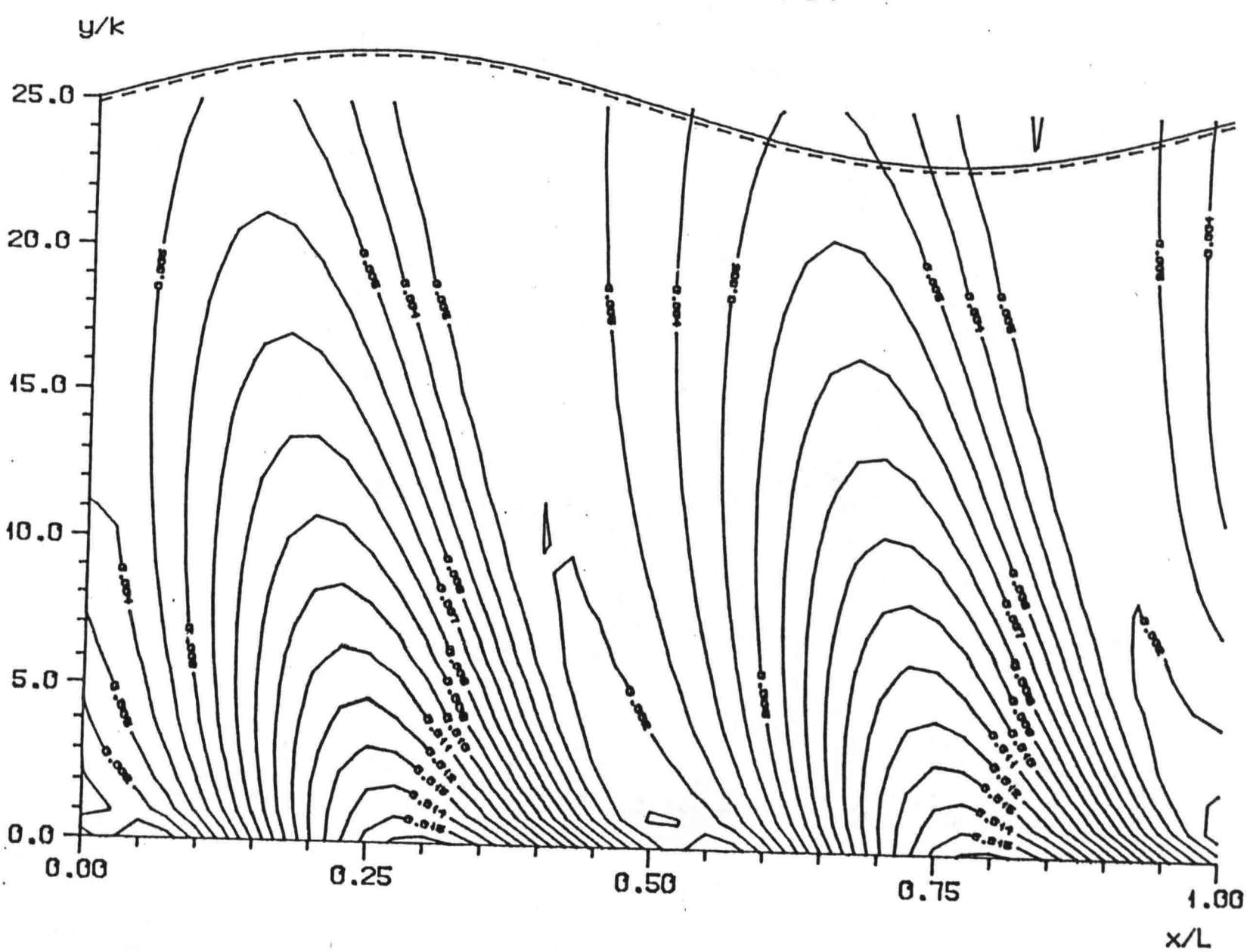

Fig. 5.9 (b) Contour plot of TKE for $a/k_w = 10^3$

In Fig. 5.8 (b) the case $a/k_N = 10$ is depicted.

To present the variation of k in a different and perhaps more comprehensive way contour plots are shown in Fig. 5.9 for the same two values of a/k_N, 10 and 10^3. They were produced by the programme TKECON, see Appendix C. The considerations above are here confirmed. It is seen how a combination of vertical diffusion and the memory effect give rise to a phase shift for the extreme values for k up through the boundary layer. As will be discussed later in connection with the eddy viscosity this phase shift is most pronounced for small a/k_N-values. This is due to a more even ratio between the period of oscillation and the time scale for the decay of turbulence. A decreasing variation over the period for the level of k at a given distance from the bed is found for smaller a/k_N-values.

Unfortunately no experimental data are available to facilitate an evaluation of the results for k in the rough wall case. The balance for TKE obtained is in good principal agreement with both theoretical and experimental results presented by Hanjalic and Launder [12] in a steady flow. One of their illustrations is reproduced in Fig. 5.10.

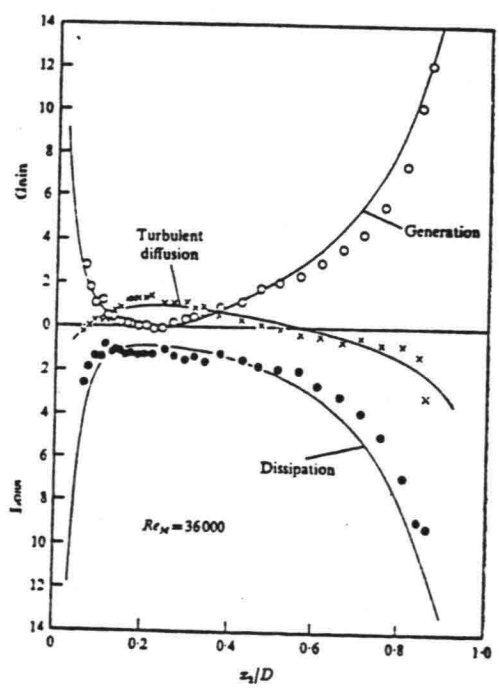

FIGURE 3. Turbulence energy balance in asymmetric channel flow. —, predictions. Experiment: ○, $-\overline{u_1 u_2}\, dU_1/dz_2)D/u_{\tau_B}^3$; ×, $-[d\frac{1}{2}(\overline{u_1^2 u_2})/dz_2]D/u_{\tau_B}^3$; ●, $\epsilon D/u_{\tau_B}^3$.

Fig. 5.10 Energy balance from Hanjalic and Launder [12] Steady turbulent flow in a channel.

Finally the turbulence intensity is considered. In some applications it might be useful to have information about the intensity of turbulent velosity fluctuations relative to the mean velocities. One example is the flow description around a seabed pipeline. Under certain conditions vortex shedding takes place which causes the pipeline to vibrate. But very high turbulence intensity in the boundary layer could affect the mechanism of vortex shedding and possibly reduce its effect. (91) Naturally we cannot give the magnitude of the three velocity fluctuations from the present model. The turbulent kinetic energy k can however provide a rough estimate.

Assume that the turbulence is isotropic even if we know from experiments that this is not correct. It follows from eq. (5.3) that

$$\sqrt{\overline{u^2}} \sim \sqrt{2k/3} \qquad (5.55)$$

In Table 5.4 this estimate is given as a function of a/k_N and in four different levels.

a/k_N	$y/k_N = 1/30$	$y/k_N = 1.13$	$y/k_N = 11.7$	$y/k_N = 122$
10^0	0.419	0.072	0	0
10^1	0.178	0.095	0.002	0
10^2	0.110	0.092	0.043	0
10^3	0.076	0.073	0.059	0.016

Table 5.4 Turbulence intensity found from BL1PJ

An extremely high intensity is present at the bed for $a/k_N = 1$ according to the results from BL1PJ.

5.5.5 Eddy viscosities

As a consequence of the improved modelling of the turbulent kinetic energy conditions in the boundary layer a better description of the eddy viscosity variations must be anticipated. To get this confirmed we first look at the eddy viscosity profiles for different a/k_N-values. Fig. 5.11 shows a picture which is very different from that in Fig. 4.14. The vertical variation is smoother and there is no snip following from a zero velocity gradient. The time variation is affected by this to give smaller fluctuations over the period. For $a/k_N=1$ it is seen that due to the transient part in the solution the eddy viscosity is steadily increasing and influencing areas further away from the bed where the solution on the other hand is seen to be well determined.

In order to investigate the variation of ε further timeseries for the eddy viscosity are depicted in Fig. 5.12 for a number of a/k_N-values. Once again the difference from the BLOBAK-results in Fig. 4.15 are remarkable. As a result of the inclusion of the memory effect in the turbulence ε does not come down to zero twice every period. There is on the contrary a mean value about which ε is fluctuating. The magnitude of this fluctuating part is clearly seen to be a function of both a/k_N as well as the distance from the bed. For small a/k_N-values the amplitude is much less than for large values. Here the time-scale for decay of TKE compared with the period in the ambient oscillatory motion is decisive. For the relatively slowly varying flows at large a/k_N-values there is a possibility for the energy to dissipate around the time of flow reversal. Hence the k-level drops and consequently smaller ε-values are found. As opposed to this for relatively high frequency oscillations at small a/k_N-numbers the time-scale for decay of TKE is comparable with the oscillation period which permits the flow to maintain an almost constant level of turbulence during the period.

To illustrate the relation between a/k_N and the magnitude of fluctuation for ε in a given level results for $\varepsilon_{max}/\varepsilon_{min}$ are presented in Fig. 5.13. 8 different levels in terms of y/k_N are included and a very consistent picture supporting the

EDDY VISCOSITY PROFILES FOR a/k_N=100
BL1PJ

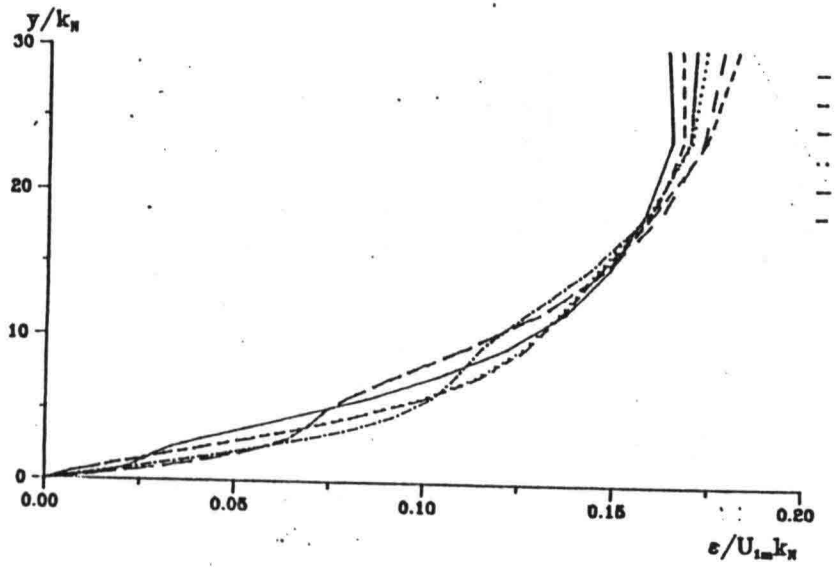

EDDY VISCOSITY PROFILES FOR a/k_N=124
BL1PJ

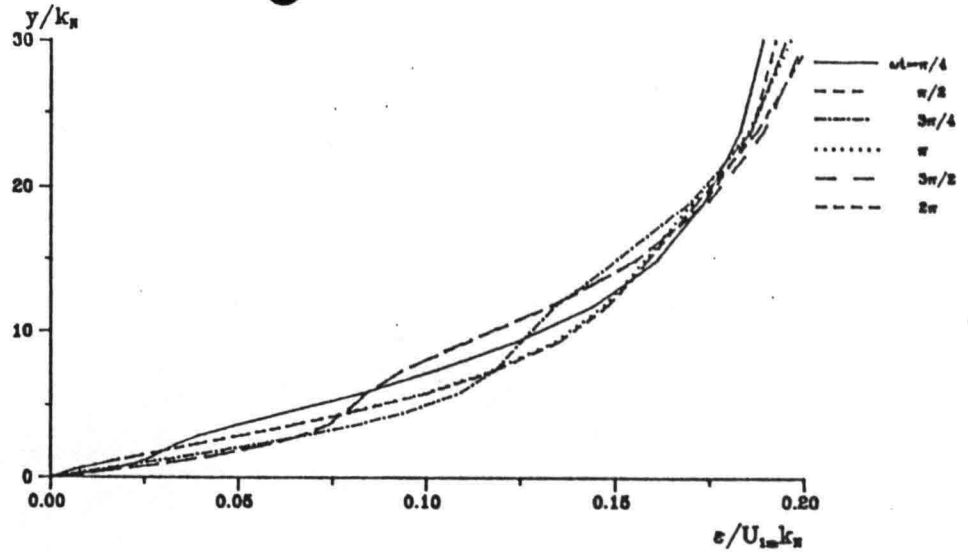

Fig. 5.11 ε-profiles for different a/k_N-values

EDDY VISCOSITY PROFILES FOR a/k_N=1
BL1PJ

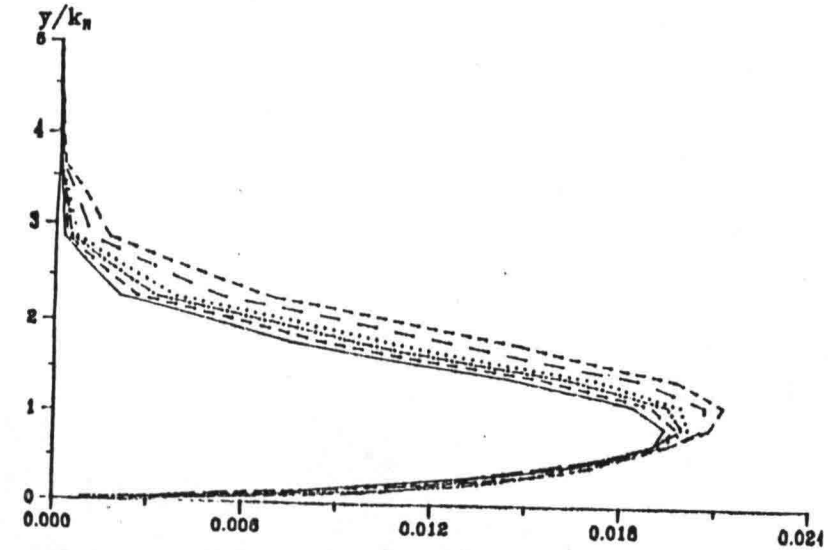

EDDY VISCOSITY PROFILES FOR a/k_N=1000
BL1PJ

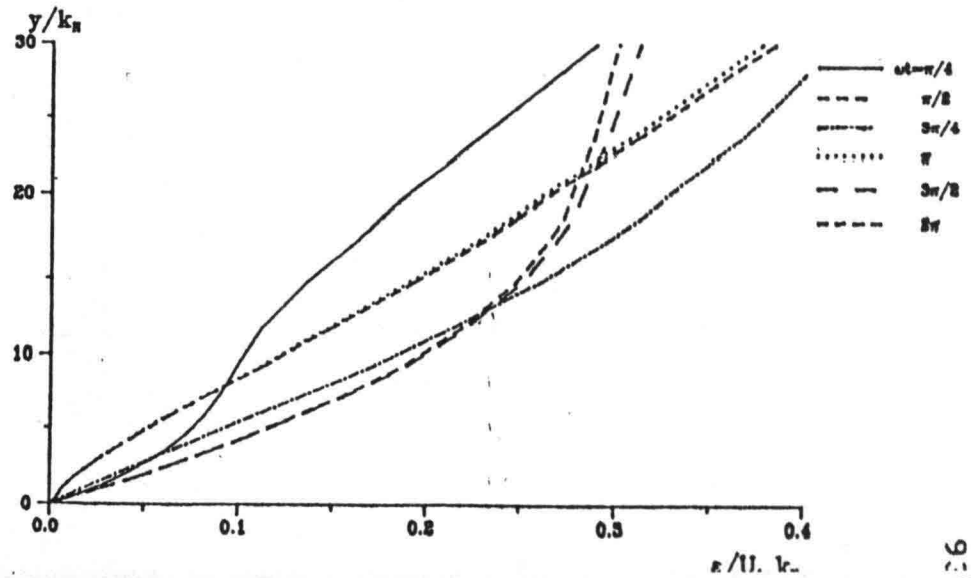

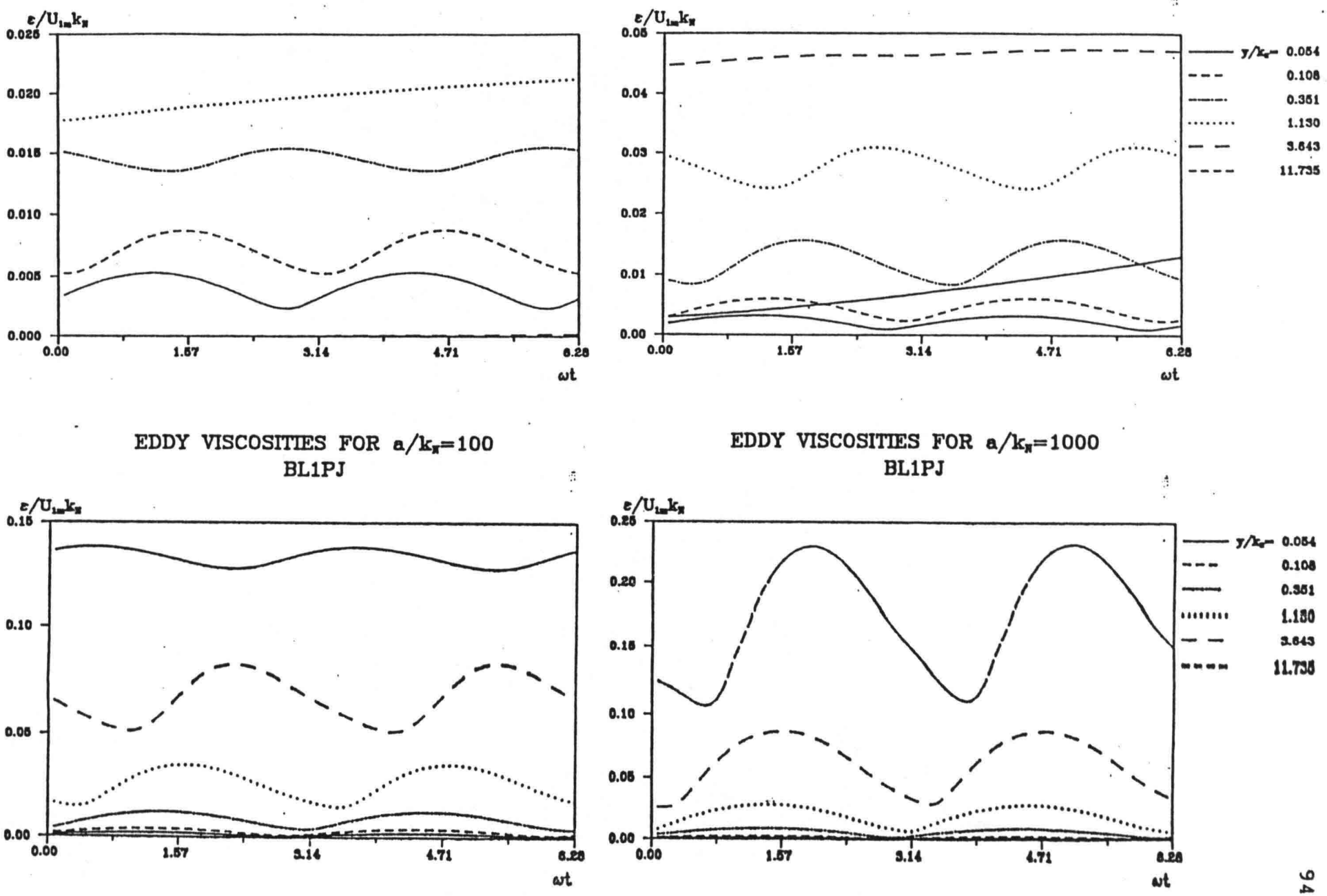

Fig. 5.12 Timeseries for ε

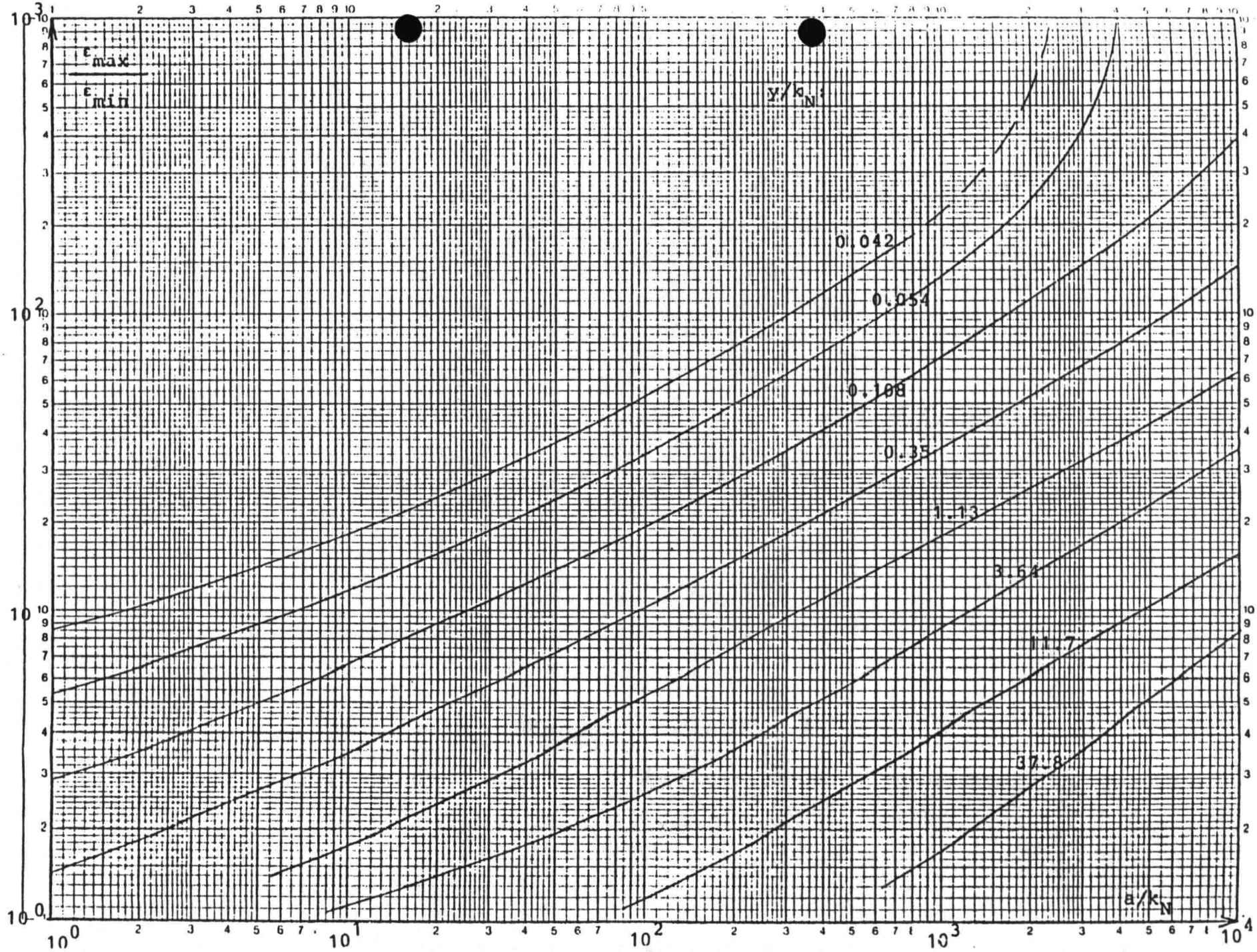

Fig. 5.13 $\varepsilon_{max}/\varepsilon_{min}$ as a function of a/k_N in different levels

speculations above appears.

Simpler models that include a time-invariant eddy viscosity will, of course, all be on the line $\varepsilon_{max}/\varepsilon_{min}=1$ in Fig. 5.13. Consequently they seem to be most relevant for small values of the amplitude/roughness ratio when it comes to describing the eddy viscosity. At the other extreme we have models like Fredsøe's which assume a logarithmic velocity profile. For very large a/k_N-values they may be successfully applied. In the important 'transition' range between, say, 5 and 10^3 it is imperative to include the transport equation for turbulent kinetic energy in the model in order to achieve a good description of the eddy viscosity. For the time-invariant-ε models it must be remembered that the flow may be expected to change its character for very small a/k_N-values due to vortex shedding behind the individual roughness elements. From Fig. 5.9 (a) it appears that most of the turbulent region can be found in a region less than one roughness from the bed.

To facilitate a comparison with experiments Fig. 4.17 includes the mean eddy viscosity profile for $a/k_N=124$ found from BL1PJ. The wave viscosity as defined by Lundgren determined in BL1PJ has been added to Fig. 4.18. Close to the bed there is agreement between BLOBAK and BL1PJ. This is in the region where local equilibrium in TKE prevails according to the observations in section 5.5.4.

5.5.6 Numerical aspects

The considerations about the numerical method that were put forward in section 4.6 concerning BLOBAK apply here as well. The meshes have been used for the same a/k_N-values and 800 timesteps per period were used in all cases. $\alpha=0.5$ corresponding to the Crank-Nicolson metod has been used throughout the study. It has been checked that the difference equations are fulfilled in all points using a special procedure ERRORV in BL1PJ. Then the local equilibrium option was checked against BLOBAK. Following this it was observed that BL1PJ yielded velocity profiles that were logarithmic close to the bed.

But before a solution of the full system of equations could be determined it was found necessary to compute a few periods assuming local equilibrium in TKE. In this way a hot start using initial profiles for both U and k could be performed. Otherwise the numerical solution did not converge and negative values of k were obtained in the vicinity of the bed. This is due to the nonlinearity and coupling in the equations. In practice four periods were run using the reduced model. Hereafter two initial periods with the full system of equations were completed with a minimum of output thus providing a solution which could be stored on an external file and reused. All results presented in this chapter were obtained during the third period with the complete model.

In some of the diagrams presented traces of the transient component have been visible. In practice it is a sign of a solution which is not in equilibrium. But it was decided that the main conclusions and a large majority of the results in general were only slightly affected by this transient so that it could not be justified to spend additional computer efforts on refining the computations through extra periods.

A typical running time for BL1PJ per period was 80 - 100 seconds on the IBM computers at NEUCC using a mesh with 43 points Every timestep the flow equation was solved 8 times whereas the k-equation required 15 times of solution. The time required depends on a/k_N. he solution is most easily found for small value of a/k_N. A list of the completed runs with BL1PJ is enclosed in Appendix B.

6. BL2PJ, A TWO-EQUATION MODEL

6.1 Introduction

To investigate the importance of the length scale in the oscillatory turbulent boundary layer a two-equation model of turbulence is developed in this chapter. The analytical work as well as the numerical method are outlined.

6.2 Construction of model

6.2.1 The equations

The transport equation for the dissipation rate reads according to chapter 2

$$\frac{\partial z}{\partial t} = \frac{\partial}{\partial y}\left(\frac{\varepsilon}{\sigma_z}\frac{\partial z}{\partial y}\right) + C_4 z \frac{\varepsilon}{k}\left(\frac{\partial U}{\partial y}\right)^2 - C_5 z C_1 \frac{\sqrt{k}}{l} \qquad (6.1)$$

where z is the dissipation rate

$$z = C_1 \frac{k^{3/2}}{l} \qquad (6.2)$$

and the length scale is now a function of both space and time. The Prandtl-Kolmogorov relation for the eddy viscosity is

$$\varepsilon = \sqrt{k}\, l = C_1 \frac{k^2}{z} \qquad (6.3)$$

Insertion of eq. (6.3) into eq. (6.1) gives

$$\frac{\partial z}{\partial t} = \frac{\partial}{\partial y}\left(\frac{C_1 k^2}{z \sigma_z}\frac{\partial z}{\partial y}\right) + C_4 C_1 k \left(\frac{\partial U}{\partial y}\right)^2 - C_5 \frac{z^2}{k} \qquad (6.4)$$

Take the length scale l as

$$l = C_1 \frac{k^{3/2}}{z} \qquad (6.5)$$

Then eqs. (6.4) and (6.5) together with the flow equation (2.18), the transport equation for turbulent kinetic energy, and

the Prandtl-Kolmogorov relation constitute a two-equation model of turbulence for the flow in a two-dimensional oscillatory boundary layer flow over a rough bed. In the literature the model is often referred to as a k-ε model, where ε means dissipation of TKE.

6.2.2 Boundary conditions

The following boundary conditions are associated with eq. (6.4)

(i) Near the bed we assume that local equilibrium in TKE prevails. Recalling a logarithmic velocity profile it is found that

$$z = c_1 \frac{k^2}{\varepsilon} = \frac{c_1}{c_1} \frac{\tau^2}{\tau} \frac{\partial U}{\partial y} = U_f^2 \frac{U_f}{\varkappa y} = \frac{U_f^3}{\varkappa y}$$

At the level where the velocity vanishes we require

$$z\,(y_b = k_N/30) = \frac{U_f^3}{\varkappa y} \qquad (6.6)$$

(ii) At the free boundary the rate of dissipation is zero

$$z(y_o) = 0 \qquad (6.7)$$

(iii) The initial profile of z is a distribution that corresponds to the given profiles for k and U, cf. 5.2.2.

(iv) The periodicity condition applies to the dissipation rate as well as to k and U.

The boundary and initial conditions for the two other equations are described in 5.2.2.

6.2.3 Constants in the z-equation

In the transport equation for the dissipation rate three empirical constants have to be enumerated. From considerations

about the decay of turbulence behind a grid, Rodi [36] comes to the result that based on experimental evidence c_5 can be taken as

$$c_5 = c_{2\varepsilon} = 1.92 \tag{6.8}$$

where $c_{2\varepsilon}$ is from [28].

The value of the diffusive constant σ_z was found from computer optimization by Hanjalic and Launder [13] and referenced by Launder and Spalding [28] as

$$\sigma_z = 1.3 \tag{6.9}$$

The constant c_4 can be related to c_5 and σ_z when local equilibrium in TKE is assumed to exist. It is found that

$$z = c_1 \frac{k^2}{\varepsilon} = \frac{U_f^3}{\varkappa y} \tag{6.10}$$

$$\frac{\partial z}{\partial y} = -\frac{U_f^3}{\varkappa y^2} \tag{6.11}$$

$$\varepsilon = U_f \varkappa y \tag{6.12}$$

Neglecting the rate of change of z in eq. (6.4) and utilizing the relations above we arrive at

$$-\frac{\partial}{\partial y}\left(\frac{U_f \varkappa y}{\sigma_z}\,\frac{U_f^3}{\varkappa y^2}\right) + c_4 \frac{1}{\sqrt{c_1}}\,U_f^2\,\frac{U_f^2}{\varkappa^2 y^2} - c_5 \frac{1}{c_1}\,\frac{U_f^6}{\varkappa^2 y^2}\,\frac{\sqrt{c_1}}{U_f^2} = 0$$

After some rearrangements this expression can be reduced to

$$c_4 = c_5 - \frac{\varkappa^2}{\sigma_z \sqrt{c_1}} \tag{6.13}$$

This equation fixes the value of the constant c_4 when the other constants have been chosen. In the present case we get

$$c_4 = 1.92 - \frac{0.40^2}{1.3 \cdot \sqrt{0.08}} = 1.48 \tag{6.14}$$

Apparently Rodi and Launder & Spalding took the von Karman constant as

κ=0.423

in order to obtain

c_4 =1.44

This value of κ stems from a paper by Patankar and Spalding [33]. Here we shall use (6.14) since κ=0.40 is prescribed throughout this report.

6.3 Numerical solution

6.3.1 General procedure

The solution procedure is similar to the one used for the one-equation model. The equations are solved sequentially starting with the z-equation then the k-equation and finally the flow equation. Knowing the solution to the z-equation the length scale l and its derivative can be determined as

$$l = C_1 \frac{k^{3/2}}{z}$$

$$\frac{\partial l}{\partial y} = C_1 \frac{3}{2}\sqrt{k}\,\frac{\partial k}{\partial y}\,\frac{1}{z} - k^{3/2}\frac{1}{z^2}C_1 = \frac{C_1}{z}\left(\frac{3}{2}\sqrt{k}\,\frac{\partial k}{\partial y} - \frac{k^{3/2}}{z}\right) \qquad (6.15)$$

In this way an easy connection to the one-equation is available.

6.3.2 Solution of the z-equation

The numerical solution procedure adopted to the transport equation for z is similar to the one used for the k-equation, cf. chapter 5.

The first order difference approximations are

$$\frac{\partial z}{\partial y} \simeq \frac{1}{2}\left(\frac{z_i^{j+1} - z_i^j}{\Delta y_{j+1}} + \frac{z_i^j - z_i^{j-1}}{\Delta y_j}\right) = G_i^j \qquad (6.16)$$

$$\frac{\partial^2 z}{\partial y^2} \simeq \frac{1}{\frac{1}{2}(\Delta y_{j+1} + \Delta y_j)}\left(\frac{z_i^{j+1} - z_i^j}{\Delta y_{j+1}} - \frac{z_i^j - z_i^{j-1}}{\Delta y_j}\right) = H_i^j \qquad (6.17)$$

Eq. (6.4) can be rewritten as

$$\frac{\partial z}{\partial t} = \frac{\varrho k c_1}{z\sigma_z}\frac{\partial k}{\partial y}\frac{\partial z}{\partial y} - \frac{c_1 k^2}{z^2\sigma_z}\frac{\partial z}{\partial y} + \frac{c_1 k^2}{z\sigma_z}\frac{\partial^2 z}{\partial y^2} + c_4 c_1 k\left(\frac{\partial U}{\partial y}\right)^2 - c_5\frac{z^2}{R} \tag{6.18}$$

Utilizing the approximations and weighing the solution in the time domain according to (5.25) yields the following difference approximation in dimensionless form

$$\begin{aligned} fz_j = -\frac{1}{t}\left(z_i^j - z_{i-1}^j\right) + \frac{a}{k_N}(1-\alpha)\left\{\frac{c_1 k_{i-1}^j}{z_{i-1}^j\sigma_z}\left[2\left(\frac{\partial k}{\partial y}\right)_{i-1}^j - \frac{k_{i-1}^j}{z_{i-1}^j}\right]G_{i-1}^j\right. \\ \left. + \frac{c_1 (k_{i-1}^j)^2}{z_{i-1}^j\sigma_z}H_{i-1}^j + c_4 c_1\left[\left(\frac{\partial U}{\partial y}\right)_{i-1}^j\right]^2 - c_5\frac{(z_{i-1}^j)^2}{k_{i-1}^j}\right\} \\ + \frac{a}{k_N}\alpha\left\{\frac{c_1 k_i^j}{z_i^j\sigma_z}\left[2\left(\frac{\partial k}{\partial y}\right)_i^j - \frac{k_i^j}{z_i^j}\right]G_i^j\right. \\ \left. + \frac{c_1 k_i^j}{z_i^j\sigma_z}H_i^j + c_4 c_1\left[\left(\frac{\partial U}{\partial y}\right)_i^j\right]^2 - c_5\frac{(z_i^j)^2}{k_i^j}\right\} \quad j = 1,\ldots,N \end{aligned} \tag{6.19}$$

Again in this case we use Newton's method to solve the system of nonlinear equations given by (6.19). The coefficients are found to be (cf. eq. (4.26))

$$A_i^j = \frac{\partial fz_j}{\partial z_i^{j-1}} = \frac{a}{k_N}\alpha\frac{c_1 k_i^j}{z_i^j\sigma_z\Delta y_j}\left\{-\left[\left(\frac{\partial k}{\partial y}\right)_i^j - \frac{1}{2}\frac{k_i^j}{z_i^j}\right] + k_i^j\frac{1}{\frac{1}{2}(\Delta y_{j+1} + \Delta y_j)}\right\} \tag{6.20}$$

$$\begin{aligned} B_i^j = \frac{\partial fz_j}{\partial z_i^j} = -\frac{1}{t} + \frac{a}{k_N}\alpha\left[\frac{c_1 k_i^j}{z_i^j\sigma_z}\left\{\frac{2}{z_i^j}\left[\frac{k_i^j}{z_i^j} - \left(\frac{\partial k}{\partial y}\right)_i^j\right]G_i^j + \left[\left(\frac{\partial k}{\partial y}\right)_i^j - \frac{1}{2}\frac{k_i^j}{z_i^j}\right]\cdot\right.\right. \\ \left.\left.\left[\frac{1}{\Delta y_j} - \frac{1}{\Delta y_{j+1}}\right] - \frac{k_i^j}{z_i^j}H_i^j - k_i^j\frac{1}{\frac{1}{2}(\Delta y_{j+1} + \Delta y_j)}\left(\frac{1}{\Delta y_{j+1}} - \frac{1}{\Delta y_j}\right)\right\} - 2c_5\frac{z_i^j}{k_i^j}\right] \end{aligned} \tag{6.21}$$

$$C_i^j = \frac{\partial fz_j}{\partial z_i^{j+1}} = \frac{a}{k_N}\alpha\frac{c_1 k_i^j}{z_i^j\sigma_z\Delta y_{j+1}}\left\{\left[\left(\frac{\partial k}{\partial y}\right)_i^j - \frac{1}{2}\frac{k_i^j}{z_i^j}\right] + k_i^j\frac{1}{\frac{1}{2}(\Delta y_{j+1} + \Delta y_j)}\right\} \tag{6.22}$$

$$D_i^j = -fz_j\left(z_i^{j,n}\right) \tag{6.23}$$

6.3.3 Implementation

The model has not been implemented.

6.4 Assessment of model capabilities

As the model has not yet been implemented as a computer programme no results are available. Assessment of BL2PJ compared with BL1PJ and BL0BAK is therefore not possible. However, it is believed that there will be no significant change in the results as long as we have a uniform ambient flow. Inclusion of the advective terms in the governing equations and second order wave theory may change this picture since gradients will then be present also in the x-direction.

7. APPLICATION OF BL0BAK AND BL1PJ TO SEDIMENT TRANSPORT CALCULATIONS

7.1 General

In order to evaluate the sediment transport in the sea knowledge about the vertical distribution of suspended sediment in waves is required. Here we will consider the situation where the bed is plane since possible ripples are normally washed away at times with large sediment transport rates under severe storm conditions in nature. The flow regime is assumed to be fully turbulent and with a rough bed.

The sediment description in this work follows that of Fredsøe et al., [10], closely. But whereas they used Fredsøe's simple boundary layer model, cf. section 3.2, to describe the flow we shall employ the turbulence models developed in this report. The purpose is to get an evaluation of the importance of these models in a sediment transport context.

7.2 Short theoretical introduction

The theory behind the calculation of the vertical concentration profiles for sediment in waves can naturally be split into two parts. One is the description of the flow. The other is the modelling of the sediment suspension given the flow conditions. These topics will be dealt with in a reverse order.

The vertical distribution of suspended sediment is usually described by the diffusion equation

$$\frac{\partial c}{\partial t} = w \frac{\partial c}{\partial y} + \frac{\partial}{\partial y}\left(\varepsilon_s \frac{\partial c}{\partial y}\right) \qquad (7.1)$$

where c is the concentration by volume, w is the fall velocity of suspended sediment and ε_s is the turbulent exchange factor for suspended sediment. In eq. (7.1) the horizontal diffusion term is neglected since it is assumed that the vertical gradient of concentration is much larger than the corresponding horizontal

gradient. The advective terms are omitted as well.

A problem is to give a value for the fall velocity. In this case we will make a comparison with experiments in which w was determined. But in practical cases it may be very difficult to evaluate w. Another problem is ε_s. This quantity is not the eddy viscosity but rather a turbulent exchange factor for sediment. Very often the particles are assumed to follow the eddies and consequently ε_s is given as

$$\varepsilon_s = \varepsilon \tag{7.2}$$

In reality, larger particles might have an inertia which causes a phase lag between big ε-values and the diffusion of the grains. However, such a discussion is beyond the scope of the present study. Presently eq. (7.2) is used for ε_s.

The boundary conditions are as follows

(i) The instantaneous concentration at the bed is assumed to be a function of the instantaneous bed shear stress. Several formulae exist but we use the same as in [10]. c_b is then a function of the dimensionless bed shear stress θ

$$c_b = c_b(\theta)$$

in which θ is defined as

$$\Theta = \frac{\tau_b}{\rho(s-1)gd} \tag{7.3}$$

In eq. (7.3) τ_b is the bed shear stress, ρ is the fluid density, s is the relative density of the grains, g is the acceleration due to gravity, and d is the mean grain diameter. θ is called Shields parameter. Using the functional relationship between τ_b and c_b from [10] the lower boundary condition for eq. (7.1) is specified.

(ii) Towards the water surface it is demanded that

$$c(t,y) \to 0 \text{ for } y \to \infty \qquad (7.4)$$

(106)

(iii) The time variation must be periodic since the 'driving force' is periodic. In a mathematical formulation this is equivalent to

$$c(t,y) = c(t+T,y) \qquad (7.5)$$

Now, the idea of this study is to see the effect of including the memory in the turbulence. The flow model used in [10] is therefore replaced by either BLOBAK or BL1PJ. From these models we get a timeseries for the friction velocity, U_*, and the eddy viscosity field during one half period.

It is now possible to solve eq. (7.1) numerically. We shall not discuss the details here, reference is made to [10].

7.3 Model implementation

The present turbulence models have been interfaced with an already existing programme P20S developed earlier, see [10]. The modifications made in P20S are as follows. Routines have been made to read U_* and ε from from an external file created by either BLOBAK or BL1PJ. Usually these data are not given in the same levels as used by P20S due to a different coordinate straining. Therefore an interpolation procedure was constructed to find intermediate values in the profiles provided in the file. In the main program the values of ε and U_* calculated by P20S were replaced by the new values. Large parts of the original program were retained since this procedure caused the least problems even if a big number of dummy statements then existed in the programme. The changed and new modules are enclosed in Appendix E.

7.4 Theoretical results and comparison with measurements

To facilitate a comparison with both the theoretical results in [10] and the measurements in [42] we have chosen to perform two computations using BLOBAK and BL1PJ for the parameters $a/k_N = 124$, $w/U_{1,0} = 0.018$, and $\theta_{max} = 1.45$ which corresponds to d=0.19 mm, s=2.65, a=1.86 m, and T=9.1 sec in the experiments. The grain diameter is related to k_N through eq. (2.50).

The instantaneous sediment concentration found using BLOBAK is depicted in Fig. 7.1. Seven different levels are included. The corresponding diagram showing the results from BL1PJ is given in Fig. 7.2 whereas the theoretical results in [10] are

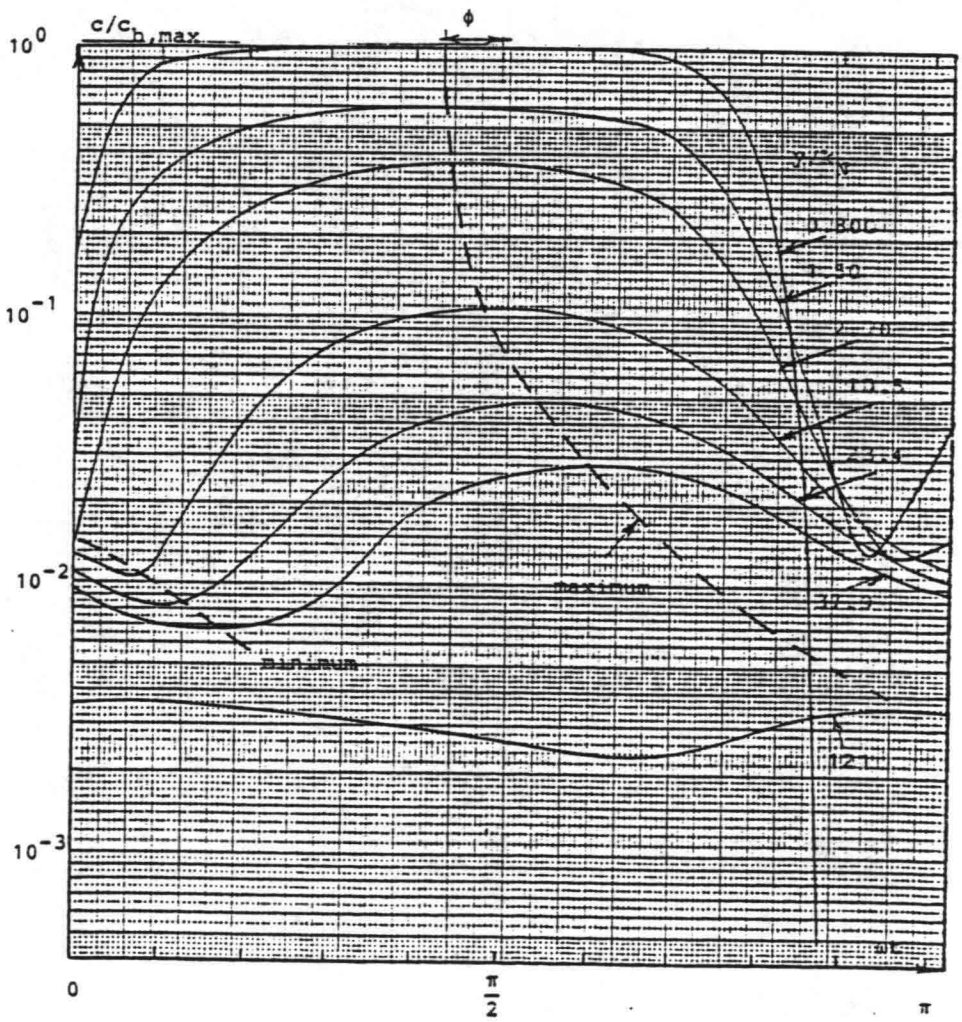

Fig. 7.1 Instantaneous sediment concentrations, BLOBAK.

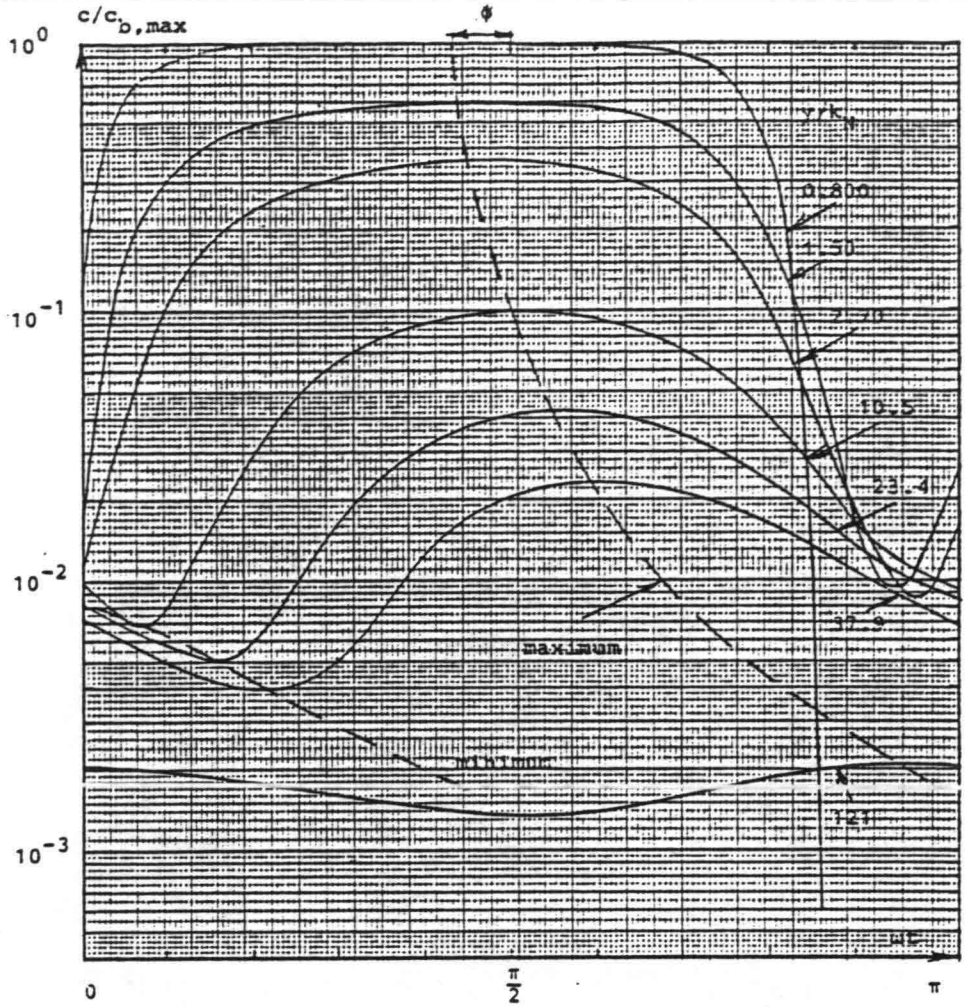

Fig. 7.2 Instantaneous sediment concentrations, BL1PJ

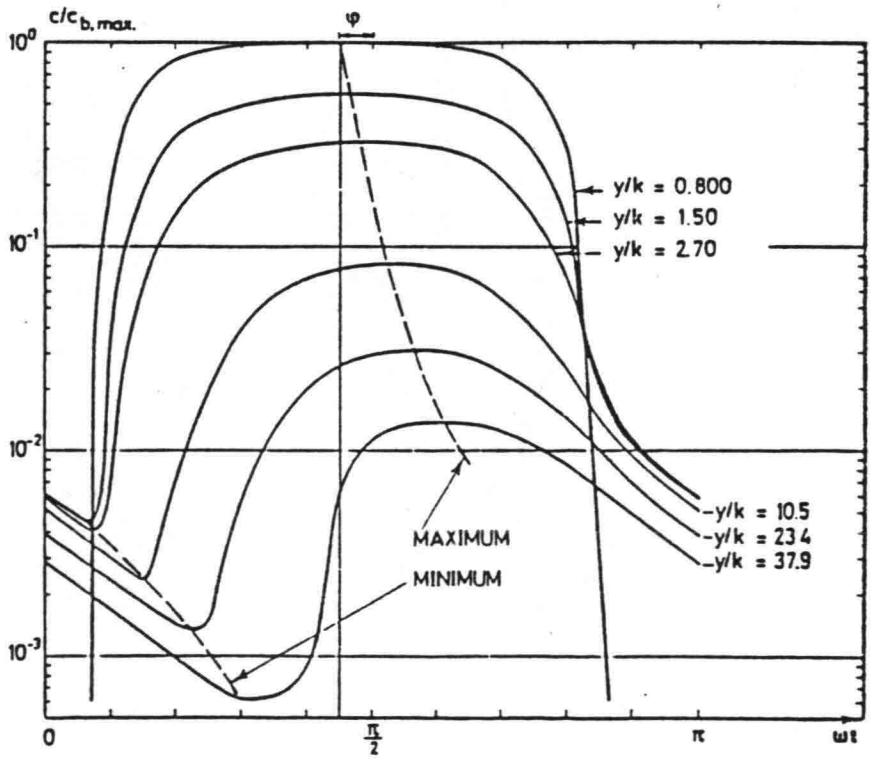

Fig. 7.3 Instantaneous sediment concentrations, from [10]

reproduced in Fig. 7.3. The general variation in the three cases is quite similar. The sediment is suspended when the bed shear stress is largest some time before the outer velocity is a maximum. The phase angle ϕ is indicated in the diagrams. The concentration is largest close to the bottom and the maximum concentration lags more and more behind the maximum bed shear stress as the distance from the bed increases. The minimum concentration has a similar phase shift one quarter of a period before It is perhaps instructive to reach back to the contour plots for the turbulent kinetic energy that were shown in Fig. 5.9. Here there are similar phase conditions for the k-level.

Note that the neglect of eddies formed in earlier half periods gives rise to a drop in the concentrations in the beginning of the period in Fig. 7.3. When the memory in the turbulence is modelled more sediment is kept in suspension at the time of flow reversal. Around $\omega t=\pi/2$ where the ambient velocity is a maximum there is little difference between the results.

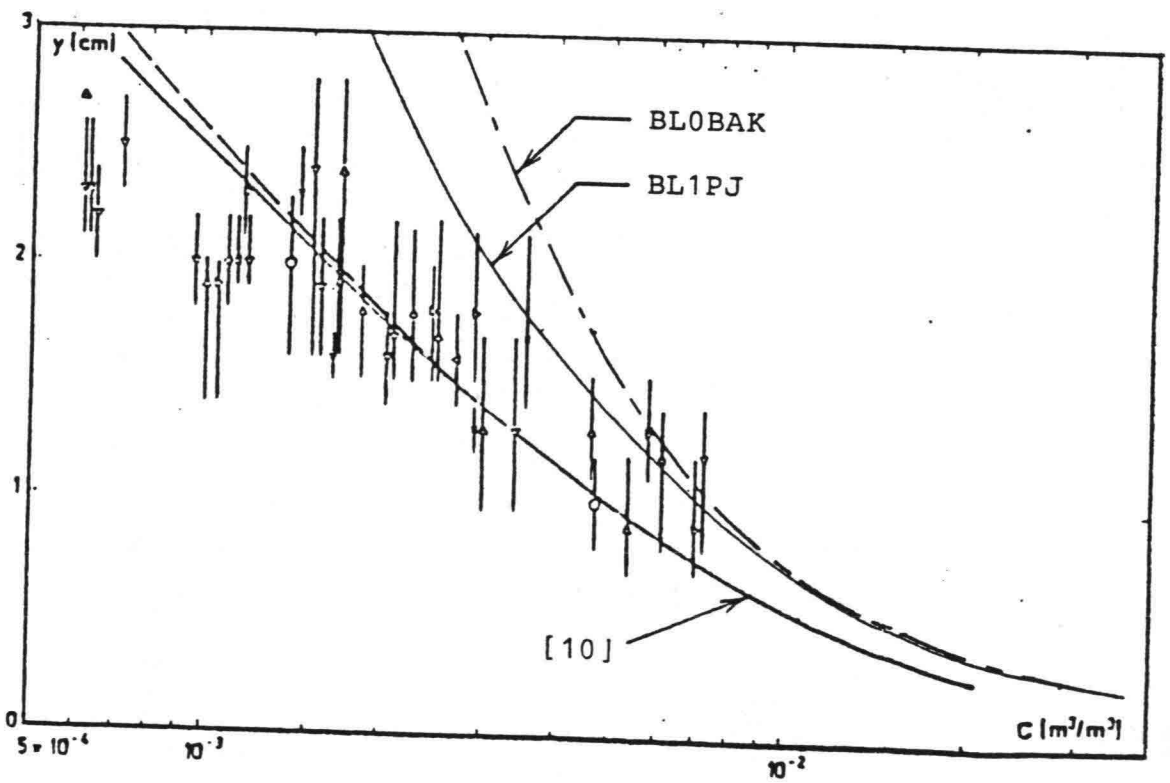

Fig. 7.4 Mean concentration profile.

Apparently BLOBAK yields higher concentrations than BL1PJ. This trend is confirmed when we look at the mean concentration profile in Fig. 7.4. Both predictions are, however, higher than the measured profiles. The explanation could be that we take $\varepsilon_s = \varepsilon$ in eq. (7.1) whereas there might be a diffusion constant which should be applied. Such a constant may be estimated by tuning model results to the experimental data. But other major uncertainties are connected to this model so that different reasons can be responsible as well. In the model a sediment containing a spectrum of different diameters is regarded as a homogeneous material consisting of grains with the median diameter. The fall velocity w is affected by great uncertainty. No field measurements are available for w.

The variation of the concentration relative to the mean concentration is depicted in Fig. 7.5 in the level $y/k_N = 37.9$. The inclusion of the memory of turbulence improves this variation compared to the results from [10]. The amplitude is now closer to the measurements whereas there is still a phase shift between the measured and predicted maximum concentration.

To documentate further that the variations predicted by these improved models may be reproducing experimental results we finally include an example of measurements by Horikawa et al. [17]. The experiment parameters can be seen in the figure caption in Fig. 7.6. This example of measurements of the time variation of c in a number of levels is similar to the diagrams 7.1 to 7.3.

Although we have not made calculations for this case a prelimenary evaluation is that the phase shifts predicted here are closer to the measured than those found in [10]. The variations of c over the period seem to be better modelled as well.

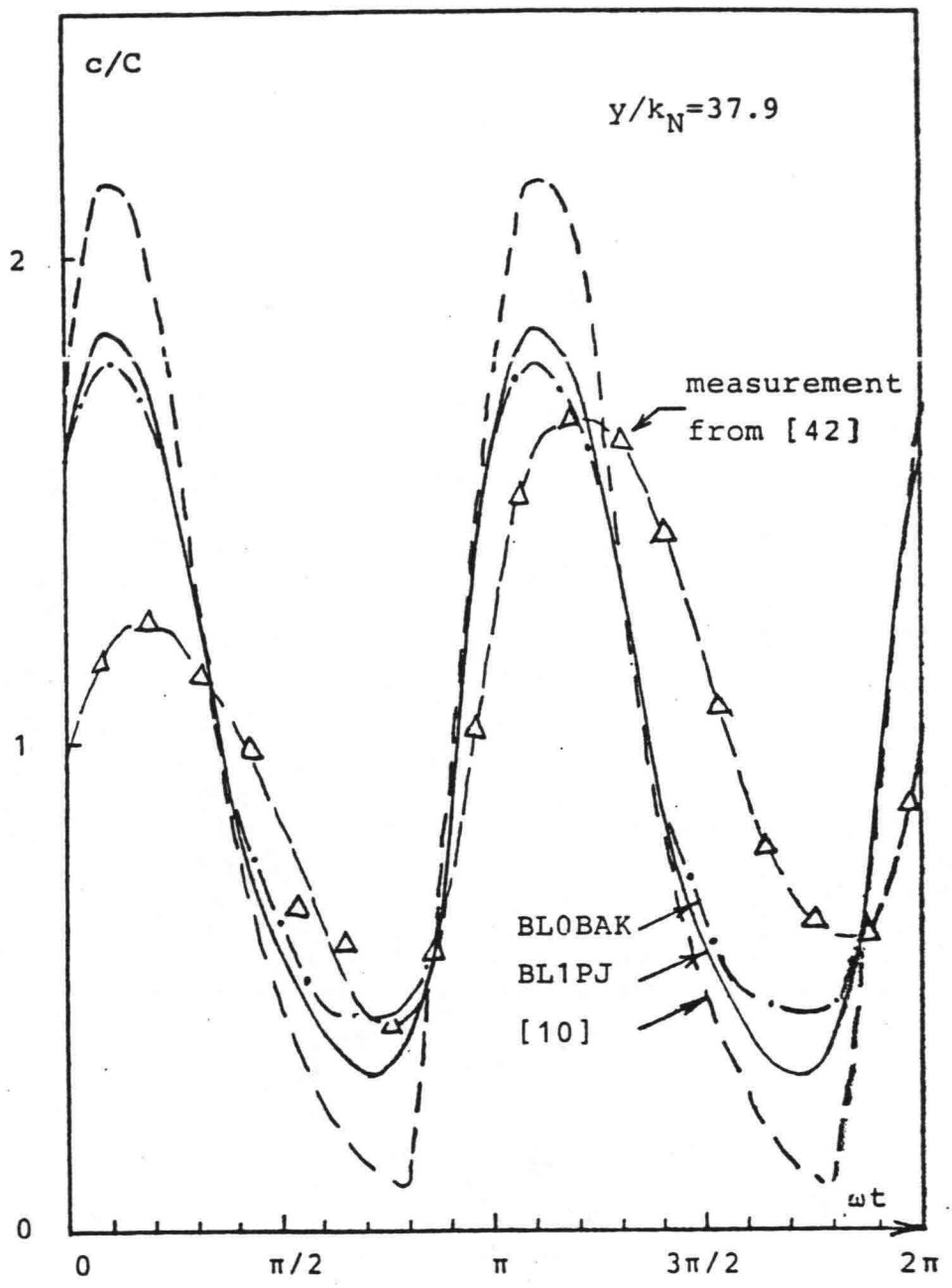

Fig. 7.5 Variation of relative concentration

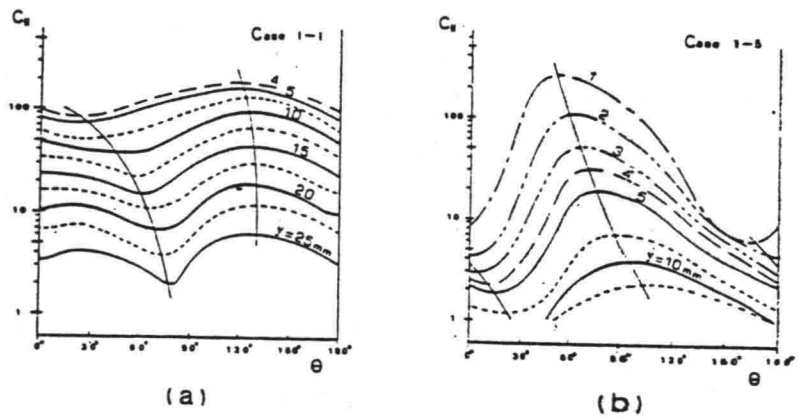

(a) (b)

Fig. 7.6 Measured variation of concentration with phase angle, from [17]. a/k_s =1140, s=2.66, d=0.20 mm,
a: $w/U_{1,m}$ =0.020
b: $w/U_{1,m}$ =0.034

8. CONCLUSIONS

The purpose of this work was to investigate the effects of th inclusion of turbulence modelling in the description of the roug turbulent oscillatory boundary layer. Three different models of increasing complexity were considered. First, the mixing-length theory was used to construct the zero-equation model BLOBAK. Modelling of the turbulent kinetic energy budget was improved by inclusion of a transport equation for turbulent kinetic energy which gave the one-equation model BL1PJ. Finally a two-equation model BL2PJ which also has a transport equation for the dissipation rate has been outlined but it has not been implemented.

No general evaluation of the use of these advanced models rather than simpler models can be made. Depending on which phenomenon is considered simpler models might yield results that are acceptable for practical purposes. We shall therefore discuss some of the applications briefly below.

It can be concluded that the description of the velocity field in an oscillatory boundary layer can be obtained from BLOBAK or BL1PJ as well as from a constant eddy viscosity model like that Myrhaug [32]. The latter model requires, however, that the boundary layer thickness is known a priory, cf. section 3.3, whereas the present models do not have this limitation.

A distinct feature which seems inherent in almost any existing model is the underestimation of the friction factor f_w in comparison with the measurements by Jonsson and Carlson [23]. This one-sidedness in the theoretical predictions may be explained by the method of simulating the natural bottom roughness in the laboratory. The discrepancy is most pronounced for smaller a/k_s values which supports the speculations in section 3.6.

In the theoretical models it has been possible to determine the energy loss factor f_e. The relative strength of f_e to f_w is an interesting quantity in connection with wave damping. We have calculated the ratio f_e/f_w and good agreement with experimental

data is observed. This applies to BLOBAK as well as to BL1PJ, the latter model yielding slightly better results.

Perhaps the most important topic in this report is the calculation of the turbulent kinetic energy conditions in the boundary layer. Using the model BL1PJ it has been innvestigated how energy is produced, diffused, dissipated, and preserved from times with a production surplus to later times where dissipation is high. The calculations show that the production is very high just before the maximum ambient velocity culminates. This surplus of energy is then preserved in the turbulent motions and is spread towards areas in which the energy level is lower. The turbulent motions are of course sustained throughout the period of oscillation. The model shows that this effect is most pronounced for low values of a/k_w. The time scale for the decay of turbulent energy is then comparable with the period of oscillation.

Unfortunately we have not been able to check the theoretical findings against measurements due to the lack of experimental data. Hino et al. [15] made tests with a smooth bed. A preliminary evaluation shows that the same tendencies with respect to the k-distribution in the boundary layer as predicted by BL1PJ in the rough bed case are present in these experiments.

(114)

The main implication of the improved description of the turbulent kinetic energy circulation is that the eddy viscosity is now related to the turbulent kinetic energy, k, rather than to the mean velocity field. ε behaves qualitatively like k when it is modelled by BL1PJ. The ability to model the memory in the turbulence has created an improved basis for sediment transport calculations in waves. We have used a newly developed model to investigate this issue. Calculations of the concentration of suspended sediment were made in three cases. One was to use an eddy viscosity distribution as given from a simple model. Another was to include the eddy viscosities from BLOBAK. The difference between those two distributions is the phase shifts. The last was to use the results from BL1PJ in which the memory is taken into account. Given the uncertainties with respect to fall velocity, sediment gradation, and the turbulent exchange factor inherent in sediment

transport calculations the general trend is that the more advanc models yield a better prediction of the tendencies whereas quant tative discrepancies do exist.

In practice it may often be sufficient to use a constant eddy viscosity model when a/k_N is close to unity while a simple model like Fredsøe's can be applied in the case of very high a/k_N - values. This is depending on the relative strength of the time scale for decay of turbulence to the period of oscillation. But a very important range for a/k_N still exists where the advanced models have an advantage in the refined description of the eddy viscosity.

The practical implications of the models developed in the present work are believed to be limited due to the computer facilities that these models require. They are, however, justified in the sense that simpler models can be checked against them.

Finally we shall outline a few of the topics that would be relevant to investigate further in the future. The effects of a variable length-scale can be studied if the model BL2PJ is implemented. It may perhaps not represent as big a step forward as the inclusion of the memory in the turbulence but some changes could be found. It should be more interesting to modify the present models to treat the smooth wall case. The viscous sublayer can be included by matching a logarithmic velocity profile in this layer to the numerical solution in the outer layer. It seems to be straightforward and would facilitate a comparison with the comprehensive experimental data by Hino et al. Another interesting extension of the present models would be the inclusion of a steady current so that a combined wave-current motion in the unidirectional case could be considered.

9. REFERENCES

[1] Bakker, W. T. (1974): Sand Concentration in an Oscillatory Flow. Coastal Engineering Conference, Copenhagen. pp. 1129-1148.

[2] Bakker, W. T. og van Doorn, T. (1978): Near-Bottom Velocities in Waves with a Current. Coastal Engineering Conference, Hamburg. pp. 1394-1413.

[3] Blottner, F. G. (1975): Investigation of Some Finite-Difference Techniques for Solving the Boundary Layer Equations. Comp. Meth. Appl. Mech. Eng. Vol. 6, pp. 1-30.

[4] Bradshaw, P. (1972): The Understanding and Prediction of Turbulent Flow. Aeronautical Journal. Vol. 76, pp. 403-418.

[5] Bradshaw, P., Cebeci, T. og Whitelaw, J. H. (1981): Engineering Calculation Methods for Turbulent Flow. Academic Press. London. xii + 311 pp.

[6] Christoffersen, J. B. (1982): Current Depth Refraction of Dissipative Water Waves. Series Paper 30, ISVA, Lyngby, v + 179 pp.

[7] Davidov, B. I. (1961): On the Statistical Dynamics of an Incompressible Turbulent Fluid. Dokl. AN SSSR, 136, 47.

[8] Fersiger, J. M. (1982): State of the Art in Subgrid Scale Modeling. In: Numerical and Physical Aspects of Aerodynamical Flows. Ed. T. Cebeci, pp. 53-68. New York, Springer Verlag. 636 pp.

[9] Fredsøe, J. (1984): The Turbulent Boundary Layer in Combined Wave-Current Motion. ASCE Journal of Hydraulic Engineering, Vol. 110, No. HY8, pp. 1103-1120.

[10] Fredsøe, J., Andersen, O. H. and Silberg, S. (1983): Distribution of Suspended Sediment in Large Waves. ASCE, Journal of Waterways, Harbours and Coastal Engineering Div. In press.

[11] Grant, W. D. og Madsen, O. S. (1979): Combined Wave and Current Interaction With a Rough Bottom. Journal of Geophysical Research. Vol. 84, No. C4, pp. 1797-1808.

[12] Hanjalic, K. and Launder, B. E. (1972): Fully Developed Assymetric Flow in a Plane Channel. JFM, Vol. 51, pp. 301-335.

[13] Hanjalic, K. and Launder, B. E. (1972): A Reynolds Stress Model of Turbulence and Its Application to Thin Shear Flows. JFM, Vol. 52, pp. 609-638.

[14] Harlow, F. H. and Nakayama, P. I. (1967): Turbulent Transport Equations. Phys. Fluids, Vol. 10, p. 2323.

[15] Hino, M., Kashiwayanagi, M., Nakayama, A. and Hara, T. (1983): Experiments on the Turbulence Statistics and the Structure of a Reciprocating Oscillatory Flow. JFM, Vol. 131, pp. 363-400.

[16] Hinze, J. O. (1959): Turbulence. McGraw Hill, New York.

[17] Horikawa, K., Watanabe, A. and Katori, S. (1982): Sediment Transport Under Sheet Flow Condition. ASCE, Coastal Engineering Conference 1982, Cape Town, pp. 1335-1352.

[18] Johns, B. (1975): The Form of the Velocity Profile in a Turbulent Shear Wave Boundary Layer. Journal of Geophysical Research. Vol. 80, No. 36, pp. 5109-5112.

[19] Johns, B. (1977): Residual Flow and Boundary Shear Stress in the Turbulent Bottom Layer Beneath Waves. J. Phys. Oceanography, Vol. 7, pp. 733-738.

[20] Jones, W. P. and Launder, B. E. (1972): The Prediction of Laminarization with a Two-Equation Model of Turbulence. Int. J. Heat and Mass Transfer. Vol. 15, p. 301.

[21] Jonsson, I. G. (1963): Measurements in the Turbulent Wave Boundary Layer. I.A.H.R. Congress, London. pp. 85-92.

[22] Jonsson, I. G. (1980): A New Approach to Oscillatory Rough Turbulent Boundary Layers. Ocean Engrg, Vol. 7, pp.109-152.

[23] Jonsson, I. G. og Carlsen, N. A. (1976): Experimental and Theoretical Investigations in an Oscillatory Turbulent Boundary Layer. Journal of Hydraulic Research. Vol. 14, No. 1, pp. 45-60.

[24] Kamphuis, J. W. (1975): Friction Factor under Oscillatory Waves. ASCE Journal of Waterway, Port and Ocean Division. Vol. 101, No. WW2, pp. 135-144.

[25] Keller, H. B. (1978): Numerical Methods in Boundary-Layer Theory. Ann. Rev. Fluid Mech., Vol. 10, pp. 417-433.

[26] Kemp, P. H. and Simons, R. R. (1982): The Interaction Between Waves and a Turbulent Current. JFM, Vol. 116, pp. 227-250.

[27] Knight, D. W. (1978): Review of Oscillatory Boundary Layer Flow. ASCE, Vol. 104, No. HY6, June, pp. 839-855.

[28] Launder, B. E. and Spalding, D. B. (1972): Mathematical Models of Turbulence. Academic Press. 170 pp.

[29] Lundgren, H. (1972): Turbulent Currents in the Presence of Waves. Coastal Engineering Conference, Vancouver. pp. 623-634.

[30] Madsen, K. and Tingleff, O. (1973): Nulpunkter for funktioner. Hæfte 15. Numerisk Institut, DTH. (In Danish).

[31] Mellor, G. L. and Herring, H. J. (1973): A Survey of the Mean Turbulent Field Closure Methods. AIAA Journal, Vol. 11, pp. 590-599.

[32] Myrhaug, D. (1982): On a Theoretical Model of Rough Turbulent Wave Boundary Layers. Ocean Engineering, Vol. 9, No. 6, pp. 547-565.

[33] Nielsen, H. B. and Madsen, K. (1972): Løsning af lineære ligningssystemer. Hæfte 23. Numerisk Institut. DTH. (In Danish).

[34] Patankar, S. V. and Spalding, D. B. (1970): Heat and Mass Transfer in Boundary Layers. 2.nd ed. Intertext Books.

[35] Reynolds, W. C. (1976): Computation of Turbulent Flows. Ann. Rev. Fluid Mech., Vol. 8, pp. 183-208.

[36] Rodi, W. (1980): Turbulence Models and Their Application in Hydraulics. I. A. H. R., Delft, The Netherlands.

[37] Rogallo, R. S. and Moin, P. (1984): Numerical Simulation of Turbulent Flow. Ann. Rev. Fluid Mech., Vol. 16, pp. 99-137.

[38] Shen, S. F. (1977): Finite Element Methods in Fluid Mechanics. Ann. Rev. Fluid Mech. , Vol. 9, pp. 421-445.

[39] Sheng, Y. P. (1982): Hydraulic Applications of a Second-Order Closure Model of Turbulent Transport. Conf. Applying Research to Hydraulic Practice. ASCE. August 17-20. pp. 106-119.

[40] Skovgaard, O., Jonsson, I. G. and Bertelsen, J. A. (1976): Computation of Wave Heights due to Refraction and Friction. Closure to paper 11100, ASCE, Journal of Waterways, Harbours and Coastal Engineering Div., Vol. 102, WW1, pp. 100-105.

[41] Sleath, J. F. A. (1984): Sea Bed Mechanics. John Wiley & Sons. xx + 335 pp.

[42] Staub, C., Jonsson, I. G. and Svendsen, I. A. (1984): Variation of Sediment Suspension in Oscillatory Flow. 19th. Coastal Engineering Conference, Houston. 14 pp. In press.

[43] Tanaka, H., Chian, C. S. and Shuto, N. (1983): Experiments on an Oscillatory Flow Accompanied with a Unidirectional Motion. Coastal Engineering in Japan, Vol. 26, pp. 19-37.

[44] Tennekes, H. and Lumley, J. L. (1972): A First Course in Turbulence. Cambridge, Mass., MIT Press. xiii + 300 pp.

[45] Throwbridge, J. and Madsen, O. S. (1984): Turbulent Wave Boundary Layers. 1. Model Formulation and First-order Solution.

J. of Geophysical Research, Vol. 89, No. C5, pp. 7989-7997.

[46] van Doorn, T. (1983): Computations and Comparison with Measurements of the Turbulent Bottom Boundary Layer in an Oscillatory Motion. Report M 1562 Part 2. Delft hydraulics Laboratory.

[47] van Kesteren, W. G. M. and Bakker, W. T. (1984): Near-Bottom Velocities in Waves with a Current; Analytical and Numerical Computation. Coastal Engineering Conference, Houston. In press.

[48] Vemuri, V. and Karplus, W. J. (1981): Digital Computer Treatment of Partial Differential Equations. Prentice-Hall, Englewood Cliffs, New Jersey. 449 pp.

10. LIST OF SYMBOLS

Symbol	Explanation	Eq.
A	coefficient matrix in system of equations	(4.26
A^j	coefficients in solution of U-equation	(5.28
A_i^n	coefficients in solution of k-equation	(5.41
B_i^n	coefficients in solution of k-equation	(5.42)
B^j	coefficients in solution of U-equation	(5.29)
C_i	coefficients	(4.27
C_i^n	coefficients in solution of k-equation	(5.43
C^j	coefficients in solution of U-equation	(5.30
D_i^n	right-hand side, solution of k-equation	(5.44
D^j	right-hand side, solution of U-equation	(5.30)
D_i^n	coefficient matrix	(4.32
E	energy loss	(4.44
E_i^n	coefficient matrix	(4.32
F_i^n	coefficient matrix	(4.32
F_i^j	coefficients in solution of k-equation	
G_i^n	right-hand side in system of eqs.	(4.32
G_i^j	approximation in z-eq.	(6.16
H	wave height	
H_i^j	approximation in z-eq.	(6.17
HS	right-hand side	(5.25)
K_i^j	coefficients in solution of k-equation	App. I
L_i^j	coefficients in solution of k-equation	App. I
L	free paths of molecules	
M_i^j	coefficients in solution of k-equation	App. I
N	number of equations	
N_i^j	coefficients in solution of k-equation	
NT	number of timesteps	
Q_x	diffusive flux in x-direction	
Q_y	diffusive flux in y-direction	
RE	amplitude Reynolds number	(2.40)
S_i	constants	(4.28)
T	period of ambient flow	
TKE	turbulent kinetic energy, k	(2.10)
U	horizontal mean velocity	
U_d	defect velocity	

U_f	friction velocity	
U_i	mean velocity in x_i-direction	
U_o	ambient flow velocity	
$U_{i\,o}$	ambient velocity amplitude	
V	vertical mean velocity	
V	velocity scale	(2.20)
a	amplitude in ambient osc. flow	
c	straining factor	(4.19)
c	wave celerity	
c	sediment concentration by volume	(7.1)
c_1	empirical constant	(5.15)
c_3	- -	(5.16)
c_4	- -	(6.13)
c_5	- -	(6.8)
$c_{2\,\varepsilon}$	empirical constant	(6.8)
d	grain diameter	
$e_{i\,j}$	deformation tensor	
f	residual vector	
f_e	energy loss factor	(4.45)
f_w	friction factor	(4.39)
fk	residual vector	(5.38)
fz	residual vector	(6.19)
g	acceleration due to gravity	
i	index	
i	imaginary unit	
j	index	
k	turbulent kinetic energy	(2.10)
k	wave number	
k_N	Nikuradse roughness	
l	length-scale	
l	index	
l_m	mixing-length	
n	index	
p	pressure	
p	internal friction velocity	
s	relative grain density	
t	time	
u	horizontal velocity fluctuation	

u_d	defect velocity amplitude	
u_i	turbulent velocity fluctuation in x_i -direction	
v	vertical velocity fluctuation	
v_i	local velocity	
w	fall velocity	
x	horizontal coordinate	
x_i	space coordinate	
y	vertical coordinate	
z	dissipation rate	(2.34)
z	vector containing unknowns	(4.24)
α	weighing factor in implicit scheme	
δ_{ij}	Kronecker delta	
δ	displacement thickness	(4.41)
δ_1	boundary layer thickness	
$\delta_{0.99}$	boundary layer thickness	
ε	eddy viscosity	
ε_s	turbulent exchange factor	(7.1)
κ	von Karmans constant (=0.40)	
η_w	wave viscosity	
π	pi, constant	
ρ	fluid density	
ν	kinematic viscosity	
μ	dynamic viscosity	
ω	angular frequency of osc. flow	
ϕ	phase shift	
ξ	strained vertical coordinate	
τ	shear stress	
σ_{ij}	stress tensor	
σ_k	empirical constant, one-eq.-model	(5.18)
σ_z	empirical constant, two-eq.-model	(6.9)
θ	momentum thickness	(4.42)
θ	Shields parameter	(7.3)

Superscripts: * - dimensionless quantity

Subscripts:
- b - bed quantity
- 1m - ambient quantity
- o - upper edge of computational region